Adsorption of element 112 on a Au surface

Inaugural-Dissertation

zur Erlangung der

Doktorwürde der Naturwissenschaften

(Dr. rer. nat.)

vorgelegt beim Fachbereich Naturwissenschaften

der Universität Kassel

von

Cristina Sarpe-Tudoran

aus Craiova, Romania

Mai 2004

Gedruckt mit Genehmigung des Fachbereichs Physik der
Universität Gesamthochschule Kassel.

1. Gutachter: Prof. Dr. B. Fricke
2. Gutachter: PD Dr. S. Fritzsche

weitere Miglieder der Prüfungskommission:

Prof. Dr. T. Baumert
Prof. Dr. M. Garcia

Tag der Disputation: 22. June. 2004

Diese Arbeit widme ich Herrn Prof. Dr. Dieter Spethmann, der mir mit einer großzügigen Spende die Fertigstellung dieser Arbeit ermöglichte.

Zusammenfassende deutsche Darstellung der in englischer Sprache abgefassten Doktorarbeit:

Adsorption des Elementes 112 auf einer Au Oberfläche

Während der letzten 20 Jahre hat sich das Periodensystem bis zu den Elementen 114 und 116 erweitert. Diese sind kernphysikalisch nachgewiesen, so dass jetzt die chemische Untersuchung an erster Selle steht. Nachdem sich das Periodensystem bis zum Element 108 so verhält, wie man es dem Periodensystem nach annimmt, wird in dieser Arbeit die Chemie des Elements 112 untersucht. Dabei geht es um die Adsorptionsenergie auf einer Gold–Oberfläche, weil dies der physikalisch/chemische Prozess ist, der bei der Analyse angewandt wird.

Die Methode, die in dieser Arbeit angwandt wird, ist die relativistische Dichtefunktionalmethode. Im ersten Teil wird das Vielkörperproblem in allgemeiner Form behandelt, und im zweiten die grundlegenden Eigenschaften und Formulierungen der Dichtefunktionaltheorie.

Die Arbeit beschreibt zwei prinzipiell unterschiedliche Ansätze, wie die Adsorptionsenergie berechnet werden kann. Zum einen ist es die sogenannte Clustermethode, bei der ein Atom auf ein relativ kleines Cluster aufgebracht und dessen Adsorptionsenergie berechnet wird. Wenn es gelingt, die Konvergenz mit der Größe des Clusters zu erreichen, sollte dies zu einem Wert für die Adsorptionsenergie führen. Leider zeigt sich in den Rechnungen, dass aufgrund des zeitlichen Aufwandes die Konvergenz für die Clusterrechnungen nicht erreicht wird. Es werden sehr ausfürlich die drei verschiedenen Adsorptionsplätze, die Top-, die Brücken- und die Muldenposition, berechnet.

Sehr viel mehr Erfolg erzielt man mit der Einbettungsmethode, bei der ein kleiner Cluster von vielen weiteren Atomen an den Positionen, die sie im Festkörpers auf die Adsorptionsenergie soweit sichergestellt ist, dass physikalisch–chemisch gute Ergebnisse erzielt werden.

Alle hier gennanten Rechnungen sowohl mit der Cluster- wie mit der Einbettungsmethode verlangen sehr, sehr lange Rechenzeiten, die, wie oben bereits erwähnt, nicht zu einer Konvergenz für die Clusterrechnungen ausreichten. In der Arbeit wird bei allen Rechnungen sehr detailliert auf die Abhängigkeit von den möglichen Basissätzen eingegangen, die ebenfalls in entscheidender Weise zur Länge und Qualität der Rechnungen beitragen. Die auskonvergierten Rechnungen werden in der Form von Potentialkurven, Density of States (DOS), Overlap Populations sowie Partial Crystal Overlap Populations analysiert.

Im Ergebnis zeigt sich, dass die Adsoptionsenergie für das Element 112 auf einer Goldoberfläche ca. 0.2 eV niedriger ist als die Adsorption von Quecksilber auf der gleichen Oberfläche. Mit diesem Ergebnis haben die experimentellen Kernchemiker einen Wert an der Hand, mit dem sie eine Anhaltspunkt haben, wo sie bei den Messungen die wenigen zu erwartenden Ereignisse finden können.

<div align="center">**Abstract**</div>

<div align="center"># Adsorption of element 112 on a Au surface</div>

The recent synthesis of element 104 to 116 attracts new interest in the field of the Super Heavy Elements (SHE) research. Once the SHE were synthesized, the question arises if they behave as their homologues in the Periodic Table. By now it is experimentally confirmed that up to Hassium, element 108, this property is perfectly accomplished by all SHE.

The production of isotopes with half-lives of ≈ 30 min for element 112 justifies chemical experiments for it to be done. Using the gas-phase-chromatography technique the adsorption energy of element 112 on a Au surface is aimed to be measured.

In this work the relativistic density functional method is used in order to calculate this quantity. The many-body problem is generally described in the first chapter, and in the second the principle and general formulation of the Density Functional Theory is presented.

This work describes two different approximations for the calculation of the adsorption energy. The first one is the so-called cluster method, in which the surface is modeled by a relatively small cluster and the adsorption energy of the ad-atom on it is calculated. All the three possible adsorption site on a (100) fcc surface were taken into account: the top-, bridge-, and hollow-position. To obtain the adsorption energy the convergence with the cluster size has to be checked. Unfortunately, due to the long computation time necessary for the self-consistent calculations, this convergence with the number of atoms in the cluster was not achieved.

The use of the embedding method was more sucessfully. Within this method a small cluster is embedded in a bigger one, formed by Au atoms placed in the (100) fcc lattice points. The atoms in the environment cluster are not treated self-consistently during the relativistic calculations, but they will produce an external potential and will contribute to the exchange correlation energy of the inner system. This procedure allows to take into account the influence of a bigger gold solid to the adsorption energy and gives a good description of the physical/chemical properties of the chemisorption process.

A large amount of time and computer memory size is required in all these calculations, for both cluster and embedding method. As mentioned above, the convergence with the cluster size for the cluster calculations was not achieved. This work contains also a detailed description of the influence of the basis on the quality of the results and the duration of the computation. For the cluster considered in the work, the potential energy curves, the total and partial Density of States (DOS) as well as the Partial Crystal Overlap Population are anlysed.

This analysis shows that the adsorption energy of element 112 on a gold surface is about 0.2 eV smaller than the corresponding value for the adsorption of Hg on the same surface. This result offers a benchmark to the experimentalist for this value, which is helpful in designing the chemical experiment with element 112.

Contents

Chapter 1

Introduction

The fundamental interest in super heavy element research is connected with the questions: How many elements exist in nature? How long is their lifetime? Which properties determine their stability? How can they be synthesized? What are their chemical properties? How are the electrons arranged in the strong field of the nuclei? e.t.c.

The recent synthesis of the elements 104 to 116 attracts new interest in this field. The properties of the nuclei are not smooth uniform functions of the proton and neutron numbers, but show non-uniformities as evidenced by variations in the measured atomic masses. Just like the electron cloud of the atom, the nuclei in the nucleus also exhibit a shell structure, whose arrangement for certain number of protons and/or neutrons (2, 8, 20, 28, 50, and 82), the so called **magic numbers** leads to particularly stable configurations.

The elements beyond uranium have been discovered as artificial elements. The transuranium elements up to fermium can be produced by neutron capture and successive β^- decay. This method of breeding of the transuranium elements in a high flux reactor allows to climb up the Periodic Table element by element up to fermium, where this process ends due to the short alpha and fission half-lives. The transfermium region is best accessible using **heavy ion reactions**: the bombardment of heavy targets with heavy ions from an accelerator. Mendelevium was the first element synthesized in a heavy–ion reaction and the first element obtained in a quantity of *one–atom–at–a–time*. There are two types of heavy–ion reactions which have been successfully used so far in the synthesis of transmendelevium elements:

- a) *cold fusion*, Pb or Bi targets and the appropriate projectile leading to low excitation energies in the completely fused species (with resulting high survival probabilities)

- b) *hot fusion*, the application of actinide targets and lighter projectile beams, leading to larger fusion cross section but reduced survival probabilities (due to the higher excitation energies of the completely fused species).

The major difference between them is the excitation energy of the compound nucleus at the lowest beam energies necessary to initiate a fusion reaction. Usually 10–20 MeV

are used in reactions with lead or bismuth targets and 35 to 45 MeV in reactions with actinide targets, which lead to the above terminology.

A second important difference is that the synthesis of an element by hot fusion reaction, compared with a cold fusion reaction, leads to more neutron rich isotopes, which are closer to the region of spherical SHEs (Super Heavy Elements) and for which also longer half-lives were expected.

The cross section is less than in the neutron capture and values are considerably below the geometrical size of the nuclei.

Historically, the first accelerators used for the production of heavy elements were the cyclotrons in Berkeley, California, and later in Dubna, Russia. These were only able to accelerate light ions up to about neon with sufficient intensity and energy high enough for fusion reactions. The U300 and U400 (300 and 400 cm diameter) cyclotrons were built in Dubna for the investigation of reactions using projectiles near calcium. In Berkeley a linear accelerator HILAC (Heavy Ion Linear Accelerator), later upgraded to SuperHILAC was built. During the years 1969–74, the UNILAC (UNIversal Linear ACcelerator) was constructed in Darmstadt, Germany, aiming the acceleration of ions as heavy as uranium. The developments in the laboratories in Berkeley, Dubna and also in Finland, France, Italy and Japan are similar and are usually made in close collaboration and exchange of known–how.

The term "super heavy element" was coined for elements which exists solely due to their nuclear shell effects. The series of super heavy elements are starting with the element 104, Rutherfordium Rf, for which the known isotopes exhibit half-lives of up to one minute. It is worth noting that Rutherfordium is also the first element in the series of transactinide elements.

Element 112 was first synthesized [1] in January–February 1996, at GSI, using the reaction:

$$^{70}Zn + ^{208}Pb \rightarrow ^{278}112^*$$
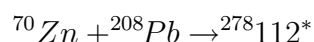
Two chains of localized alpha–emitters were identified as originating with $^{277}112$, the first two shown in Fig. 1.1. These were assigned to the one–neutron emission channel and the observed cross section was of 0.5 pb. The first chain has subsequently been eliminated [2] after the reanalysis of the data. The experiment was repeated in May 2000 aiming to confirm the synthesis of $^{277}112$ [3]. During a similar measuring time one more decay chain (on the left–hand side in Fig. 1.1) was observed, which was in agreement with the one observed in the first experiment.

In 1999, a Dubna-GSI-RIKEN collaboration [4] reported the successful synthesis of $^{283}112$ using the reaction

$$^{48}Ca + ^{238}U \rightarrow ^{286}112^* \rightarrow ^{283}112 + 3n$$
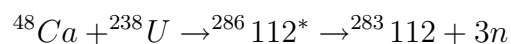
in which the two events decay by spontaneous fission with a lifetime of 2 min. Two fission events were measured with a cross section of 5.0 pb. The experiments were continued in

2

Confirmation of element 112

1st Experiment 1996:
$E^* = 10$ MeV
2 events

^{277}112 CN
11.65 MeV
0.4 ms
^{273}110
9.73 MeV
170 ms
^{269}Hs
9.17 MeV
7.1 s
^{265}Sg
8.77 MeV
24.1 s
^{261}Rf
1.22 MeV
32.7 s
^{257}No
Date: 01 Feb 1996

^{277}112 CN
11.45 MeV
0.2 ms
^{273}110
11.08 MeV
0.11 ms
^{269}Hs
9.23 MeV
19.7 s
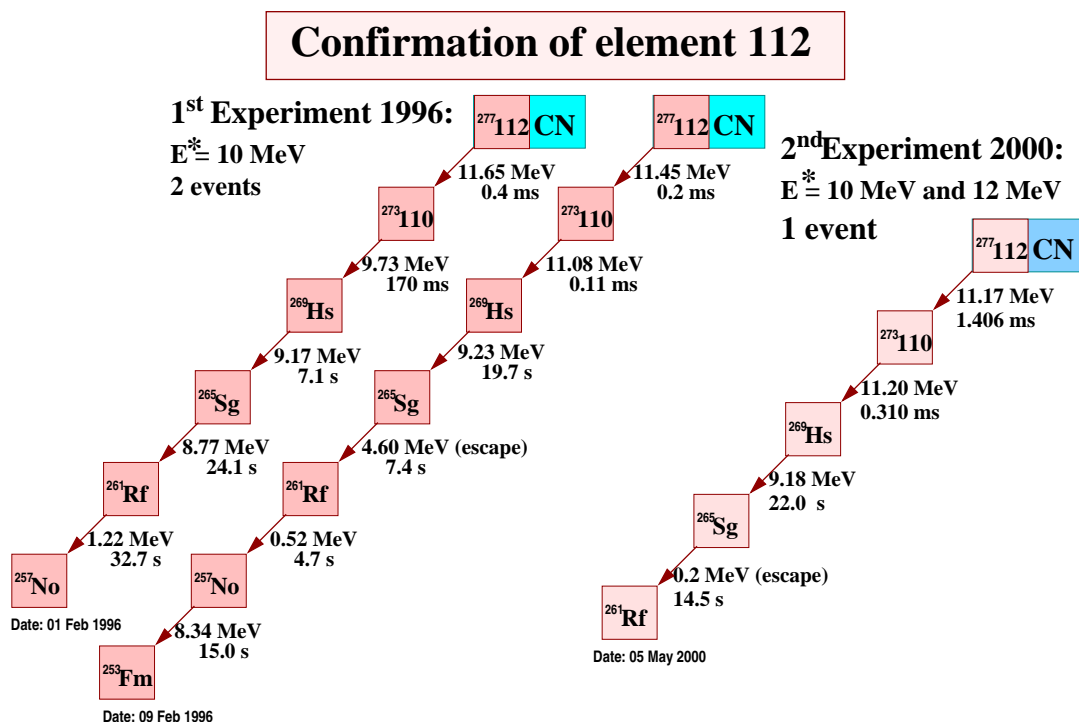^{265}Sg
4.60 MeV (escape)
7.4 s
^{261}Rf
0.52 MeV
4.7 s
^{257}No
8.34 MeV
15.0 s
^{253}Fm
Date: 09 Feb 1996

2nd Experiment 2000:
$E^* = 10$ MeV and 12 MeV
1 event

^{277}112 CN
11.17 MeV
1.406 ms
^{273}110
11.20 MeV
0.310 ms
^{269}Hs
9.18 MeV
22.0 s
^{265}Sg
0.2 MeV (escape)
14.5 s
^{261}Rf
Date: 05 May 2000

Figure 1.1: Three decay chains measured in experiments at SHIP in the cold fusion reaction $^{70}Zn + ^{208}Pb \rightarrow ^{278}112^*$. The chains were assigned to the isotope $^{277}112$ produced by evaporation of one neutron from the compound nucleus.

March 1999 and the element $^{287}114$ was produced [5], and element $^{283}112$ resulted in the α decay chain. The element $^{289}114$ was produced [6] in the reaction $^{48}Ca + ^{244}Pu$, which decayed through $^{285}112$. The isotope $^{284}112$ was obtained [7] in the alpha decay chain of element $^{292}116$, obtained in the reaction $^{48}Ca + ^{248}Cm \rightarrow ^{284}116^*$.

One of the most important question for chemists is: do the rules of the Periodic Table still hold for the heaviest elements? The position of an element is determined by its atomic number and electronic configuration. Very early theoretical predictions of this chemical behaviour have been made on the basis of Dirac–Fock type calculations. A review of 1975 summarizes the results for all superheavy elements from $Z = 100$ to $Z = 172$ [8]. The general trend of the predictions still holds true nowadays. Of course experimentally this structure cannot be measured, and information on their chemical behaviour or obtained from the relation with its daughter products is often used to place an element in a chemical group. For the SHEs, which have very small cross sections and half–lives, fast chemistry techniques based on chromatographic separations are used. Chemistry of elements 104 and 108 performed by these techniques, proved that they behave as their homologues in the Periodic Table. Some chemical experiments with element 112 were performed and new other are planed to be made, based on gas phase chromatography technique, where one observes the adsorption of it on metal surfaces. The chemical information obtained from experiments with elements with very short half–lives is limited to proof if the new element behaves similarly or differently than its

lighter congeners in the chromatographic separation process. The deviations in their behaviour is due to the very strong relativistic effects on the valence electronic shells of the heavy and super heavy elements. The experiments performed with element 112, aimed to determine if it behaves like Hg or rather as a noble gas, Rn. The metal used in the chromatographic column is Au, on which both Hg and element 112 are well adsorbed and the physical quantity to be measured is the adsorption energy. Theoretical predictions of experimentally studied properties are especially valuable in order to design the sophisticated and expensive experiments.

Chapter 2

The many-body problem

Prediction of the electronic and geometric structure of a solid requires calculation of quantum-mechanical total energy of the system and subsequent minimisation of that energy with respect to the electronic and nuclear coordinates. If one looks at small atoms the non-relativistic theory is a very good approximation, but when heavy atoms are involved, the relativistic effects must be considered.

The Hamilton operator describing a system of N nuclei and M electrons described by position vectors $\vec{R}_A$ and $\vec{r}_i$, respectively, with a pair (Coulomb) interaction between the components is given, in atomic units, by:

$$\mathcal{H} = \sum_{A=1}^{N} \hat{T}_A + \sum_{i=1}^{M} \hat{t}_i - \sum_{i=1}^{M}\sum_{A=1}^{N} \frac{Z_A}{|\vec{r}_i - \vec{R}_A|} + \frac{1}{2} \sum_{\substack{i,j=1 \\ i \neq j}}^{M} \frac{1}{|\vec{r}_i - \vec{r}_j|} + \frac{1}{2} \sum_{A,B=1}^{N} \frac{Z_A Z_B}{|\vec{R}_A - \vec{R}_B|}. \quad (2.1)$$

The first two summations are the kinetic energy operators of the nuclei and electrons; the third term represents the Coulomb interaction between electrons and nuclei; third fourth and fifth terms represent the repulsion between electrons and between nuclei, respectively.

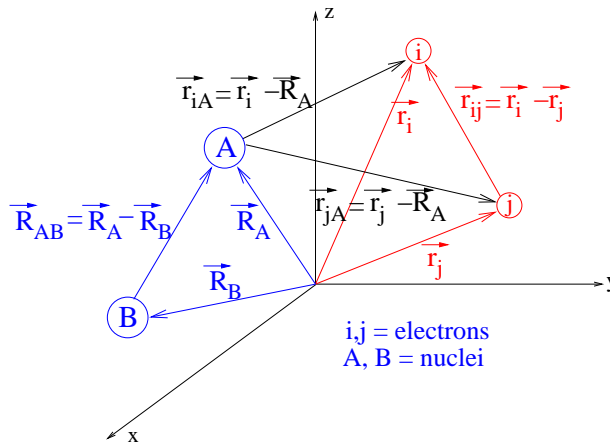To find the total ground state energy the following eigenvalue equation:

Figure 2.1: A molecular coordinate system: i, j = electrons; A, B = nuclei.

5

$$\mathcal{H}\Psi = E\Psi \tag{2.2}$$

is solved under the constraint

$$\langle\Psi|\Psi\rangle = 1$$

E is the total energy of the system and ψ is the total quantum state of this system. It is impossible to solve exactly this equation and several approximations have to be made.

2.1 The Born-Oppenheimer approximation

Since nuclei are much heavier than electrons, they move more slowly. The total energy of a given nuclear configuration can be then estimated by keeping the nuclei fixed, and minimising the energy of the electrons in the constant external potential originating from the nuclei. The kinetic energy of the nuclei in (2.1) can be neglected and the last term, the repulsion between the nuclei, can be considered to be constant. The remaining terms 2,3 and 4 in (2.1) are called the electronic Hamiltonian, and the corresponding eigenvalue equation is now:

$$\mathcal{H}_{el}\Psi_{el} = E_{el}\Psi_{el} \tag{2.3}$$

where the electronic wave function,

$$\Psi_{el} = \Psi_{el}(\{\vec{r}_i\}; \{\vec{R}_A\})$$

depends on the electronic coordinates but depends parametrically on the nuclear coordinates, as does the electronic energy $E_{el} = E_{el}(\{\vec{R}_A\})$. If the thermal energy of the atoms is expected to have any influence on the nuclear motion, it can be included afterwards. Fixing the nuclei like this is called the Born-Oppenheimer approximation.

2.2 The Hartree–Fock method

For a system of N non-interacting fermions the wave function can be constructed as a Slater determinant of the orthonormalized single-particle spin-orbitals:

$$|\Psi_{el}\rangle = \frac{1}{\sqrt{M!}} \begin{pmatrix} \psi_1(\vec{r}_1, s_1) & \psi_1(\vec{r}_2, s_1) & ... & \psi_1(\vec{r}_M, s_1) \\ \psi_2(\vec{r}_1, s_1) & \psi_2(\vec{r}_2, s_1) & ... & \psi_2(\vec{r}_M, s_1) \\ \psi_3(\vec{r}_1, s_1) & \psi_3(\vec{r}_2, s_1) & ... & \psi_3(\vec{r}_M, s_1) \\ \vdots & \vdots & & \vdots \\ \psi_M(\vec{r}_1, s_1) & \psi_M(\vec{r}_2, s_1) & ... & \psi_M(\vec{r}_M, s_1) \end{pmatrix} \tag{2.4}$$

where s_i indicates that each spatial orbital is multiplied by a spin function. Such a Slater determinant is total anti-symmetric. Furthermore, it is easily verified that the Slater

determinant obeys the Pauli exclusion principle: If two electrons are in the same state, they have the exact same orbitals, then two column vectors of the Slater determinant are identical, and the wave function equals zero.

The minimisation of the total energy of a Slater determinant wave function using the interacting Hamiltonian (2.3), keeping the orthogonality between the single-particle spin orbitals, is known as the Hartree–Fock method [9, 14].

This method conceptually implies solving an eigenvalue equation (2.5) for all single particle quantum states, with a mean field effective potential for each state:

$$\hat{\mathcal{F}}(\vec{r})|\psi_i\rangle = \sum_{i=1}^{M} \epsilon_{ij}|\psi_i\rangle, \qquad i = 1, ..., M \ . \tag{2.5}$$

$\hat{\mathcal{F}}$ is the Hartree-Fock operator given by:

$$\hat{\mathcal{F}}(\vec{r}) = \hat{t} - \sum_{A=1}^{N} \frac{Z_A}{|\vec{r} - \vec{R}_A|} + \sum_{j=1}^{M} \int \psi_j^*(\vec{r}') \frac{1}{|\vec{r} - \vec{r}'|} \psi_i(\vec{r}') d^3\vec{r}' + V^{ex}(\vec{r}), \tag{2.6}$$

where the exchange potential $V^{ex}(\vec{r})$ is a non-local operator:

$$V^{ex}(\vec{r})\psi_i(\vec{r}) = -\sum_{j=1}^{M} \int \psi_j^*(\vec{r}', s') \frac{1}{|\vec{r} - \vec{r}'|} \psi_i(\vec{r}') d^3\vec{r}' ds' \psi_j(\vec{r}, s) \tag{2.7}$$

The evaluation of the exchange term is difficult for the non-local character of the operator. Dirac [10] and Bloch [11] showed that the exchange integral is expressible in terms of the electronic density.

Since the mean field has to be known to solve the eigenvalue problem, and the eigenstates have to be known to calculate the mean field potential, the equations can not be solved directly. The way they are solved in practical calculations is to use an iterative procedure: An initial guess is made for the single-particle states, and this is used to calculate the mean field potential. The mean field potential thereby obtained is then used to calculate an improved approximation to the single-particle states. This iteration procedure is continued until the mean field is self-consistent with the quantum states within some small error margin. Such a method is called a Self Consistent Field (SCF) procedure. At self-consistency the Hartree-Fock wave function, Ψ_{HF}, is the Slater determinant of single particle states.

The Hartree-Fock energy is determined:

$$E_{HF} = T_{HF} + U_{HF} + W_{HF} \tag{2.8}$$

where T_{HF} and U_{HF} are the expectation values of $\hat{t}$ and the electron-nuclei Coulomb potential using Ψ_{HF}, and the later one is the Hartree-Fock electron-electron interaction energy, which includes the Hartree energy and the (HF-)exchange energy.

$$W_{HF} = \frac{1}{2} \sum_{i,j=1}^{M} \int \psi_i^*(\vec{r}', s')\psi_j^*(\vec{r}, s) \frac{1}{|\vec{r} - \vec{r}'|} \psi_i(\vec{r}'s')\psi_j(\vec{r}, s) d^3\vec{r} \, d^3\vec{r}' ds ds'$$

$$-\frac{1}{2} \sum_{i,j=1}^{M} \int \psi_i^*(\vec{r}', s')\psi_j^*(\vec{r}, s) \frac{1}{|\vec{r} - \vec{r}'|} \psi_j(\vec{r}', s')\psi_i(\vec{r}, s) d^3\vec{r} \, d^3\vec{r}' ds ds' \tag{2.9}$$

In quantum physics the definition of the exchange energy is slightly different, as it is the same summation of integrals but using the Kohn-Sham single-particle states instead of the Hartree-Fock states. The HF-exchange energy is a non-positive function that has the important property that in the two summations of (2.7) its terms with i=j cancels with equivalent terms of the Hartree energy. An electron does not experience any repulsion due to itself. The energy cancellation is therefore a correction to the wrongly determined Coulomb interaction in the individual electron clouds and is called the self–energy Hartree-correction.

2.3 Scaling behaviour of quantum mechanical methods

The Hartree-Fock energy is not the correct ground state energy, as one Slater determinant does not provide enough variational freedom to expand the entire Hilbert space of a set of fully interacting fermions. The difference between the total ground state energy and the Hartree-Fock energy is the chemists definition of the so called correlation energy:

$$E_{corr}^{chem} = E_{tot} - E_{HF} \tag{2.10}$$

In atoms the relativistic energy correction is already larger than the correlation energy in an Aluminium atom (with Z=13), and it grows much more rapidly than the correlation energy with increasing atomic number. This could seem to indicate that the relativistic corrections rapidly become more important than correlation corrections in the description of molecules and solids containing heavy elements. This is however not the case, as the relativistic energy is related almost exclusively to the inert core electrons. The electron correlation energy on the other hand is closely related to the bonding between atoms.

Whereas all other quantities discussed so far are easy to obtain (in the sense that they are well defined and can be found for a medium sized system in relatively short time on a computer), the correlation energy is a very difficult quantity to calculate. This is because the correlation energy is so directly related to the degrees of freedom in the Hilbert space, which can not be spanned by the single Slater determinant. The large majority of wave function methods tries to span the Hilbert space by introducing multiple Slater determinants and including the unoccupied Hartree-Fock one-electron orbitals in this expansion. The ultimate goal of this would be to give a correct representation of the full electronic wave function. The wave function in the Born-Oppenheimer approximation is a 3M dimensional complex function with M spin coordinates, where M is the number of electrons. The multi-dimensional search of such a wave function is prohibitively expensive from a computational point of view for even very small systems. This is the motivation for the use of the density functional theory.

The quick development of computational methods in Physics and Chemistry nowadays allows to calculate energies and other properties of atoms, molecules and small clusters with ab-initio methods. First of all there are the 'classical' but still very popular methods

in quantum chemistry such as the Hartree- (Dirac-) Fock-Methods [12–14], Configuration Interaction (CI), Multiconfiguration Dirac-Fock (MCDF), second order Møller-Plessed MP2 [15], coupled cluster single double (triple) excitation CCSD(T) [16–19] and s.o. The great advantage of all these methods is the possibility to achieve the 'exact' solution (within the chosen method) just by increasing the number of configurations. Unfortunately this number increases as power of 4, 5 or even 7 with the number of active electrons, so that all these methods fight with the limit of the memory and CPU-power. Therefore these methods can nowadays only be applied to systems with relatively small numbers of active electrons such as atoms, small molecules and small clusters. The results achieved for these systems are very good and serve as benchmarks. In the last two decades however many computational improvements are made to make these methods more efficient. With some approximations for example it was possible to achieve first a quadratic [20, 21] and later on even a linear [22, 23] scaling for the Hartree-Fock method. A linear scaling has been also achieved for the MP2 [24, 25] as well as for the CCSD(T) [26] methods.

Chapter 3

Density Functional Theory

In the recent years DFT has become a widely used formalism for providing a theoretical picture into the microscopic physical process which determine the macroscopic properties of interacting electronic systems. The DFT is based on the earlier fundamental work of Hohenberg and Kohn [27] and Kohn and Sham [28].

3.1   The Hohenberg-Kohn Theorems

The Hohenberg-Kohn theorems relate to any system consisting of electrons moving under the influence of an external potential. Stated simply they are as follows:

Theorem 1
The external potential $v_{ext}(\vec{r})$, and hence the total energy, is a unique functional of the electron density $\rho(\vec{r})$.

The energy functional $E[\rho(\vec{r})]$ alluded to in the first Hohenberg-Kohn theorem can be written in terms of the external potential in the following way,

$$E[\rho(\vec{r})] = \int d^3\vec{r}\rho(\vec{r})v_{ext}(\vec{r}) + F[\rho(\vec{r})] \qquad (3.1)$$

where $F[\rho(\vec{r})]$ is an unknown, but otherwise universal functional of the electron density only. Correspondingly, a Hamiltonian for the system can be written such that the electron wavefunction that minimises the expectation value gives the ground state energy (assuming a non-degenerate ground state):

$$E[\rho(\vec{r})] = \langle \Psi | \mathrm{H} | \Psi \rangle \qquad (3.2)$$

Theorem 2
The ground state energy can be obtained variationally: the density that minimises the total energy is the exact ground state density.

Although the Hohenberg-Kohn theorems are extremely powerful, they do not offer a way of computing the ground-state density of a system in practice. About one year after the seminal DFT paper by Hohenberg and Kohn, Kohn and Sham [9] derived a simple method for carrying out DFT calculations, that retains the exact nature of DFT.

3.2 The Kohn-Sham Formulation

The Kohn-Sham formulation centres on mapping the full interacting system with the real potential, onto a fictitious non-interacting system whereby the electrons move within an effective "Kohn-Sham" single-particle potential $v_{KS}(\vec{r})$. The Kohn-Sham method is still exact since it yields the same ground state density as the real system, but greatly facilitates the calculation.

First consider the variational problem presented in the second Hohenberg-Kohn theorem - the ground state energy of a many-electron system can be obtained by minimising the energy functional

$$\delta \left[F[\rho(\vec{r})] + \int d^3\vec{r}\rho(\vec{r})\mathcal{V}_{ext}(\vec{r}) - \mu(\int d^3\vec{r}\rho(\vec{r}) - N) \right] = 0 \qquad (3.3)$$

where μ is the Lagrange multiplier associated with the constraint of constant N. The idea of Kohn and Sham was to set up a system where the kinetic energy could be determined exactly, since this was a major problem in Thomas-Fermi theory. This was achieved by invoking a non-interacting system of electrons.

The universal functional $F[\rho(\vec{r})]$ was then partitioned into three terms, the first two of which are known exactly and constitute the majority of the energy, the third being a small unknown quantity

$$F[\rho(\vec{r})] = T_S[\rho(\vec{r})] + E_H[\rho(\vec{r})] + E_{xc}[\rho(\vec{r})]. \qquad (3.4)$$

$T_S[\rho(\vec{r})]$ is the kinetic energy of a non-interacting electron gas of density, $E_H[\rho(\vec{r})]$ is the classical electrostatic (Hartree) energy of the electrons,

$$E_H[\rho(\vec{r})] = \int \int d^3\vec{r}d^3\vec{r}' \frac{\rho(\vec{r})\rho(\vec{r}')}{|\vec{r} - \vec{r}'|}, \qquad (3.5)$$

and $E_{xc}[\rho(\vec{r})]$ is the exchange-correlation energy, which contains the difference between the exact and non-interacting kinetic energies and also the non-classical contribution to the electron-electron interactions, of which the exchange energy is a part.

Application of the Hohenberg-Kohn variational principle to Kohn-Sham orbitals gives the canonical Kohn-Sham orbital equations:

$$\left(\hat{t} + \mathcal{V}_{KS}(\vec{r}) \right) \psi_j(\vec{r}) = \varepsilon_j \psi_j(\vec{r}). \qquad (3.6)$$

where j runs over all the electrons, ψ_j and ε_j are the Kohn-Sham wave function of electronic state j and the Kohn-Sham eigenvalue, respectively.

Here the Kohn-Sham potential $\mathcal{V}_{KS}(\vec{r})$ is given by

$$\mathcal{V}_{KS}(\vec{r}) = \mathcal{V}_{ext}(\vec{r}) + \mathcal{V}_H(\vec{r}) + \mathcal{V}_{xc}(\vec{r}) = \mathcal{V}^{eff}[\rho(\vec{r})] + \mathcal{V}^{ex}[\rho(\vec{r})], \qquad (3.7)$$

with the Hartree potential $\mathcal{V}_H(\vec{r})$

$$\mathcal{V}_H(\vec{r}) = \int d^3\vec{r}' \frac{\rho(\vec{r}')}{|\vec{r} - \vec{r}'|}, \qquad (3.8)$$

$$\mathcal{V}^{eff}(\vec{r}) \;\; = \;\; \mathcal{V}_{ext}(\vec{r}) + \mathcal{V}_H(\vec{r}) \tag{3.9}$$

and the exchange-correlation potential $\mathcal{V}_{xc}(\vec{r})$,

$$\mathcal{V}_{xc}(\vec{r}) \;\; = \;\; \frac{\delta E_{xc}[\rho(\vec{r})]}{\delta \rho(\vec{r})}. \tag{3.10}$$

The ground state density is obtained by solving the Kohn-Sham equations, and the density is constructed from

$$\rho(\vec{r}) \;\; = \;\; \sum_{j=1}^{N} |\psi_j(\vec{r})|^2 \,. \tag{3.11}$$

These equations are nonlinear like the Hartree-Fock equations and are thus solved by an equivalent self consistent procedure.

Although exact in principle, Kohn-Sham theory is approximate in practice because of the unknown exchange-correlation functional $E_{xc}[\rho(\vec{r})]$. An implicit definition of $E_{xc}[\rho(\vec{r})]$ can be given through 3.4 as,

$$E_{xc}[\rho(\vec{r})] \;\; = \;\; T[\rho(\vec{r})] - T_S[\rho(\vec{r})] + E_{ee}[\rho(\vec{r})] - E_H[\rho(\vec{r})], \tag{3.12}$$

where $T[\rho(\vec{r})]$ and $E_{ee}[\rho(\vec{r})]$ are the exact kinetic and electron-electron interaction energies respectively.

An exchange-correlation energy functional has to be supplied in order to obtain useful results by the Kohn-Sham scheme.

3.3 The relativistic Kohn–Sham equations

One fundamental limitation of the density functional theory is that it is based on non-relativistic quantum theory and therefore is not applicable when relativistic effects are large. This limitation is more significant when the description of heavy metals and molecules is involved. It has already been pointed out by Rajagopal and Callaway [29] that the two theorems given by Hohenberg and Khon [27], on which the density functional formalism is based, can be generalised to include relativistic effects.

The first theorem, the existence theorem, becomes [32]:

There exists a one-to-one correspondence between the class of external potential just differing by gauge transformations, the associated class of ground states and the ground state four current j^ν.

The existence of a unique relation between the ground state and j^ν has as consequence that all ground state observables are unique functionals of the four current, in particular the ground state energy:

$$E_{tot}[j^\nu] \;\; = \;\; \langle \Psi[j^\nu]|H|\Psi[j^\nu]\rangle. \tag{3.13}$$

The variational principle for the RDFT gives:

$$\frac{\delta}{\delta j^\nu[\vec{r}]}\left[E_{tot}[j^\nu] - \frac{\mu}{c}\int d^3x j^0(\vec{x})\right]_{j=j_0} \;\; = \;\; 0, \tag{3.14}$$

with the inclusion of the charge conservation.

The four current components are defined by

$$j_0(\vec{r}) = \rho(\vec{r}) = \sum_i n_i \psi_i{}^+(\vec{r})\psi_i(\vec{r}), \quad j_k(\vec{r}) = \sum_i n_i \psi_i^+(\vec{r})\alpha_k\psi_i(\vec{r}), \tag{3.15}$$

where $\psi_i(\vec{r})$ are the four–component Dirac spinors, and α_k are the 4 x 4 Dirac-matrices

$$\vec{\alpha} = \begin{pmatrix} 0 & \vec{\sigma} \\ \vec{\sigma} & 0 \end{pmatrix}, \quad \beta = \begin{pmatrix} I & 0 \\ 0 & -I \end{pmatrix} \tag{3.16}$$

.

In the above equation $\vec{\sigma}$ and I are respectively the 2x2 Pauli matrices and the unit matrix.

The relativistic Kohn-Sham equations are

$$\left(\hat{t} + \mathcal{V}^{ex}(\vec{r}) + \mathcal{V}_{eff}[j_\mu] + \mathcal{V}^{xc}[j_\mu]\right)\psi_j(\vec{r}) = \varepsilon_j\psi_j(\vec{r}), \tag{3.17}$$

with the kinetic energy operator being the Dirac operator

$$\hat{t} = \vec{\alpha}\vec{p} + c^2(\beta - 1). \tag{3.18}$$

3.4 Non-collinear form of Kohn-Sham equations

Practical experience has shown that the functionals which depend on the density only cannot reproduce the experimental results [30,31]. One of the reasons was that the three dimensional current for a relativistic electron gas is zero, and therefore these functionals cannot describe system with internal magnetic field properly. One can rewrite the functional using the Gordon decomposition as functional dependent on the density and magnetization density. In the Gordon decomposition the three-dimensional current is represented as the sum of the orbit current and the magnetization. The first term is usually neglected because in most cases it is small in comparison to the second one. A general derivation can be found in [32,33]. One can prove [32,33] that the ground state energy is an unique functional of the ground state density ρ and magnetization density $\vec{m}$, provided the system is not subject to an external magnetic field. This means that the system can be completely described by its density and magnetization density. Within this method the total energy of a molecular system is given by the expression

$$E = \sum_{i=1}^M n_i \langle \psi_i \mid \hat{t} \mid \psi_i \rangle + \int V^N \rho \, d^3\vec{r} + \frac{1}{2}\int V^H \rho \, d^3\vec{r} + E^{xc}[\rho, \vec{m}] + \sum_{p>q} \frac{Z_p Z_q}{|\vec{R}_p - \vec{R}_q|} \tag{3.19}$$

with the density ρ and magnetization density $\vec{m}$ which are defined by

$$\rho(\vec{r}) = \sum_{i=1}^M n_i \, \psi_i^+(\vec{r})\psi_i(\vec{r}) \tag{3.20}$$

$$\vec{m}(\vec{r}) = -\mu_B \sum_{i=1}^M n_i \psi_i^+(\vec{r})\beta\vec{\Sigma}\psi_i(\vec{r}). \tag{3.21}$$

13

Here n_i are the occupation numbers, $\vec{r}$, $\vec{R}_q$ are the electronic and nuclear coordinates respectively and μ_B is the Bohr-magneton. The index i runs over all occupied molecular orbitals M, which in our case are four-component Dirac-spinors. The four-component spin-operator $\vec{\Sigma} = (\Sigma_x, \Sigma_y, \Sigma_z)$ is built from the two component Pauli matrix σ. The Dirac kinetic energy operator has the form (we use atomic units throughout)

$$\hat{t} = c\,\vec{\alpha}\cdot\hat{\vec{p}} + c^2(\beta - I)\,, \tag{3.22}$$

where $\vec{\alpha} = (\alpha_x, \alpha_y, \alpha_z)$ and β are the four-component Dirac matrices in the standard representation [34] and I is the four-component unit matrix.
V^N is the nuclear potential

$$V^N = \sum_p -\frac{Z_p}{|\vec{r} - \vec{R}_p|}\,, \tag{3.23}$$

where the index p runs over all nuclei in the molecular system.
E^{xc} is the exchange-correlation energy functional. V^H is the electronic Hartree potential

$$V^H(\vec{r}) \;\; = \;\; \int \frac{\rho(\vec{r}')}{|\vec{r} - \vec{r}'|}\, d^3\,\vec{r}'\,. \tag{3.24}$$

The variation of the energy functional (3.19) leads to the relativistic Kohn-Sham (KS) equations in their general form for the molecular orbitals ψ_i

$$\left\{ \hat{t} + V^N + \tilde{V}^H + \frac{\delta E^{xc}[\rho, \vec{m}]}{\delta\rho} - \mu_B\beta\vec{\Sigma}\cdot\frac{\delta E^{xc}[\rho, \vec{m}]}{\delta\vec{m}} \right\}\psi_i = \epsilon_i\psi_i \qquad i = 1, ..., M' \tag{3.25}$$

Here $\tilde{V}^H$ is the Hartree potential from the model-density and $M' \geq M$ is the number of molecular orbitals.

3.5   Choise of the Exchange-Correlation Functional

Functionals essentially try to model the exchange-correlation hole. This is done with varying degrees of sophistication depending on the approach taken. However, all functionals can be written in the following general form,

$$E_{xc}[n(\vec{r})] \;\; = \;\; \int d^3\vec{r}\, n(\vec{r})\varepsilon_{xc}(\vec{r}), \tag{3.26}$$

where $\varepsilon_{xc}(\vec{r})$ is the exchange-correlation energy per particle, or energy density for short.

3.5.1   Local–density approximation

The oldest, simplest and probably the most important functional is the local density approximation (LDA), which was proposed by Hohenberg and Kohn in their original DFT paper [27]. The LDA consists of locally approximating the true exchange-correlation
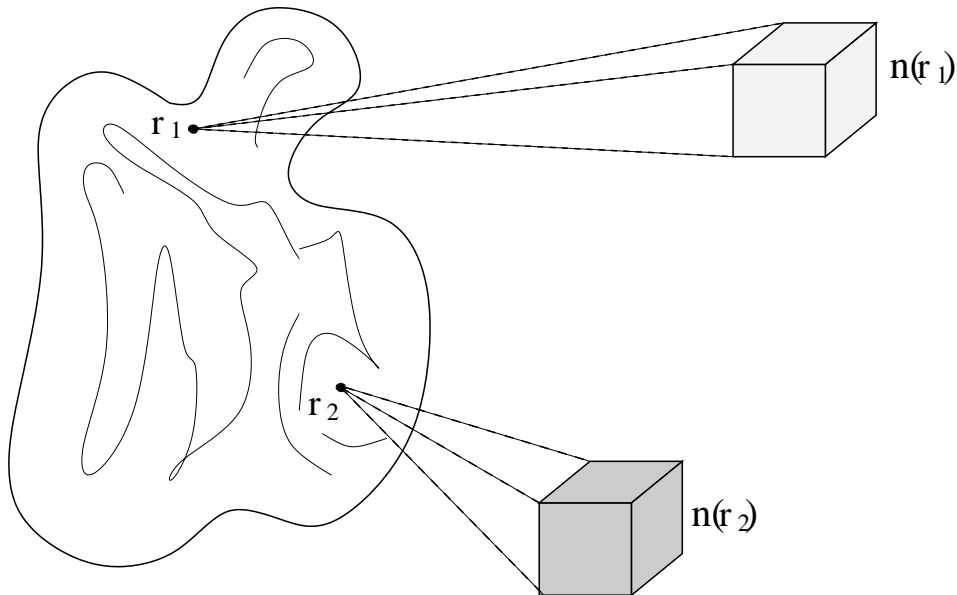
Figure 3.1: Schematic representation of the local density approximation. $v_{xc}(\vec{r_1}) = v_{xc}[n(\vec{r_1})]$ and $v_{xc}(\vec{r_2}) = v_{xc}[n(\vec{r_2})]$.

energy of a system by the exchange-correlation energy associated with a homogeneous electron gas of the same density. The homogeneous gas is the only system for which the form of the exchange-correlation energy is known precisely.

The LDA is only dependent on the local density, and the total energy is commonly written as,

$$E_{xc}^{LDA}[n(\vec{r})] = \int d^3\vec{r}\, n(\vec{r})\varepsilon_{xc}^{hom}(\vec{r}) \tag{3.27}$$

where $\varepsilon_{xc}^{hom}(\vec{r})$ is the exchange-correlation energy density corresponding to a homogeneous electron gas of density $n(\vec{r})$.

3.5.2 The Generalised Gradient Approximation (GGA)

Hohenberg and Kohn presumed that the LDA would be too simplistic to work for real systems and so proposed an extension to the LDA known as the gradient expansion approximation (GEA) [27]. The GEA is a series expansion of increasingly higher order density gradient terms. The first order form of the GEA was subsequently implemented and tested for atoms and molecules and was a complete failure. Despite the disappointing results, the GEA provided the basis for the generalised gradient approximation (GGA) which is currently the most popular exchange-correlation functional in condensed matter physics.

The vital steps that lead to the GGA were principally made by Perdew and co-workers [35] who devised a cutoff procedure that sharply terminates the GEA exchange-correlation hole in real-space using delta functions, in order to restore the sum rule and non-positivity

hole conditions. As a result of this procedure the GGA can be conveniently written in terms of an analytic function known as the enhancement factor, $F_{xc}[n(\vec{r}), \nabla n(\vec{r})]$, that directly modifies the LDA energy density,

$$E_{xc}^{GGA}[n(\vec{r})] \;\; = \;\; \int d^3\vec{r}\, n(\vec{r}) \varepsilon_{xc}^{hom}(\vec{r}) F_{xc}[n(\vec{r}), \nabla n(\vec{r})]. \qquad (3.28)$$

The development of gradient corrections, which actually improves the local functionals, has been following two different ideas. The idea primarily advocated by Becke ([36–42] is that "everything is legal". The argument here is that going away from the local density functionals, the true first principles or ab initio aspect is generally lost. One can therefore choose any functional for any reason, and the quality of the functional is then determined afterwards by actual application to physical systems. The idea of Becke stands in contrast to the idea primarily advocated by Perdew [43–50] that the development of exchange-correlation functionals should be based on basic principles derived from quantum mechanics. These basic principles can be scaling relations, correct limits for high and low densities, correct Local Spin Density Approximation limit for slowly varying densities as well as fulfilment of exact relations on the exchange and correlation holes.

Chapter 4

Technical aspects

4.1 MO-LCAO Method

To solve the Kohn-Sham equations (3.6) we use the MO-LCAO (Molecular Orbital – Linear Combination of Atomic Orbitals) method. Within this method we expand the molecular orbitals $\psi_i(\vec{r})$ in a series of symmetry-adapted orbitals (SO) $\chi_j(\vec{r})$

$$\psi_i(\vec{r}) = \sum_j c_{ji} \chi_j(\vec{r}) \, . \tag{4.1}$$

The SO's themselves are expanded in a series of atomic orbitals φ_ν

$$\chi_j(\vec{r}) = \sum_\nu d_{\nu j} \varphi_\nu(\vec{r}) \tag{4.2}$$

where the expansion coefficients $d_{\nu j}$ can be determined from Group theory [51]. Atomic orbitals are solutions of the atomic Kohn-Sham equation.

Inserting 4.1 in the equation 3.6 gives the matrix equation in the symmetry orbital representation

$$\underline{\underline{H}}\,\underline{c} \;=\; \underline{\underline{S}}\,\underline{c}\,\underline{\underline{\varepsilon}} \tag{4.3}$$

where $\underline{\underline{H}}$ and $\underline{\underline{S}}$ are the Fock and overlap matrices respectively, $\underline{c}$ is the coefficient-matrix, and $\underline{\underline{\varepsilon}}$ is the eigenvalue diagonal matrix.

According to the Group theory [51] both the Overlap-Matrix and Fock-Matrix have in the SO-representation a block structure. Due to this fact the matrix equation (4.3) is split up into g (number of irreducible representations of the symmetry group) independent systems of linear equations. The dimension of each of these sub-matrix-equations is smaller than the original matrix-equation (4.3). This reduces considerable the calculation time.

Another big advantage of the SO-representation is the possibility to reduce the number of integration points. In fact the SO have already the symmetry properties of the molecular system and therefore only the so called symmetry points are requiread for the calculation of the matrix elements. Depending on the symmetry of the system the difference could be up to factor 10 what again reduces the total calculation time.

4.2 Calculation of the Hartree potential

One important aspect in connection with the computation of the total energy is the calculation of the Hartree energy (3.5) via the Hartree potential (3.8). The evaluation of $\mathcal{V}_H(\vec{r})$ on the foundation of 3.8 would be too time consuming for the implied three-dimensional integration.

4.2.1 The model density

Several suggestions have been made to obviate this impediment. The basic idea is to introduce an auxiliary density, $\tilde{\rho}(\vec{r})$ which fits the "true" density $\rho(\vec{r})$, and leads to a considerable simplification in calculating the Hartree potential. Thus

$$\rho(\vec{r}) = \tilde{\rho}(\vec{r}) + \Delta\rho(\vec{r}), \tag{4.4}$$

where the modelled density $\tilde{\rho}(\vec{r})$ is obtained by a multipolar expansion [52] over spherical harmonics $Y_l^m(\theta_k, \phi_k)$ and radial functions $F_k^j(r_k)$ centred on the atoms of the system.

$$\tilde{\rho}(\vec{r}) = \sum_{k=1}^{N_A}\sum_{j=1}^{M_k}\sum_{l=0}^{L_j}\sum_{m=-l}^{l} Q_{jm}^{kl} F_k^j(r_k)Y_l^m(\theta_k, \phi_k) \equiv \sum_{\nu} q_{\nu}\,\varphi_{\nu}. \tag{4.5}$$

Here k runs over all N_A atoms, and j over all basis functions on each centre k. The insertion of (4.5) into (3.8) gives corresponding approximate expression for the $\mathcal{V}_H(\vec{r})$

$$\tilde{\mathcal{V}}_H(\vec{r}) = \sum_{k=1}^{N_A}\sum_{j=1}^{M_k}\sum_{l=0}^{L_j}\sum_{m=-l}^{l} Q_{jm}^{kl} \int \frac{F_k^j(r_k')Y_l^m(\theta_k', \phi_k')}{|\vec{r}-\vec{r}'|}d^3\vec{r'}. \tag{4.6}$$

After the expansion of $1/|\vec{r}-\vec{r}'|$ in terms of Legendre polinoms,

$$\frac{1}{|\vec{r}-\vec{r}'|} = \begin{cases} \sum_{l'=0}^{\infty} \frac{r'^{l'}_k}{r^{l'+1}_k} P_{l'}(\cos\omega_k) & r_k > r_k', \\ \sum_{l'=0}^{\infty} \frac{r^{l'}_k}{r'^{l'+1}_k} P_{l'}(\cos\omega_k) & r_k < r_k' \end{cases} \tag{4.7}$$

and by putting them down through real spherical harmonics,

$$P_{l'}(\cos\omega_k) = \frac{4\pi}{2l'+1} \sum_{m'=-l'}^{l'} Y_{l'}^{m'}(\theta_k, \phi_k)Y_{l'}^{m'}(\theta_k', \phi_k'), \tag{4.8}$$

we will have

$$\frac{1}{|\vec{r}_k-\vec{r}'_k|} = \begin{cases} \sum_{l'=0}^{\infty} \frac{r'^{l'}_k}{r^{l'+1}_k} \frac{4\pi}{2l'+1} \sum_{m'=-l'}^{l'} Y_{l'}^{m'}(\theta_K, \phi_k)Y_{l'}^{m'}(\theta_k', \phi_k') & r_k > r_k', \\ \sum_{l'=0}^{\infty} \frac{r^{l'}_k}{r'^{l'+1}_k} \frac{4\pi}{2l'+1} \sum_{m'=-l'}^{l'} Y_{l'}^{m'}(\theta_k, \phi_k)Y_{l'}^{m'}(\theta_k', \phi_k') & r_k < r_k' \end{cases} \tag{4.9}$$

By introducing this expression in (4.6) and in view of the fact that

$$\int d\Omega_K' \, Y_l^m(\theta_K', \phi_K') \, Y_{l'}^{m'}(\theta_K', \phi_K') = \delta_{l\,l'}\, \delta_{m\,m'}, \tag{4.10}$$

one obtain for the approximate Hartree potential

$$\tilde{\mathcal{V}}_H(\vec{r}) = \sum_{k=1}^{N_A} \sum_{j=1}^{M_k} \sum_{l=0}^{L_j} \sum_{m=-l}^{l} Q_{jm}^{kl} \frac{4\pi}{2l+1} Y_l^m(\theta_k, \phi_k)$$

$$\times \left[\frac{1}{r_k^l} \int_0^{r_k^l} r'_k{}^l F_k^j(r'_k) dr'_k + \int_{r_k^l}^{\infty} \frac{1}{r_k^{l+1}} r'_k{}^l F_k^j(r'_k) dr'_k \right] \quad (4.11)$$

4.2.2   The least-square-fit of the molecular density

To determine the expansion coefficients q_ν a least–square–fit to the true density $\rho(\vec{r})$ is usually made of:

$$\int \left(\rho(\vec{r}) - \tilde{\rho}(\vec{r}) \right)^2 \, d^3\vec{r} = min \quad (4.12)$$

Alternatively the minimisation of the difference in the Hartree energy can also be utilised:

$$\int \int \frac{\left(\rho(\vec{r}) - \tilde{\rho}(\vec{r}) \right) \left(\rho(\vec{r}') - \tilde{\rho}(\vec{r}') \right)}{|\vec{r} - \vec{r}'|} \, d^3\vec{r} \, d^3\vec{r}' = min \quad (4.13)$$

$$\int \left(\rho(\vec{r}) - \sum_\nu q_\nu \, \varphi_\nu(\vec{r}) \right)^2 \, d^3\vec{r} = min \quad (4.14)$$

respectively

$$\int \int \frac{\left(\rho(\vec{r}) - \sum_\nu q_\nu \, \varphi_\nu(\vec{r}) \right) \left(\rho(\vec{r}') - \sum_\nu q_\nu \, \varphi_\nu(\vec{r}') \right)}{|\vec{r} - \vec{r}'|} \, d^3\vec{r} \, d^3\vec{r}' = min \quad (4.15)$$

The variation of (4.14) and (4.15) relations is made by the use of the Lagrange multipliers, with the supplementary conditions of multipole moment conservation. Thus one have the conservation of the monopol (charge)

$$\sum_\nu q_\nu \int \varphi_\nu \, d^3\vec{r} = Q \,,$$

dipole moment $\vec{d}$

$$\sum_\nu q_\nu \int x \, \varphi_\nu \, d^3\vec{r} = d_x \quad \sum_\nu q_\nu \int y \, \varphi_\nu \, d^3\vec{r} = d_y \quad \sum_\nu q_\nu \int z \, \varphi_\nu \, d^3\vec{r} = d_z$$

and quadrupole moment D_{ij}

$$\sum_\nu q_\nu \int x^2 \, \varphi_\nu \, d^3\vec{r} = D_{xx} \quad \sum_\nu q_\nu \int x \, y \, \varphi_\nu \, d^3\vec{r} = D_{xy} \quad \sum_\nu q_\nu \int y^2 \, \varphi_\nu \, d^3\vec{r} = D_{yy}$$

$$\sum_\nu q_\nu \int (xz + yz) \, \varphi_\nu \, d^3\vec{r} = D_{xz} + D_{yz} \quad \sum_\nu q_\nu \int z^2 \, \varphi_\nu \, d^3\vec{r} = D_{zz} \quad (4.16)$$

$$\underline{\underline{A}} \, \underline{x} = \underline{b} \,, \quad (4.17)$$

4.3   Frozen-Core Approximation

In the last two decades the development in the computer industry follows Moore's Law: both the amount of memory and the speed of a CPU (Central Processor Unit) are doubled every 1.5 years. Due to this development it is possible nowadays to calculate big systems with several hundreds of light atoms or systems with up to 100 heavy or very heavy atoms. However even on fast computers such calculations take weeks and months.

The requirement on the CPU time and memory for solving the Kohn-Sham equations 3.25 grows with the square of the number of atomic basis functions. For heavy elements this number grows very rapidly due to the large number of electrons in such atoms. On the other hand if one is only interested on chemical properties the inner-shell electrons do not contribute to the chemical binding. This means that these orbitals can be kept fixed (frozen) during the solution of the Kohn-Sham equations. This approximation is called the frozen–core approximation. It allows to keep the number of valence molecular orbitals small which drastically, at least for heavy systems, reduces the calculation time.

4.3.1   Molecular orbitals in frozen-core approximation

In section 4.1 we discussed the MO-LCAO method and saw which advantages the SO-representation of the overlap- and Fock-matrix has. In order to keep these very important properties we have in general not to freeze the atomic orbitals but the symmetry orbitals which are of course only linear combinations of the last ones. We devide the symmetry orbitals of each symmetry block in two parts: the core part ψ_c with orthonormal SO's[1] and the valence part ψ_v to which all other SO's belong. The overlap matrix reads

$$\underline{\underline{S}} = \begin{pmatrix} S_{cc} & S_{cv} \\ S_{vc} & S_{vv} \end{pmatrix}. \tag{4.18}$$

In order to eliminate the core parts in the valence part of the Hilbert-space we orthogonalize the valence orbitals to the core orbitals and get new valence SO's

$$\psi_v = \tilde{\psi}_v - S_{vc}S_{cc}^{-1}\tilde{\psi}_c \tag{4.19}$$

In this new basis the overlap matrix has the form

$$\underline{\underline{S}} = \begin{pmatrix} 1 & 0 \\ 0 & S_{vv} \end{pmatrix}. \tag{4.20}$$

and the Fock-matrix can be written in the form

$$\underline{\underline{H}} = \begin{pmatrix} H_{cc} & 0 \\ 0 & 0 \end{pmatrix} + \begin{pmatrix} 0 & 0 \\ 0 & H_{vv} \end{pmatrix} + \begin{pmatrix} 0 & H_{cv} \\ H_{vc} & H_{vv} \end{pmatrix}. \tag{4.21}$$

---

[1]Atomic orbitals of any atom are already orthonormal to each other. The orthonormality of all frozen core SO's means that core orbitals of different atoms do not overlap.

The last part of the Fock-matrix (off-diagonal elements) is due to an appropriate choice of the core orbitals quite small and can be neglected. In this case the secular equation for each symmetry block splits up in two sub-systems. The sub-system describing the core part is very simple and can be very easy calculated. On the other hand if one is interested only on bond length and bond distances then this can be neglected; however it can even be larger than the valence part.

4.3.2 Calculation of the total energy in frozen-core approximation

We saw above that the molecular orbitals in the frozen-core approximation can be written in the form

$$
\psi_i = \begin{cases}
\psi_i^c = \chi_i \equiv \sum_{K=1}^{N_A} \sum_{\mu=1}^{N_K^c} d_{\mu i}^K \varphi_\mu^K & i = 1, ..., M^c, \\
\psi_i^v = \tilde{\psi}_v - S_{vc} S_{cc}^{-1} \tilde{\psi}_c & i = M^c + 1, ..., M'.
\end{cases}
\tag{4.22}
$$

where M^c is the total number of frozen SO's. The electronic density build from these MO's has the form

$$
\rho(\vec{r}) = \sum_{i=1}^{M^c} n_i^c \chi_i^+ \chi_i + \sum_{i=M^c+1}^{M'} n_i^v (\psi_i^v)^+ \psi_i^v \equiv \rho_c + \rho_v
\tag{4.23}
$$

The atomic basis functions φ_μ^K are solutions of the atomic Kohn-Sham-equation

$$
\left(\hat{t} + {}^K\hat{V}^N + {}^K\hat{V}^C + {}^K\hat{V}^{ex} \right) \varphi_\mu^K(\vec{\xi}) = \epsilon_\mu^K \varphi_\mu^K(\vec{\xi}).
\tag{4.24}
$$

If we add and substract to the total energy (3.19) the eigenvalues of the frozen symmetry orbitals then we can write it in the form

$$
\begin{aligned}
E =\ & \sum_{i=1}^{M^c} n_i^c \left(\sum_{K'=1}^{N_A} \sum_{\nu=1}^{N_{K'}^c} \sum_{K=1}^{N_A} \sum_{\mu=1}^{N_K^c} \frac{1}{2} \left(\epsilon_\nu^{K'} + \epsilon_\mu^K \right) d_{i\nu}^{*K'} d_{\mu i}^K \left\langle \varphi_\nu^{K'} | \varphi_\mu^K \right\rangle \right) \\
& + \left[\sum_{i=1}^{M^c} n_i^c \left(\epsilon_i - \sum_{K'=1}^{N_A} \sum_{\nu=1}^{N_{K'}^c} \sum_{K=1}^{N_A} \sum_{\mu=1}^{N_K^c} \frac{1}{2} \left(\epsilon_\nu^{K'} + \epsilon_\mu^K \right) d_{i\nu}^{*K'} d_{\mu i}^K \left\langle \varphi_\nu^{K'} | \varphi_\mu^K \right\rangle \right) \right] \\
& + \sum_{i=M^c+1}^{M'} n_i^v \epsilon_i - \frac{1}{2} \int \left(V_c^C + V_v^C \right) (\rho_c + \rho_v)\ d^3\vec{r} - \int V^{ex} \rho\ d^3\vec{r} + E^{xc}.
\end{aligned}
\tag{4.25}
$$

This equation can also be written in the form

$$
\begin{aligned}
E =\ & \sum_{i=1}^{M^c} n_i^c \left(\sum_{K'=1}^{N_A} \sum_{\nu=1}^{N_{K'}^c} \sum_{K=1}^{N_A} \sum_{\mu=1}^{N_K^c} \frac{1}{2} \left(\epsilon_\nu^{K'} + \epsilon_\mu^K \right) d_{i\nu}^{*K'} d_{\mu i}^K \left\langle \varphi_\nu^{K'} \middle| \varphi_\mu^K \right\rangle \right) \\
& + \int V^N \rho_c\, d^3\vec{r} + \frac{1}{2} \int V_c^C \rho_c\, d^3\vec{r} \\
& - \sum_{i=1}^{M^c} n_i^c \left(\sum_{K'=1}^{N_A} \sum_{\nu=1}^{N_{K'}^c} \sum_{K=1}^{N_A} \sum_{\mu=1}^{N_K^c} d_{i\nu}^{*K'} d_{\mu i}^K \int \frac{1}{2} \left({}^{K'}\hat{V}^N + {}^{K}\hat{V}^N \right) \varphi_\nu^+ \varphi_\mu\, d^3\vec{r} \right) \\
& - \sum_{i=1}^{M^c} n_i^c \left(\sum_{K'=1}^{N_A} \sum_{\nu=1}^{N_{K'}^c} \sum_{K=1}^{N_A} \sum_{\mu=1}^{N_K^c} d_{i\nu}^{*K'} d_{\mu i}^K \int \frac{1}{2} \left({}^{K'}\hat{V}^C + {}^{K}\hat{V}^C \right) \varphi_\nu^+ \varphi_\mu\, d^3\vec{r} \right) \\
& - \sum_{i=1}^{M^c} n_i^c \left(\sum_{K'=1}^{N_A} \sum_{\nu=1}^{N_{K'}^c} \sum_{K=1}^{N_A} \sum_{\mu=1}^{N_K^c} d_{i\nu}^{*K'} d_{\mu i}^K \int \frac{1}{2} \left({}^{K'}\hat{V}^{ex} + {}^{K}\hat{V}^{ex} \right) \varphi_\nu^+ \varphi_\mu\, d^3\vec{r} \right) \\
& + \sum_{i=M^c+1}^{M'} n_i^v \epsilon_i - \frac{1}{2} \int V_v^C \rho_v\, d^3\vec{r} - \int V^{ex} \rho_v\, d^3\vec{r} + E^{xc} .
\end{aligned}
\tag{4.26}
$$

According to our definition of frozen-core SO's given above the frozen atomic orbitals are ortho-normal to each other

$$
\left\langle \varphi_\mu^{K'} \middle| \varphi_\nu^K \right\rangle = \delta_{\mu\nu} \delta_{K'K} .
\tag{4.27}
$$

We introduce the atomic frozen-core densities

$$
\rho_c^K = \sum_{i=1}^{M^c} n_i^c \sum_{\mu=1}^{N_K^c} \left| d_{i\mu}^K \right|^2 \rho_\mu^K = \sum_{\mu=1}^{N_K^c} n_K^{c\mu} \rho_{c\mu}^K ,
\tag{4.28}
$$

where $n_K^{c\mu}$ are the atomic occupation numbers $n_K^{c\mu} = \sum_{i=1}^{M^c} n_i^c \left| d_{i\mu}^K \right|^2$. The nuclear potential $V^N = \sum_{K=1}^{N_A} {}^K V^N$ and according to eqn. (4.27) the core density becomes $\rho_c = \sum_{K=1}^{N_A} \rho_c^K$ and the core Hartree potential takes the form $V_c^C = \sum_{K=1}^{N_A} {}^K V_c^C$. Inserting this equations in (3.19) we get

$$
\begin{aligned}
E =\ & \sum_{K=1}^{N_A} \sum_{\mu=1}^{N_K^c} n_K^{c\mu} \epsilon_\mu^K + \sum_{K=1}^{N_A} \sum_{K' \neq K}^{N_A} \int {}^K V^N \rho_c^{K'}\, d^3\vec{r} + \frac{1}{2} \sum_{K=1}^{N_A} \sum_{K' \neq K}^{N_A} \int {}^K V_c^C \rho_c^{K'}\, d^3\vec{r} \\
& - \frac{1}{2} \sum_{K=1}^{N_A} \int {}^K V^C \rho_c^K\, d^3\vec{r} - \sum_{K=1}^{N_A} \int {}^K V_v^C \rho_c^K\, d^3\vec{r} - \sum_{K=1}^{N_A} \int {}^K V^{ex} \rho_c^K\, d^3\vec{r} \\
& + \sum_{i=M^c+1}^{M'} n_i^v \epsilon_i - \frac{1}{2} \int V_v^C \rho_v\, d^3\vec{r} - \int V^{ex} \rho_v\, d^3\vec{r} + E^{xc} .
\end{aligned}
\tag{4.29}
$$

In most cases the internal structure of the frozen-core part in the equation can be neglegted and the atomic cores considered as point charges centered on the nuclei. In this

case the core density has the form $\rho_c^{K'}(\xi_K) = \frac{n_K^c}{4\pi\xi_K}\delta(\xi_K - R_K + R_{K'})$. Inserting this equation in (4.29) we get for the total energy in the frozen-core approximation

$$
\begin{aligned}
E &= \sum_{K=1}^{N_A}\sum_{\mu=1}^{N_K^c} n_K^{c\,\mu}\,\epsilon_\mu^K \;-\; \sum_{K=1}^{N_A}\sum_{K'\neq K}^{N_A}\frac{Z_K\,n_{K'}^c}{|\vec{R}_K - \vec{R}_{K'}|} + \frac{1}{2}\sum_{K=1}^{N_A}\sum_{K'\neq K}^{N_A}\frac{n_K^c\,n_{K'}^c}{|\vec{R}_K - \vec{R}_{K'}|} \\
&\quad -\; \frac{1}{2}\sum_{K=1}^{N_A}\int {}^K V_c^C \rho_c^K \; d^3\vec{r} - \sum_{K=1}^{N_A}\int {}^K V_v^C \rho_c^K \; d^3\vec{r} - \sum_{K=1}^{N_A}\int {}^K V^{ex}\rho_c^K \; d^3\vec{r} \\
&\quad +\; \sum_{i=M^c+1}^{M'} n_i^v\,\epsilon_i - \frac{1}{2}\int V_v^C \rho_v \; d^3\vec{r} - \int V^{ex}\rho_v \; d^3\vec{r} + E^{xc}
\end{aligned}
\tag{4.30}
$$

Here $n_K^c = \sum_{\mu=1}^{N_K^c} n_K^{c\,\mu}$ is the frozen-core charge of the atom K.

4.4   Mulliken analyses, DOS and COOP

To analyse the chemical bonding it is convenient to present the molecular electron density as a sum of the atomic densities of the orbitals j, centred on different atoms. In the MO–LCAO method, the molecular orbitals are taken as linear combination of atomic orbitals

$$
\psi_i \;=\; \sum_j b_{ji}\varphi_j,
\tag{4.31}
$$

where j runs over all AO's. The total electronic density can consequently be expressed as follows

$$
\rho(\vec{r}) = \sum_{i=1}^{N}\psi_i^+(\vec{r})\psi_i(\vec{r}) = \sum_{i=1}^{N}\sum_j\sum_k b_{ij}^* b_{ki}\varphi_j^+\varphi_k
\tag{4.32}
$$

The total number of electrons in the system is

$$
\int \rho(\vec{r})d^3\vec{r} = \sum_{i=1}^{N}\sum_j\sum_k b_{ij}^* b_{ki}\int \varphi_j^+\varphi_k d^3\vec{r},
\tag{4.33}
$$

which gives,

$$
N = \sum_{i=1}^{N} N(i) = \sum_{i=1}^{N}\left[\sum_j b_{ij}^*\left(b_{ji} + \sum_{k\neq j} b_{ki}S_{jk}\right)\right],
\tag{4.34}
$$

where S_{jk} is the atomic overlap matrix.

The expression in square bracket in the right–hand side of this equation is called in the literature the net population of the molecular orbital ψ_i:

$$N(i) = \sum_j b_{ij}^* \left(b_{ji} + \sum_{k \neq j} b_{ki} S_{jk} \right). \tag{4.35}$$

The sum runs over all the atomic orbitals, thus the contribution from a given atomic orbitals φ_j to the MO ψ_i will be

$$N(i,j) = b_{ij}^* \left(b_{ji} + \sum_{k \neq j} b_{ki} S_{jk} \right). \tag{4.36}$$

The term $|b_{ij}|^2$ originates from the atomic orbital φ_j, while the second one, $\sum_{k \neq j} b_{ij}^* b_{ki} S_{jk}$, comes from the overlap between the atomic orbitals j and k. This later quantity, called overlap population, is associated with interaction, and is connected to the bond order. According to Mulliken, when two orbitals overlap, the term $b_j^* b_k S_{jk} + b_k^* b_j S_{kj}$ is "democratic" divided to the AO contribution of φ_j and φ_k. Summation over all MOs provides the total population of φ_j:

$$\mathcal{N}(j) = \sum_{i=1}^{N} N(i,j). \tag{4.37}$$

The effective transfer of charge from/to the φ_j is given by

$$q(j) = \mathcal{N}_0(j) - \mathcal{N}(j) \tag{4.38}$$

where $N_0(j)$ is the number of electrons in φ_j in the neutral isolated atom.

The net number of electrons associated with a given atom in the molecule are obtained by summing over all basis functions j_A centred on atom A, and the effective charge of that atom will be

$$q(A) = Z_A - \sum_{j_A} q(j_A) = \sum_{j_A} \mathcal{N}(j). \tag{4.39}$$

Another interpretative tool is given by the Density Of States (DOS), defined as the number of orbitals per unit energy range $\frac{dN}{d\epsilon}$.

$DOS(\epsilon)d\epsilon$ is equal to the number of levels in the energy interval ϵ and $\epsilon + d\epsilon$. The above decomposition of the molecular electron density allows to divide up the DOS among atoms. The integral of these projections up to the Fermi level gives then the total electron density on a given atom or in a specific orbital (PDOS, Partial Density Of States).

A bond indicator for a molecule, can be defined on the base of the overlap population defined above, by summing $b_j^* b_k S_{jk}$ over all orbitals in the atoms, over all occupied MOs. This quantity is called COOP, which stands for Cristal Orbital Overlap Population.

This gives information about the bonding (with positive contribution $b_j^* b_k S_{jk}$) and anti-bonding (negative). The amplitudes in the COOP curves depend on the number of states in that energy interval, the magnitude of the coupling overlap, and the size of the coefficients in the MOs.

The DOS and COOP can be seen as differential versions of electronic occupation and bond order indices in crystal. The integral of DOS to the Fermi level gives the total number of electrons, and that of the COOP curve gives the total overlap population, which is connected with the bond order.

4.5 Optimization of the atomic basis functions

Of great importance in molecular calculations is the basis which is used for the expansion of the molecular orbitals. The basis which we use is an optimised one, that consists of two parts, a minimal basis set and an extended basis. The former consists of all occupied four-component wave functions of the neutral atoms. As an example, for Au it contains the $1s_{1/2}$ to $6s_{1/2}$ orbitals. The optimisation procedure implies dimer calculations and implies the next steps:

- The total energy curve for the dimer of the species to be considered is determined for the minimal basis. In general a clear minimum is observed at a certain distance, corresponding to the bond length of the molecule.

- Basis functions of the next sub–shell from a calculation of an atom with a certain degree of ionisation (we use non-integer occupation numbers) are added and the total energy of the dimer at a fixed internuclear distance (corresponding to the minimum in the previous step) is recalculated. Next, the total energy of the system is minimised as function of the degree of ionisation.

- Further, the partial occupation numbers for these two basis sets is fixed and additional basis functions of the next sub–shell are optimised in the same way as before. This procedure is continued until the change in the total energy by further increase of the number of basis functions is smaller than a chosen value.

The degree of ionisation lies typical in the range from 0 to a few degrees of ionisation [53]. At last the potential energy curve is determined but using the optimised basis. As a result, the binding energy and the bond length can be compared with the corresponding experimental values.

Chapter 5

Adsorption on metal surfaces

In the last years, the methods to calculate of adsorption were intensively developed. Nowadays, it reaches a level where it is possible to calculate adsorption energies, as well as the electronic and atomic structure of medium–sized systems with predictive accuracy. Adsorption phenomena are commonly classified, according to the value of the binding energy, in two classes:

- the domain of *physisorption* corresponding to "small" binding energies,

- and the domain of *chemisorption* corresponding to "large" binding or adsorption energies.

In the first case, the substrate–adsorbate interactions are mainly due to Van der Waals forces and involve almost no mixing between the orbitals of the adsorbate and the substrate. The adsorption energy is typically less than 0.3 eV per adsorbed particle (6.9 kcal mol^{-1}). For chemisorption systems there is a further classification of the nature of the binding in: covalent, metallic and ionic. This is based on survey of electronic, electrical, vibrational, and thermal properties. The adsorption theory can be approached from three complementary points of view:

- the macroscopic or thermodynamical approach, used to derive relations between the properties of the system at equilibrium;

- the microscopic approach in which the principles of quantum mechanics are used to compute various physical quantities describing the substrate–absorbate interactions;

- and the methods of statistical mechanics, which establish the connection between macroscopic and microscopic quantities and relates the two previous approaches.

In the case which we are interested in this work is the adsorption of the elements of interest which are studied in a gas-phase thermochromatography column. Models for

adsorption equilibria of reversible mobile adsorption [54,55] (without any superimposed chemical reaction) show that the following equation holds:

$$\frac{a \cdot t_r \cdot V_0}{s \cdot T_{dep} \cdot \frac{V}{100 \cdot A}} = \left(\frac{R \cdot T_0}{-\Delta H^0_{ads}} \right) \cdot exp \left(\frac{-\Delta H^0_{ads}}{R \cdot T_{dep}} \right) \cdot exp \left(\frac{-\Delta S^0_{ads}}{R} \right), \qquad (5.1)$$

where the parameter a describes the variation of the temperature along the chromatography column (approximated to be linear): $T = T_s - a \cdot y$. The additional parameters s and t_r are the partition coefficient for the solid phase and the retention time, which for a short-lived radioactive species is calculated as the radioactive lifetime of the nuclide:

$$t_r = \frac{T_{1/2}}{ln(2)}$$

or equals the duration of the experiment for a long-lived species.

Thus, the deposition temperature T_{dep} and the adsorption enthalpy ΔH^0_{ads} of the process are combined and can be easily determined from each other. This stresses the importance of our theoretical calculations of the adsorption energy of element 112. The evaluation of this quantity is used to predict the adsorption temperature in the thermochromatographic column, on the base of relation 5.1

Adsorption of atoms and molecules has been extensively studied using a different theoretical methods. Initially, mainly theoretical approaches applicable to semi-infinite systems were used. In the last decade the cluster and embedded cluster methods proved their utility in the treatement of this phenomenon. These releaved that the adsorption is both a geometric and energetically local phenomenon. It has been found that the strength of the chemisorption bond is directly related to the width of the energy region of the substrate local density of states that is probed. This can be understood by considering the strength of the interaction to be proportional with an overlap term and inversely proportional to ΔE. The influence of the details of the surface electronic structure to the chemisorption bond is found to decrease with the ratio of the adsorbate-surface interaction strength to the metal-metal interaction strength. From later work ([56]) it has followed that this ratio fluctuates around the value of one, which constitutes the intermidiate binding limit. In the case of Hg on a Au surface this ratio is below one therefore we expect that the calculation of the adsorption properties to be sensible to the local density of states of the clusters which model the surface. The fact that the details of the surface electronic structure are essential for the chemisorption bond only on a relativley small scale compared with the overall surface density of states, can be the reason for the succes of the analysis of the chemisorption phenomenon by means of the cluster approach. An appealing aspect of this conceptually simple strategy for tackling such a complicated problem consists in the possibility to use the entire wealth of methods and interpretative tools of quantum chemistry available in the treatment of chemisorption.

5.1 Cluster method

The cluster–model approach has proven very useful for theoretical investigations of local defects in solids (such as vacancies or adsorption of atoms or molecules). The use of a this kind of model rests on the assumption that the adsorption is an local phenomenon. As already mentioned above, treating the surface as a molecule allows an analysis of the chemical bond by mean of the orbital overlap population. To probe the electronic interaction one has to look to the occupation of bonding and antibonding orbital fragments, these fragments being conveniently defined as adsorbate and substrate separately by means of the orbital overlap population. The occupation of binding orbital fragments results in an attractive contribution to chemical bond. On the other side, the occupation of antibonding orbital fragments results in a bond weakening or a repulsive interaction. The relative stability of atoms (or molecules) adsorbed in different adsorption sites depends on both the occupation of bonding orbitals and that of antibonding orbitals.

It has been shown that the population of bonding orbital fragments tends to favour bonding to high coordination sites (i.e. for our systems in the hollow position). Population of antibonding orbitals leads to repulsive interactions that tend to become minimized in low coordination sites (top position). The final preference is controlled by the balance of these two opposing "forces". Bond formation between the adsorbate and cluster tends to result in a weakening of the substrate metal-metal bonds between atoms to which the adsorbate coordinate. This may results in a displacement of the metal-subtrate atoms and a reconstruction of the surface.

Results may converge slowly with cluster size. Several contributing factors can be mentioned:

- When one particular surface is modeled, the geometry of the surface-metal atoms interacting with the adsorbate has to be the same to at least the first coordination shell. Thus, at a (100) surface of a face centered cubic metal, surface atoms have eight metal-atom neighbours. Four of them are in the plane and four are located in the second layer. Clusters modelling chemisorption atop such a surface atom in a (100) surface should include at least these eight metal-atom neighbours.

- There is another difficulty that arises, even when the first coordination shell of the surface-metal atom is fully included in the cluster model. On a real surface, the surface metal atoms have a lower number of neighbours than bulk atoms do. However, in the nine atoms metal cluster mentioned above, the central atom has eight neighbours, but these neighbour atoms share only four or five neighbour atoms amongst themselves. These reversal from the real surface situation leads to significantly different electron-distribution relative to that of a true surface atom.

- Another deficiency of this method is given by the discrete substrate density of states, due to the finite number of atoms included in the cluster model. Therefore,
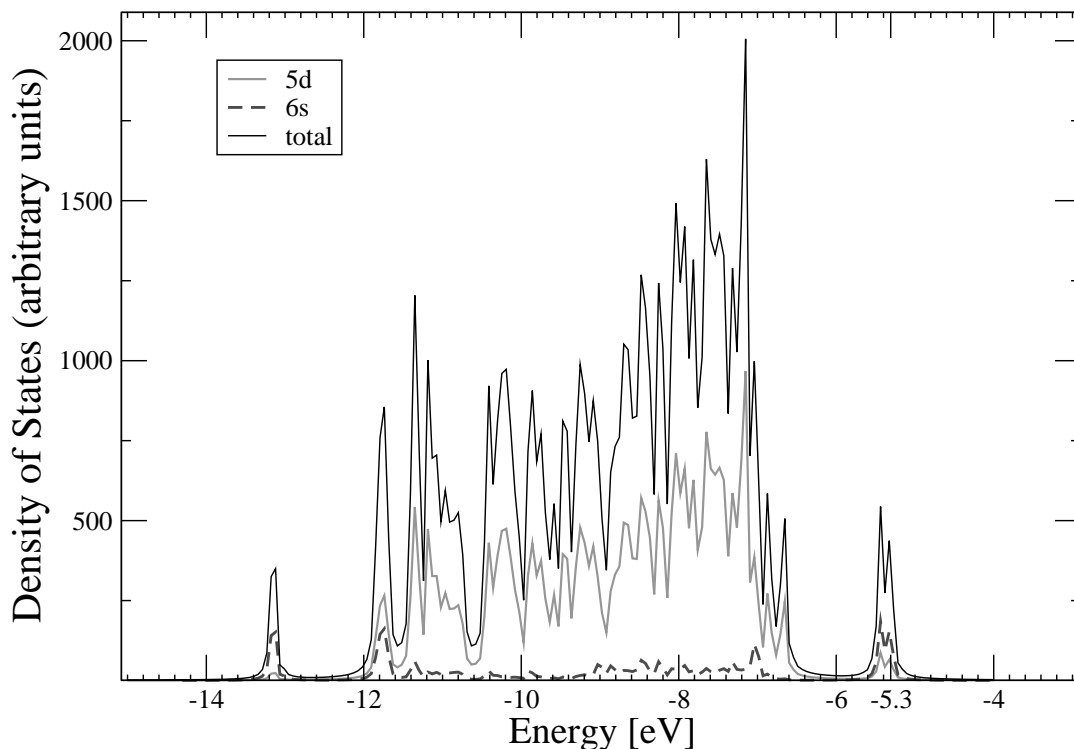
Figure 5.1: The total density of states for a Au$_{14}$ cluster (black line) and the corresponding 5d (grey line) and 6s (dashed line) differential density of states. The Fermi level, situated at -5.3 eV, is indicated along the energy axis.

one important requirement is that the number of atoms included in the cluster should be big enough to ensure bands formation. The large number of d-aotmic levels in a cluster results rapidly in a d-molecular orbital valence electron band, with very small orbital energy differences resembling the continuum of the bulk d-valence electron density. The situation is different for the molecular orbitals of predominantly $s-p$ character since there are fewer $s-p$ states, which additionally are more spread in energy. For these, the convergence to a continuous bulk valence band is slow. Figure 5.1 shows the total DOS of a Au$_{14}$(9,5,1) cluster, together with the 5d and 6s projected density of states.

5.2 Cluster-Embedding method

In section 5.1 the cluster method was presented. There it was shown that this method works quit well for describing adsorbtion phenomena. However the disadvantage of this method is the big number of atoms which should be included in such calculations. This makes this method often inapplicable. To avoid this kind of problems a so called Cluster-embedding method was developed [57] in our group. It was applied to several systems [57, 58] and gives reasonable results.

Lets consider a system with N nuclei and M electrons. The total energy of this system

(3.19) is

$$E = \sum_{i=1}^{M} n_i \langle \psi_i \,|\, \hat{t} \,|\, \psi_i \rangle + \int V^N \rho \, d^3 \vec{r} + \frac{1}{2} \int V^H \rho \, d^3 \vec{r} + E^{xc}[\rho] + \frac{1}{2} \sum_{K=1}^{N} \sum_{K' \neq K}^{N} \frac{Z_{K'} Z_K}{|\vec{R}_{K'} - \vec{R}_K|} \quad (5.2)$$

where the density

$$\rho(\vec{r}) = \sum_{i=1}^{M} n_i \, \tilde{\psi}_i^+(\vec{r}) \tilde{\psi}_i(\vec{r}) \tag{5.3}$$

is build from the solutions of the Kohn-Sham equation

$$\left(\hat{t} + \hat{V}^N + \hat{V}^H + \hat{V}^{xc} \right) \tilde{\psi}_i(\vec{r}) = \epsilon_i \tilde{\psi}_i(\vec{r}). \tag{5.4}$$

There are the equations (3.19), (3.21) and (3.25) without taking in the account the magnetic density contribution. Here n_i are the occupation numbers of the MO's. We divide this system in two parts which we will call cluster and environment. The cluster contains N^{Cl} nuclei and M^{Cl} electrons the rest of the nuclei $N^{Env} = N - N^{Cl}$ and $M^{Env} = M - M^{Cl}$ electrons belong to the environment. Now we have to divide the density of the system in two parts. It is clear that we cannot do this using the solutions of the Kohn-Sham equation (5.4) because the are strongly de-localized. Fortunately it can be shown that there exists a set of orthonormal functions ψ_i which allows us to do this derivation.

The density in this basis has the form

$$\rho \equiv \sum_{i=1}^{M} n_i \, \tilde{\psi}_i^+(\vec{r}) \tilde{\psi}_i(\vec{r}) = \sum_{i=1}^{M^{Cl}} n_i^{Cl} \, \psi_i^{Cl+}(\vec{r}) \psi_i^{Cl}(\vec{r}) + \sum_{i=M^{Cl}+1}^{M} n_i \, \psi_i^{Cl+}(\vec{r}) \psi_i^{Cl}(\vec{r}) \equiv$$
$$\equiv \rho^{Cl} + \rho^{Env} \tag{5.5}$$

Inserting this equation in (5.2) leads to

$$E^{tot} = \sum_{i=1}^{M^{Cl}} n_i^{Cl} \langle \psi_i^{Cl} \,|\, \hat{t} \,|\, \psi_i^{Cl} \rangle + \int V^N \rho^{Cl} \, d^3 \vec{r} + \frac{1}{2} \int V^C \rho^{Cl} \, d^3 \vec{r} + E^{xc} + \frac{1}{2} \sum_{K=1}^{N^{Cl}} \sum_{K' \neq K}^{N^{Cl}} \frac{Z_{K'} Z_K}{|\vec{R}_{K'} - \vec{R}_K|}$$
$$+ \sum_{i=1}^{M^{Env}} n_i^{Env} \langle \psi_i^{Env} \,|\, \hat{t} \,|\, \psi_i^{Env} \rangle + \int V^N \rho^{Env} \, d^3 \vec{r} + \frac{1}{2} \int V^C \rho^{Env} \, d^3 \vec{r} + \frac{1}{2} \sum_{K=1}^{N^{Env}} \sum_{K' \neq K}^{N^{Env}} \frac{Z_{K'} Z_K}{|\vec{R}_{K'} - \vec{R}_K|}$$
$$+ \sum_{K=1}^{N^{Cl}} \sum_{K'=1}^{N^{Env}} \frac{Z_{K'} Z_K}{|\vec{R}_{K'} - \vec{R}_K|} \tag{5.6}$$

The Hartree energy is linear in the density and can be written in the form

$$V^C \equiv V^C(\rho) = V^C(\rho^{Cl}) + V^C(\rho^{Env}) \equiv V_{Cl}^C + V_{Env}^C. \tag{5.7}$$

Inserting this equation in (5.6) leads to

$$
E^{tot} = \sum_{i=1}^{M^{Cl}} n_i^{Cl} \left\langle \psi_i^{Cl} \right| \hat{t} \left| \psi_i^{Cl} \right\rangle + \int V^N \rho^{Cl} \, d^3\vec{r} + \frac{1}{2} \int V_{Cl}^C \, \rho^{Cl} \, d^3\vec{r} + E^{xc} + \frac{1}{2} \sum_{K=1}^{N^{Cl}} \sum_{K' \neq K}^{N^{Cl}} \frac{Z_{K'} Z_K}{|\vec{R}_{K'} - \vec{R}_K|}
$$

$$
+ \sum_{i=1}^{M^{Env}} n_i^{Env} \left\langle \psi_i^{Env} \right| \hat{t} \left| \psi_i^{Env} \right\rangle + \int V_{Env}^N \rho^{Env} \, d^3\vec{r} + \frac{1}{2} \int V_{Env}^C \, \rho^{Env} \, d^3\vec{r} + \frac{1}{2} \sum_{K=1}^{N^{Env}} \sum_{K' \neq K}^{N^{Env}} \frac{Z_{K'} Z_K}{|\vec{R}_{K'} - \vec{R}_K|}
$$

$$
+ \int V_{Cl}^N \rho^{Env} \, d^3\vec{r} - \int V_{Cl}^C \rho^{Env} \, d^3\vec{r} + \sum_{K=1}^{N^{Cl}} \sum_{K'=1}^{N^{Env}} \frac{Z_{K'} Z_K}{|\vec{R}_{K'} - \vec{R}_K|} \qquad (5.8)
$$

In order to derive an equation for the cluster orbitals we hold in the total energy functional (5.8) the environment orbitals fixed and vary the cluster orbitals only. This procedure leads to the Kohn-Sham equation in the cluster embedding method

$$
\left(\hat{t} + \hat{V}_{Cl}^N + \hat{V}_{Cl}^C + \hat{V}^{xc}(\rho) + \hat{V}^{Ext} \right) \psi_i^{Cl}(\vec{r}) = \epsilon_i^{Cl} \psi_i^{Cl}(\vec{r}). \qquad (5.9)
$$

where $\hat{V}^{Ext} = \hat{V}_{Env}^N + \hat{V}_{Env}^C$ is the external potential. This equation contains one additional term V^{Ext} in comparison to a similar equation in cluster method (3.17). A further difference is the exchange-correlation potential which depends not only from the density in the cluster but from the total density. These two terms contain the whole information about the environment. The total energy can thus be written as

$$
E^{tot} = \sum_{i=1}^{M^{Cl}} n_i^{Cl} \left\langle \psi_i \right| \hat{t} \left| \psi_i \right\rangle + \int V_{Cl}^N \rho^{Cl} \, d^3\vec{r} + \frac{1}{2} \int V_{Cl}^C \, \rho^{Cl} \, d^3\vec{r} + E^{xc}(\rho) + \frac{1}{2} \sum_{K=1}^{N^{Cl}} \sum_{K' \neq K}^{N^{Cl}} \frac{Z_{K'} Z_K}{|\vec{R}_{K'} - \vec{R}_K|}
$$

$$
- \int V_{Cl}^C \rho^{Env} \, d^3\vec{r} + \sum_{K=1}^{N^{Cl}} \sum_{K'=1}^{N^{Env}} \frac{Z_{K'} Z_K}{|\vec{R}_{K'} - \vec{R}_K|} + E^{Env} \qquad (5.10)
$$

where

$$
E^{Env} = \sum_{i=1}^{M^{Env}} n_i^{Env} < \psi_i | \hat{t} | \psi_i > + \int V^N \, \rho^{Env} \, d^3\vec{r} + \int V^{xc} \, \rho^{Env} \, d^3\vec{r}
$$

$$
- \frac{1}{2} \int V_{Env}^C \, \rho^{Env} \, d^3\vec{r} + \frac{1}{2} \sum_{K=1}^{N^{Env}} \sum_{K' \neq K}^{N^{Env}} \frac{Z_{K'} Z_K}{|\vec{R}_{K'} - \vec{R}_K|} + \sum_{K=1}^{N^{Cl}} \sum_{K'=1}^{N^{Env}} \frac{Z_{K'} Z_K}{|\vec{R}_{K'} - \vec{R}_K|} \qquad (5.11)
$$

depends only on the density distribution in the environment.

5.2.1 Exchange-correlation energy in cluster embedding method

The equation (5.9) is not applicable for practical calculation because the exchange-correlation potential still depends on the total density of a molecular system. Due to the non-linearity of the xc-potential and xc-energy a simple deviation of the total density is not possible. Therefore we extended our model described in the previous section. A scheme of this model is presented in figure (5.2).
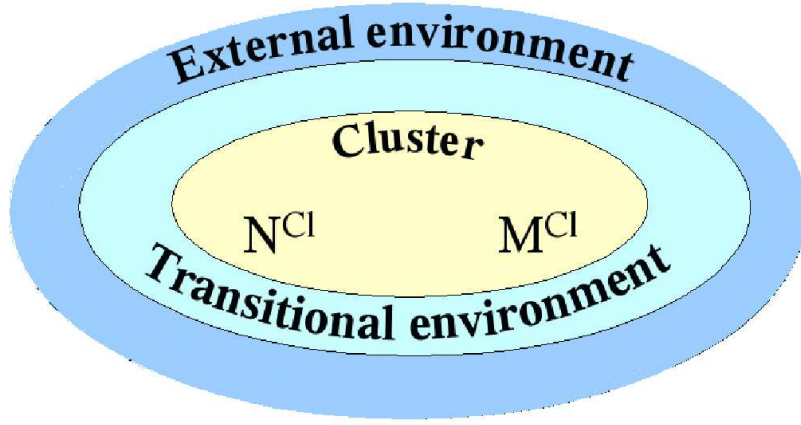
Figure 5.2: The system is divided in three parts which are treated differently: cluster, trans–environment and exterior–environment .

There we use the fact that if the wave functions of two electrons do not overlap then the exchange-correlation energy for these electrons is zero. We divide the environment in two parts: exterior- and trans-environment. The transitional–environment is chosen in such a way that wave functions from cluster and exterior environment do not overlap. We can now write the total environment density in the form

$$\rho^{Env} = \rho^E + \rho^T \tag{5.12}$$

The exchange-corelation potential in the equation (5.9) can be approximated by

$$V^{xc} \equiv V^{xc}(\rho^{Cl} + \rho^E + \rho^T) = V^{xc}(\rho^{Cl} + \rho^T) \equiv V^{xc}_{Cl} \tag{5.13}$$

and the exchange-correlation energy by $E^{xc}(\rho) = E^{xc}(\rho^{Cl} + \rho^T)$.

5.2.2 Choice of the environment density

In section 4.2.1 has been shown that the density of a molecular system can very well be approximated by a sum of multipole one-center densities

$$\rho(\vec{r}) = \sum_{K=1}^{N_A} \sum_{j=1}^{M_K} \sum_{l=0}^{L_j} \sum_{m=-l}^{l} Q^{Kl}_{jm} F^j_K(\xi_K) Y^m_l(\theta_K, \phi_K) \equiv \sum_{\nu} q_\nu \, \varphi_\nu \,. \tag{5.14}$$

We use in our calculations this expansion to approximate the density of the environment where we have however in general too many free parameters: all expansion coefficient q_ν. From charge conservation law follows that the sum of the monopole occupation numbers should give the number of electrons N^{Env} in the environment. On the other hand inside a solid the micro charge balance should be valid and therefore the electronic charge of each atom in the solid should be equal to their nuclear charge. And indeed our experience shows that occupation numbers for quasi neutral atoms used for the environment lead to a better agreement with experiment. One example are the occupation numbers of free atoms. One other example are average occupation numbers from a cluster

calculation. The third possibility are average occupation numbers from a cluster embedding calculation. In this case one a cluster is embedded in an environment and after each SCF-iteration one takes the average occupation numbers of the cluster atoms for the environment. Occupation numbers obtained in such a way deliver best 'solid state' occupation numbers of an atom.

In this case the energy E^{Env} is not constant anymore and should be calculated at each SCF-iteration. Due to this fact we have to extend equation (5.11) to this case. In general there a four possible types of occupation numbers for the environment

1. Atoms with constant occupation numbers q_{ic}^{EK} which belong to exterior environment

2. Atoms with variable occupation numbers q_{iv}^{EK} which belong to exterior environment

3. Atoms with constant occupation numbers q_{ic}^{TK} which belong to trans-environment

4. Atoms with variable occupation numbers q_{iv}^{TK} which belong to trans-environment

The environment density has the form

$$\rho^{Env} = \rho_c^E + \rho_v^E + \rho_c^T + \rho_v^T \tag{5.15}$$

Inserting this equation in (5.11) leads to

$$
\begin{aligned}
E^{Env} = & \sum_{K=1}^{N_c^E} \sum_{i=1}^{M_c^E} q_{ic}^{EK} <\phi_i|\hat{t}|\phi_i> + \sum_{K=1}^{N_v^E} \sum_{i=1}^{M_v^E} q_{iv}^{EK} <\phi_i|\hat{t}|\phi_i> \\
& + \sum_{K=1}^{N_c^T} \sum_{i=1}^{M_c^T} q_{ic}^{TK} <\phi_i|\hat{t}|\phi_i> + \sum_{K=1}^{N_v^T} \sum_{i=1}^{M_v^T} q_{iv}^{TK} <\phi_i|\hat{t}|\phi_i> \\
& + \int V_{Cl}^N \left(\rho_c^S + \rho_v^E\right) d^3\vec{r} + \int V_{Cl}^N \left(\rho_c^R + \rho_v^T\right) d^3\vec{r} \\
& + \int V^{Ext} \left(\rho_c^S + \rho_v^E\right) d^3\vec{r} + \int V^{Ext} \left(\rho_c^R + \rho_v^T\right) d^3\vec{r} \\
& - \frac{1}{2} \int V_{Env}^C \left(\rho_c^E + \rho_v^E\right) d^3\vec{r} - \frac{1}{2} \int V_{Env}^C \left(\rho_c^T + \rho_v^T\right) d^3\vec{r} \\
& + \frac{1}{2} \sum_{K=1}^{N^{Env}} \sum_{K' \neq K}^{N^{Env}} \frac{Z_{K'} Z_K}{|\vec{R}_{K'} - \vec{R}_K|} + \sum_{K=1}^{N^{Cl}} \sum_{K'=1}^{N^{Env}} \frac{Z_{K'} Z_K}{|\vec{R}_{K'} - \vec{R}_K|} \, .
\end{aligned}
$$

In order to be able to calculate the interaction energy between the cluster and environment some additional integration points are required explicitly in the exterior part of the environment. However there are extra points needed in the trans-environment because the contribution from these regions are constant and do not contribute for example to the binding energy of an ad-atom.

But we can make some estimations for this constant contributions if we approximate all atomic densities in the trans environment to be point-charges:

$\rho_\mu^{TK}(\xi_K) = \frac{q_\mu^{TK}}{4\pi \xi_K} \delta(\xi_K - T_K + T_{K'})$ where $\mu = c, v$. Inserting this in the expression of the E^{Env} leads to

$$
\begin{aligned}
E^{Env} = &\sum_{K=1}^{N_c^E} \sum_{i=1}^{M_c^E} q_{ic}^{EK} <\phi_i|\hat{t}|\phi_i> + \sum_{K=1}^{N_c^T} \sum_{i=1}^{M_c^T} q_{ic}^{TK} <\phi_i|\hat{t}|\phi_i> \\
&+ \sum_{K=1}^{N_v^E} \sum_{i=1}^{M_v^E} q_{iv}^{EK} <\phi_i|\hat{t}|\phi_i> + \sum_{K=1}^{N_v^T} \sum_{i=1}^{M_v^T} q_{iv}^{TK} <\phi_i|\hat{t}|\phi_i> \\
&+ \int V_{Cl}^N \left(\rho_c^E + \rho_v^E\right) d^3\vec{r} + \int V^{Ext} \left(\rho_c^E + \rho_v^E\right) d^3\vec{r} - \frac{1}{2} \int V_{Env}^C \left(\rho_c^E + \rho_v^E\right) d^3\vec{r} \\
&+ \mathcal{E}_c^N + \mathcal{E}_v^N + \mathcal{E}_c^E + \mathcal{E}_v^E + \frac{1}{2} \sum_{K=1}^{N^{Env}} \sum_{K' \neq K}^{N^{Env}} \frac{Z_{K'} Z_K}{|\vec{R}_{K'} - \vec{R}_K|} + \sum_{K=1}^{N^{Cl}} \sum_{K'=1}^{N^{Env}} \frac{Z_{K'} Z_K}{|\vec{R}_{K'} - \vec{R}_K|}
\end{aligned}
$$

where

$$
\mathcal{E}_\mu^N = \sum_{K'=1}^{N_\mu^R} \sum_{K=1}^{N^{Cl}} \begin{cases} q_\mu^{TK'}\, {}^K V_{Cl}^N(\vec{R}_{K'}) & |\vec{R}_{K'} - \vec{R}_K| > \epsilon \\ \int \rho_\mu^{TK'}\, {}^K V_{Cl}^N\, d^3\vec{r} & |\vec{R}_{K'} - \vec{R}_K| < \epsilon \end{cases} \tag{5.16}
$$

and

$$
\mathcal{E}_\mu^E = \sum_{K'=1}^{N_\mu^R} \sum_{K=1}^{N_\mu^{Env}} \begin{cases} q_\mu^{RK'} \left({}^K V_{Env}^N(\vec{R}_K') - \frac{1}{2}{}^K V_{Env}^C(\vec{R}_K')\right) & |\vec{R}_{K'} - \vec{R}_K| > \epsilon \\ \int \rho_\mu^{TK'} \left({}^K V_{Env}^N(\vec{R}_K) - \frac{1}{2}{}^K V_{Env}^C(\vec{R}_K)\right) d^3\vec{r} & |\vec{R}_{K'} - \vec{R}_K| < \epsilon . \end{cases}
$$

Chapter 6

Atomic properties

The detailed calculations of the electronic-ground states of the atoms represents the first step towards predicting the chemical and physical properties of super heavy elements. When one compares these properties for two elements in the same chemical group, which often have the same outer electronic structure, one finds some differences due to the differences in sizes, ionisation potentials, energies and radial distributions of the wave functions between analogues shells. Slater [59] showed that the size of the atom or ion is strongly correlated with the principal maximum of the outermost electronic shell, and hence giving a first estimate of this important magnitude. Sometimes the expectation value of $\langle r \rangle$ of the outermost shell (which roughly agrees with the principal maximum) is used as the radius, but the agreement with the experiment is not so good.

For the heavy and super heavy elements the increased number of shells and the decrease of the binding energy of the outer electrons lead to a competition between shells. As a consequence, the inner electrons will play also an important role. The relativistic effects become now important and the coupling between the electrons changes from LS to JJ coupling.

The relativistic effects on atomic orbitals can be classified in:

- the spin–orbit (SO) splitting of the levels with $l \neq 0$ ($p, d, f \ldots$ electrons) into $j = l \pm 1/2$.

- a direct relativistic contraction and stabilisation of the ns and $p_{1/2}$ orbitals,

- an indirect relativistic expansion of outer d and f orbitals

The SO splitting originates in the inner region in the vicinity of the nucleus. For a given l, the SO splitting decreases with increasing the number of sub-shells, i.e., it is much stronger for inner (core) shells than for outer shells (see table 6.1). For a given principal quantum number, the SO splitting decreases with increasing l, i.e. the $np_{1/2} - np_{3/2}$ splitting is larger than $nd_{3/2} - nd_{5/2}$, which is in turn larger than the $nf_{5/2} - nf_{7/2}$, as is evident from table 6.1 and figure 6.1. In transactinide compounds SO coupling leads to splittings comparable with (or even larger than) the typical bond energies. The SO splitting for the 6d valence electrons for element 112 is 3.18 eV in comparison with the corresponding value of 1.84 eV for the 5d valence electrons.
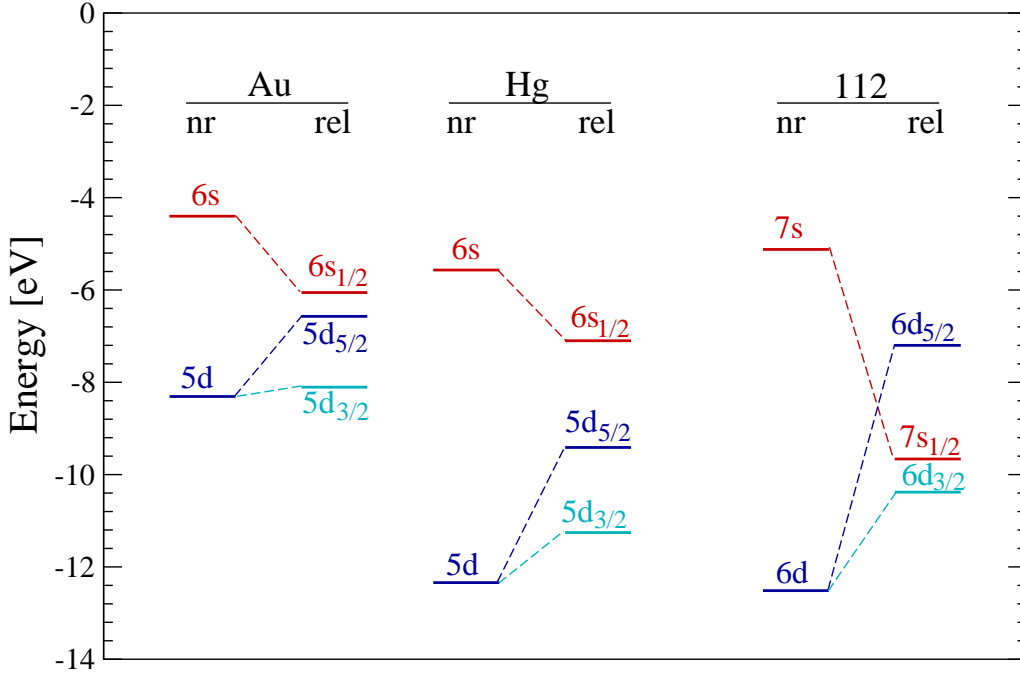
Figure 6.1: Relativistic (DF) and nonrelativistic (HF) energy levels of the valence electrons of Au, Hg and element 112.

Initially it had been assumed that the direct relativistic effect, i.e. the contraction and stabilisation of s and $p_{1/2}$ orbitals, are important only for "fast" electrons in inner core shells of heavy atoms. However, actual relativistic calculations [60] showed that this effect is still large for the outer valence AO of s and p type. In general, the relative relativistic correction Δa_μ of a property a of atomic orbital μ is given by:

$$\delta a_\mu \simeq c_{l,j}^a \left(\frac{Z}{c}\right)^2 \tag{6.1}$$

where Z is the unshielded nuclear charge [61]. In several cases $c_{l,j}^a$ is even somewhat larger for valence orbitals than for core orbitals, this effect being maximal in the 6th row on Au and in the 7th row on element 112 (the so–called gold maximum and group 12 maximum, respectively).

The direct relativistic effects for a valence orbital smoothly increases along a periodic row. Tables 6.2 and 6.3 show the relativistic contractions of the ns and n$p_{1/2}$ orbitals for Hg and element 112. The relative relativistic contraction $\Delta < r >= (< r >_{nr} - < r >_{rel}) / < r >_{nr}$ of the ns orbital is 14.1 for Au, 12.4 for Hg and 27.1 for element 112, see figure 6.2 and tables 6.2 and 6.3. For element 112 one see that for the 6s orbital $< r >_{nr}=$ 1.16 a.u. and $< r >_{rel}=$ 0.93 a.u., and for the 7s orbital $< r >_{nr}=$ 3.36 a.u. and $< r >_{rel}=$ 2.45 a.u. Thus the relativistic orbital contraction is much larger for the 7s orbital compared to the 6s orbital. The relative relativistic contraction of the valence 6s of Hg is bigger than that of the 6s of element 112, and smaller than that for
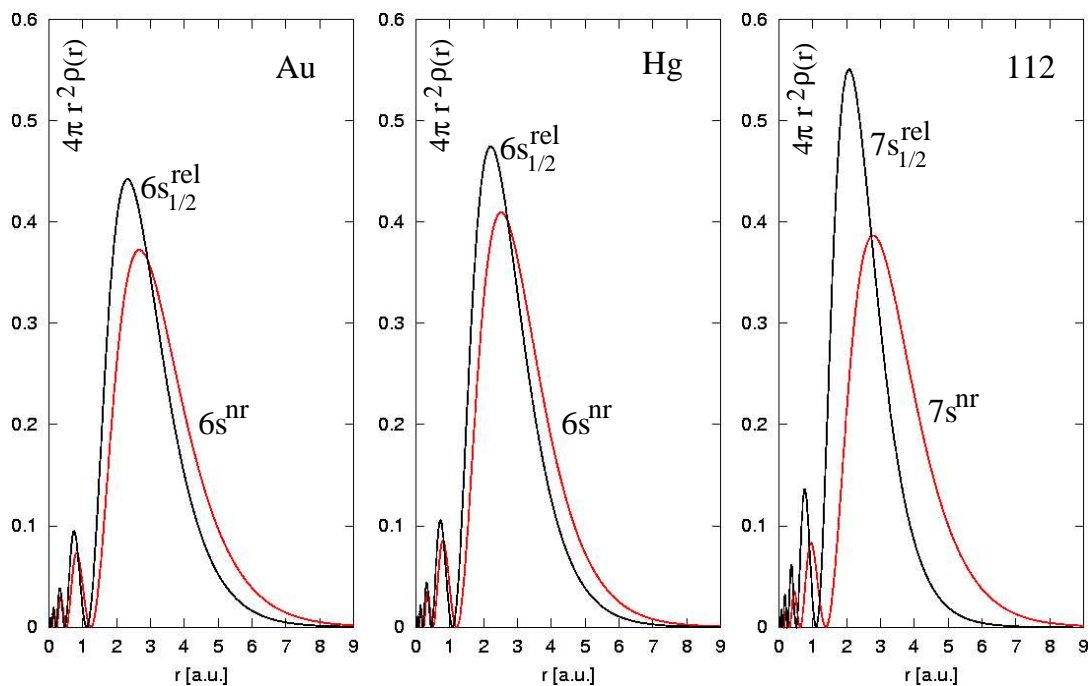
Figure 6.2: Relativistic and non–relativistic radial distribution of the ns valence electrons in Au, Hg and element 112

the 7s of 112. Both n$p_{1/2}$ and n$p_{3/2}$ orbitals of the elements discussed above contract relativistically.

For the indirect relativistic effect, an important role is played by the region between the innermost and outermost shells. The effect of the relativistic contraction of the s and p *core orbitals* is the increase in the Coulomb repulsion on the valence electrons. The s and p *valence orbitals* have their main maximum well outside the core and therefore, the effect of the *outer core* on them is not so strong. These orbitals, however, penetrate in the inner core and, as a consequence, they experience weak destabilising effects from the innermost shell.

The d and f AO will experience a strong indirect destabilisation (and expansion) from the relativistic contraction of the *outer s, p core orbitals* which have a similar extent. Furthermore, the relativistically expanded d and f orbitals will stabilise the penetrating s, p *valence orbitals*. From these reasonings one can conclude:

- the d and especially f orbitals are in general significantly destabilised;
- the occupation of the inner s, p, d and f orbitals determines if the indirect destabilisation predominates for s and p valence AO or weather it is compensated (or even over-compensated) by indirect stabilisation.

These considerations clarify the the very large relativistic stabilisation of the 6s and 7s orbitals in Au and element 112 respectively. Thus for element 112 as well as element 111 the electronic configuration is $d^q s^2$ whereas it changes from Au ($d^{10}s^1$) to Hg ($d^{10}s^2$).

37

Table 6.1: The relativistic spin-orbit splitting for Au, Hg and element 112 neutral atoms.

	the SO splitting [eV]		
	Au	Hg	Element 112
$2p_{1/2} - 2p_{3/2}$	1811.2	1921.54	10686.7
$3p_{1/2} - 3p_{3/2}$	400.10	426.08	2589.74
$3d_{3/2} - 3d_{5/2}$	86.49	91.83	443.19
$4p_{1/2} - 4p_{3/2}$	96.24	103.19	738.40
$4d_{3/2} - 4d_{5/2}$	18.02	19.34	119.29
$4f_{5/2} - 4f_{7/2}$	3.81	4.19	35.24
$5p_{1/2} - 5p_{3/2}$	16.51	18.29	212.275
$5d_{3/2} - 5d_{5/2}$	1.53	1.84	30.02
$5f_{5/2} - 5f_{7/2}$			6.31
$6p_{1/2} - 6p_{3/2}$			43.69
$6d_{3/2} - 6d_{5/2}$			3.18

Here the nd shells become fully populated and the indirect stabilisation of the valence s, p orbitals achieves its maximum.

As one can see in the tables 6.3 and 6.2 the $6p_{1/2}$ and $6p_{3/2}$ of 112 are stronger contracted than the $5p_{1/2}$ and $5p_{3/2}$ of Hg, whereas the $5f_{5/2}$ and $5f_{7/2}$ of 112 are stronger expanded and destabilised in comparison to the $4f_{5/2}$ and $4f_{7/2}$ of Hg.

Table 6.2: The nonrelativistic and relativistic radii of the principal maximum r^{max} and of the expectation values $\langle r \rangle$ for the valence orbitals of Hg.

nonrelativistic			relativistic			$\Delta \langle r \rangle$
orbital	r_{nr}^{max}[a.u.]	$\langle r \rangle_{nr}$ [a.u.]	orbital	r_{rel}^{max}[a.u.]	$\langle r \rangle_{rel}$ [a .u.]	[%]
4f	0.36	0.47	$4f_{5/2}$	0.36	0.48	–2.1
			$4f_{7/2}$	0.37	0.49	–4.2
5s	0.91	0.99	$5s_{1/2}$	0.82	0.90	9
5p	0.97	1.08	$5p_{1/2}$	0.88	0.97	10.2
			$5p_{3/2}$	0.95	1.07	0.9
5d	1.15	1.46	$5d_{3/2}$	1.15	1.46	0.02
			$5d_{5/2}$	1.17	1.53	–4.9
6s	2.52	3.07	$6s_{1/2}$	2.23	2.69	12.4

The effect is so strong that the $6p_{1/2}$ energy level is situated below the $5f$ levels for the SHE. Because of the large relativistic $7s$ contraction and the relativistic $6d$ expansion, the $7s$ electrons are more strongly bound than the $6d_{5/2}$ electrons.

For the same reason the ground–state configuration for the positively charged species 112^+ and 112^{+2} are $6d^9 7s^2$ and $6d^8 7s^2$, respectively [62]. As a result one expects large

Table 6.3: The nonrelativistic and relativistic radii of the principal maximum r^{max} and of the expectation values $\langle r \rangle$ for the valence orbitals of element 112.

nonrelativistic			relativistic			$\Delta \langle r \rangle$
orbital	r_{nr}^{max}[a.u.]	$\langle r \rangle_{nr}$ [a.u.]	orbital	r_{rel}^{max}[a.u.]	$\langle r \rangle_{rel}$ [a .u.]	[%]
5f	0.60	0.68	$5f_{5/2}$	0.62	0.70	−2.9
			$5f_{7/2}$	0.62	0.72	−5.9
6s	1.07	1.16	$6s_{1/2}$	0.87	0.93	19.8
6p	1.15	1.26	$6p_{1/2}$	0.93	1.00	20.6
			$6p_{3/2}$	1.12	1.23	2.4
6d	1.38	1.16	$6d_{3/2}$	1.35	1.67	−43.9
			$6d_{5/2}$	1.44	1.83	−57.8
7s	2.81	3.36	$7s_{1/2}$	2.08	2.45	27.1

contributions from $6d$ involving in the chemical bonding for element 112. In the case of Hg the relativistic $6s$ contraction is not enough to change the order of the valence levels in the neutral atom. This is also reflected in the fact that the ground state configuration for the positively charged species Hg$^+$ and Hg^{2+} are $5d^{10}6s^1$ and $5d^{10}$. From these reasoning we expect that both the $6s$ and $5d$ electrons will participate to the binding.

To be complete one should mention here that the quantum electrodynamic effects (QED) are very important in accurate calculations of X–ray spectra, for highly charged few electron atoms. In the case of neutral atom, the effects are less than 1%, and therefore are not of interest in our calculations.

Chapter 7

Diatomic calculations

One important step in performing molecular calculations consists in the optimization of the basis, described in Section 4.5. First the procedure is applied to the Au atoms, since they are constituting the cluster which simulate the surface.

As starting point we consider the dimer Au_2. The first choice is the minimal basis set for the expansion of the MO. These are the 4-component wave functions corresponding to all the occupied states in the neutral atom. The total energy of the Au_2 molecule is determined as function of the internuclear distance. A clear minimum is obtained for a certain distance, defining the bond length of the molecule. It was found that the total energy has a minimum of -1033972.3946 eV at an internuclear distance of 4.82 a.u. One should mention that during the optimization procedure the RLDA value of the total energy is considered.

Two kinds of optimization procedures were applied for all the atoms involved, giving two different types of basis sets, which we will call A and B.

Type A

In this case a basis set is construct as follows:

- the $1s_{1/2}$ to $5p_{3/2}$ Dirac 4–component spinors obtained by solving the Kohn-Sham equation for the neutral atom,

- the valence $5d_{3/2}$, $5d_{5/2}$ and $6s_{1/2}$ orbitals obtained by solving the same equation, but for the ionized atoms.

The total energy of the Au_2 molecule is again calculated, keeping the internuclear distance equal to 4.8 a.u., for different degrees of ionization. The corresponding potential energy curve is plotted in figure 7.1 (the small curve in the top left-hand side of the figure), and it presents a minimum (-1033972.4209 eV) for an degree of ionization equal to 0.29. One mention that this values for the ionization of the atom have nothing to do with a real system, but the aim is to produce wave functions with a smaller radius of the principal maximum than that corresponding to the neutral atom.

Further on, to this basis are added the $6p_{1/2}$ and $6p_{3/2}$ wave functions, obtained again from atomic calculations for the ionized atom. The total energy of the dimer for this extended basis is shown by dots in figure 7.1 and a minimum is found (-1033972.6555
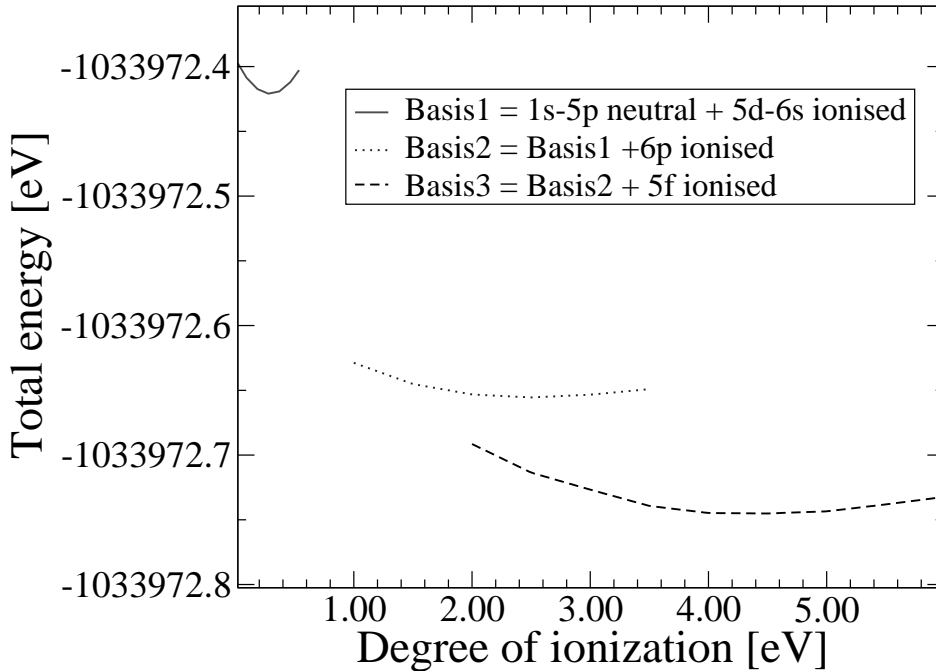
Figure 7.1: The total energy of the Au$_2$ dimer when different basis functions are used.

eV) for a degree of ionization of +2.5. In a similar way, the $5f_{5/2}$ and $5f_{7/2}$ functions are added (the dashed curve) with an degree of ionization of +4.5, the corresponding minimum of total energy being -1033972.7451 eV. The reason for adding the $5f$ functions instead of $6d$, was that the former produced a bigger change in the total energy than the later one. The optimization procedure was stopped in this point since we are limited in the number of wave functions contained in our basis, due to the required memory which is proportional to N^2, where N represents the number of functions in the basis set used for the MO–LCAO expansion.

Using this optimized basis, the potential energy curve of the dimer is again determined and its minimum is found to be at 4.67 a.u., which differs slightly from the experimental value ($R_e = 4.67$ a.u., $D_e = 2.29 + -0.02$ eV [63]). The corresponding RLDA binding energy is found to be 3.15 eV, and the GGA (with B88 for exchange and Perdew 86 for correlation) value 2.61 eV. The differences to the above experimental values are due to the fact that in the case of the Au$_2$ the spin–polarized collinear (SP) and the the spin–polarized non–collinear (SP,non) (described in 3.4) calculation should be performed, as shown by Anton et al. [64] The total energy of the dimer calculated by the three methods is essentially the same, since the molecule has no open spins and therefore it behaves around the minimum of the potential energy curve as a closed shell system. The mean difference in bond energy comes from the atomic calculations for the open shell system of the Au atom.

It is worth noting that generally the GGA bond length is larger than the RLDA value

(in our case 4.8 a.u). Therefore the geometry of the system is better described by the RLDA values, while the binding energy by the GGA value.

Type B

The second type of basis contains the entire minimal basis as starting point. Keeping fixed the interatomic distance to the value of 4.8 a.u., the $6p$ and $5f$ functions (from ionized atoms) are added (forming Basis No. 2 in table 7.1) with a degree of ionization of 4.0. The RLDA bonding energy for this type of basis is -3.07 eV with a bond length of 4.7 a.u., and the GGA value is -2.55 eV for an internuclear distance of 4.8 a.u. One has a difference of 0.06 eV in the binding energy corresponding to the two types of basis. Basis B, although somewhat weaker bound, has the advantage that it allows an analysis of the density of states and overlap populations in molecules.

Table 7.1: Total energy (RLDA) for the Au_2 dimer, for minimal and optimized basis (type B), and the degree of ionization for the optimized atomic basis functions.

Basis	Basis functions (type B)	Degree of ionization	Total energy [a.u.]
1	$1s_{1/2}$ to $6s_{1/2}$		−1033972.4208
2	Basis No. 1 + $6p_{1/2}$,$6p_{3/2}$	+4.0	−1033972.5701
3	Basis No. 2 + $5f_{5/2}$,$5f_{7/2}$	+4.0	−1033972.6703

Table 7.2: Total energy (RLDA) for the HgAu dimer, for minimal and optimized basis, and the degree of ionization for the optimized atomic basis functions.

Basis	Basis functions	Degree of ionization	Total energy [eV]
	Type A		
1	$1s_{1/2}$ to $5p_{3/2}$ neutral + 5d-6s ionized	+0.2	−1050625.2228
2	Basis No. 1 + $6p_{1/2}$,$6p_{3/2}$	+1.0	−1050625.8313
3	Basis No. 2 + $5f_{5/2}$,$5f_{7/2}$	+4.0	−1050625.8914
	Type B		
1	$1s_{1/2}$ to $6s_{1/2}$	neutral	−1050625.2449
2	Basis No. 1 + $6p_{1/2}$,$6p_{3/2}$	+1.5	−1050625.8234
3	Basis No. 2 + $5f_{5/2}$,$5f_{7/2}$	+4.0	−1050625.8715
4	Basis No. 3 + $6d_{3/2}$,$6d_{5/2}$	+4.0	−1050625.8921
5	Basis No. 4 + $5g_{7/2}$,$5g_{9/2}$	+6.0	−1050625.9072
6	Basis No. 5 + $6f_{5/2}$,$6f_{7/2}$	+5.5	−1050625.9144

In the next step we performed in a similar way the optimization for the dimers HgAu and 112Au, using the previous by optimized sets for Au. We start with the minimal basis for Hg and 112 respectively. The optimization procedure for the two types of basis is pointed in tables 7.2 and 7.3.

Table 7.3: Total energy (RLDA) for the 112Au dimer, for minimal and optimized basis, and the degree of ionization for the optimized atomic basis functions.

Basis	Basis functions	Degree of ionization	Total energy [eV]
	Type A		
1	$1s_{1/2}$ to $6p_{3/2}$ neutral + 6d-7s ionized	+0.2	–1050625.2228
2	Basis No. 1 + $7p_{1/2},7p_{3/2}$	+0.15	–1805404.9588
3	Basis No. 2 + $6f_{5/2},5f_{7/2}$	+0.9	–1805405.7101
4	Basis No. 3 + $5g_{7/2},5g_{9/2}$	+4.0	–1805405.7928
	Type B		
1	$1s_{1/2}$ to $7s_{1/2}$	neutral	–1805404.7711
2	Basis No. 1 + $7p_{1/2},7p_{3/2}$	+1.0	–1805405.6734
3	Basis No. 2 + $6f_{5/2},5f_{7/2}$	+4.0	–1805405.7467
4	Basis No. 3 + $5g_{7/2},6d_{9/2}$	+6.0	–1805405.7747
5	Basis No. 4 + $7d_{3/2},7d_{5/2}$	+3.5	–1805405.7936
6	Basis No. 5 + $7f_{5/2},7f_{7/2}$	+3.5	–1805405.8036

For further reference, the second type of optimization (type B) is performed till the achievement of the completeness of the basis sets for Hg and element 112. The calculations were performed for both types of basis with atomic spinors including up to 5f for Au and Hg, and up to 6f for element 112, respectively. From tables 7.2 and 7.3 one can see that one loses (by these limitation of the basis) 0.04 eV for HgAu and 0.06 eV for 112Au in the precision of value of the binding energy.

Table 7.4: Binding energy and bond distance (RLDA) for the AuX dimers (for optimized basis), with X=Hg, element 112.

System	Binding energy [eV]		Distance[a.u.]	
	RLDA	GGA	RLDA	GGA
HgAu	–1.03	–0.55	4.92	5.12
HgAu(SP)	–1.01	–0.52		
HgAu(SP, non)	–1.02	–0.53		
112Au	–0.93	–0.41	4.99	5.20
112Au(SP)	–0.89	–0.38		
112Au(SP, non)	–0.90	–0.39		

Figure 7.2 shows how the total energy (RLDA) and the bond distance of the dimer are influenced by the extension of the basis. The bond length for the minimal basis set is situated at 6.9 a.u, differing then substantially from the experimental value. The effect of the optimization of the valence wave functions is a smooth increase in the total energy of the system and a decrease of the bond length to 5.4 a.u. The main change in both the total energy and bond length results from the addition of the np atomic wave functions,
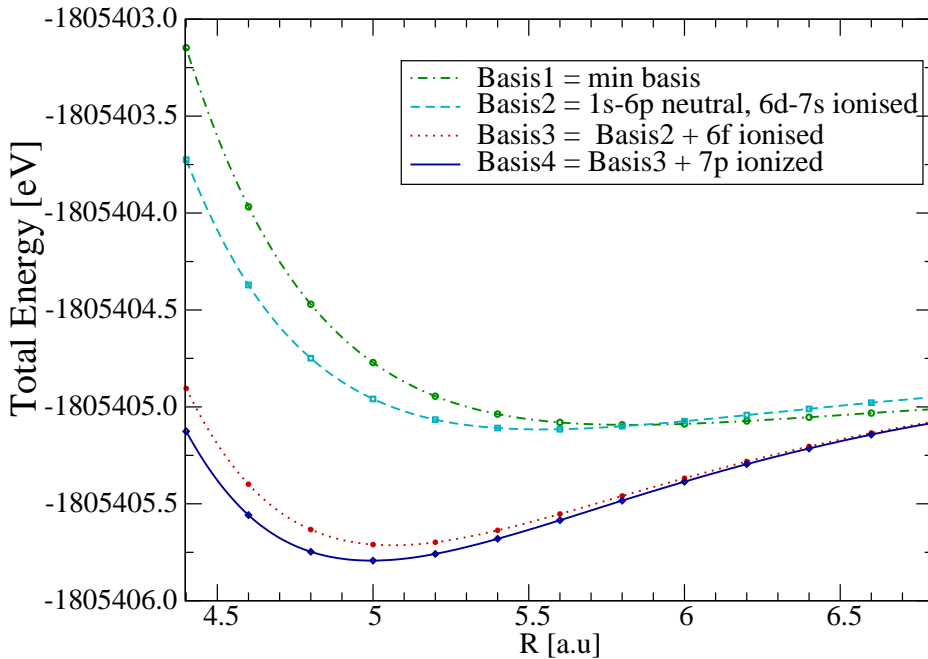
Figure 7.2: Energy potential curves for the dimer 112Au, when different basis are used.

whereas the correction induced by the next nf atomic spinors is only 0.06 eV in the energy and 0.05 a.u. in the bond length.

To see the effect of the spin–polarized method on the XAu dimer results, calculations were performed using basis type A. The obtained binding energies shown in table 7.4 reveals no significant improvement in comparison to the non–SP ones. This is understandable since in the XAu molecule both Hg and element 112 are closed shell systems, and only the Au atom has an open spin. Therefore the entire molecule has an open spin, and the corrections due to the SP (collinear and non–collinear) method are of the same order of magnitude for both the XAu molecule and for the Au atom system. These results show that it is not necessary to use the improved method in studying XAu_n systems, since the corrections given for the total energy of the system will be canceled by the total energy of the cluster Au_n system.

Figure 7.3 shows the binding energies as a function of the internuclear distances. One sees in the first picture that the difference $E_b^{112} - E_b^{Hg}$ is almost the same for the two types of basis (A and B) discussed above. In comparison to the GGA (B88 for exchange, P86 for correlation) values —the second plot— the RLDA values of the binding energy are 0.44 eV greater. On the right–hand side the energy potential curves for the dimer Au112, containing the element of interest, are plotted for basis B and for the minimal basis sets, to illustrate again the effect of the extended basis. The use of the extended sets results in an increase of the electronic density in the region between the atoms (figure 7.4), corresponding to an increasing of the binding energy.

44
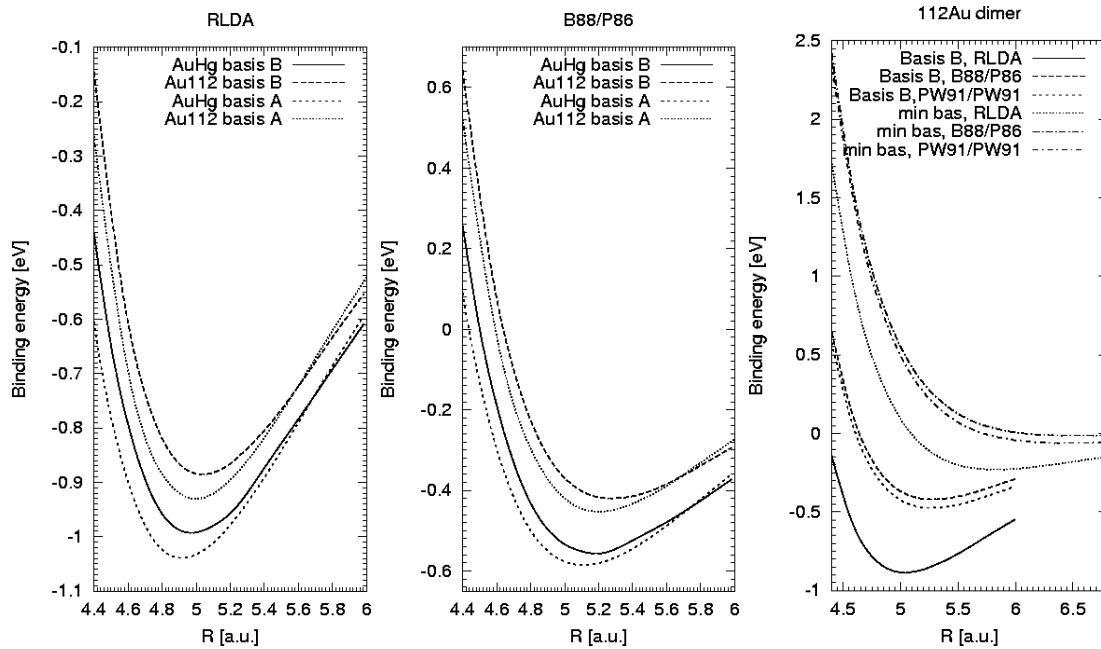
Figure 7.3: Potential energy curves for the dimers XAu, with X = Hg, element 112. The RLDA binding energies for the two types of basis are shown on the left, the GGA (B88/P86) curves—in the middle. On the right the energy potential curves for the dimer 112Au only, for basis B and minimal basis, for RLDA and GGA.
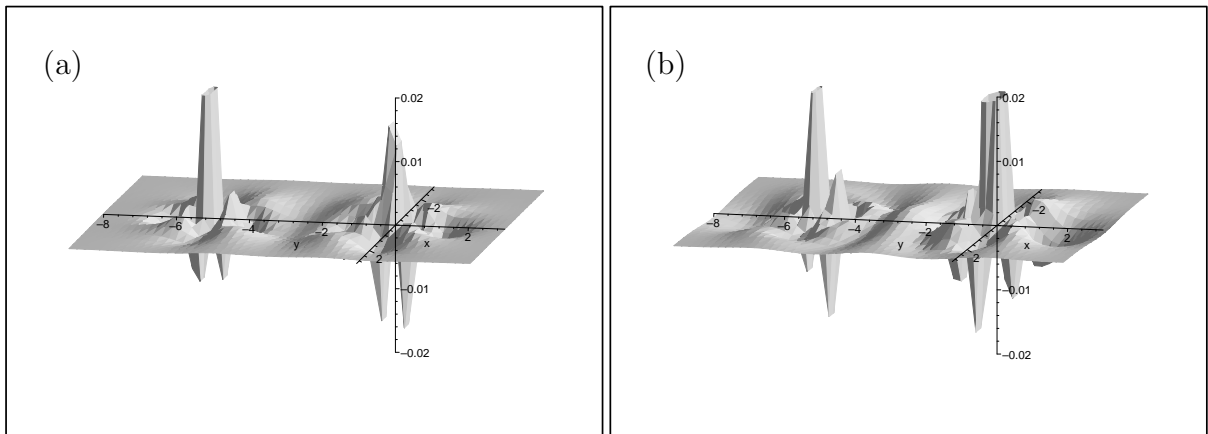
Figure 7.4: The difference between the electronic density of a Au112 molecule and the electronic densities of the neutral isolated atoms localized in the positions of dimer atoms $(\rho_{dimer}(\vec{r}) - \rho_{Au}(\vec{r}) - \rho_{112}(\vec{r}))$; (a) with minimal basis and (b) with the optimized basis sets type B.

Chapter 8

Cluster calculations

8.1 Geometry

The ideal Au(100) surface exhibits a 2-dimensional square lattice with a lattice constant a= 4.08 $\overset{\circ}{A}$ (=7.712 a.u.) chosen according to the bulk fcc phase of Au [65]. A 2 to 5 layer slabs are used to model this surface, designed to describe on-top, bridge and fourfold adsorption processes. The cluster models are constructed by successive addition of neighboring shells starting with the atoms that forms the adsorption site.

The clusters will be denoted by $Au_n(m_1,m_2,...)$, where n denotes the total number of atoms and m_i the number of atoms in the i-th crystal layer parallel to the (100) surface, starting with the surface layer. Individual groups (called blocks in the following tables) of symmetry-equivalent atoms are labeled as in figures 8.1, 8.2 and 8.3. Both top and hollow positions have a C_{4v} symmetry, whereas the bridge position has only C_{2v}.

8.2 Unperturbed surface clusters

One price which one have to pay when the surface is modeled by a cluster is given by the polarization of the cluster in both horizontal and vertical directions. Tables 8.1, 8.2 and 8.3 monitorize this effect by the Mulliken analysis of the cluster–atoms.

Table 8.1: Mulliken charge of the surface-metal atoms of different clusters used in the study of adsorption on the top position when the cluster method is used.

basis	system	Bl.1	Bl.2	Bl.3	Bl.4	Bl.5	Bl.6	Bl.7	Bl.8	Bl.9
opt (B)	Au_9	78.95	79.04	78.96						
opt (A)	Au_{13}	78.97	79.05	78.96	79.00					
min	Au_{14}	79.14	79.03	78.91	79.01	79.07				
opt (A)	Au_{14}	78.99	79.03	78.93	79.03	79.05				
opt (B)	Au_{14}	79.02	79.03	78.89	79.06	79.09				
opt (A)	Au_{34}	78.97	79.01	78.94	78.99	79.03	78.99	79.01	79.03	78.91
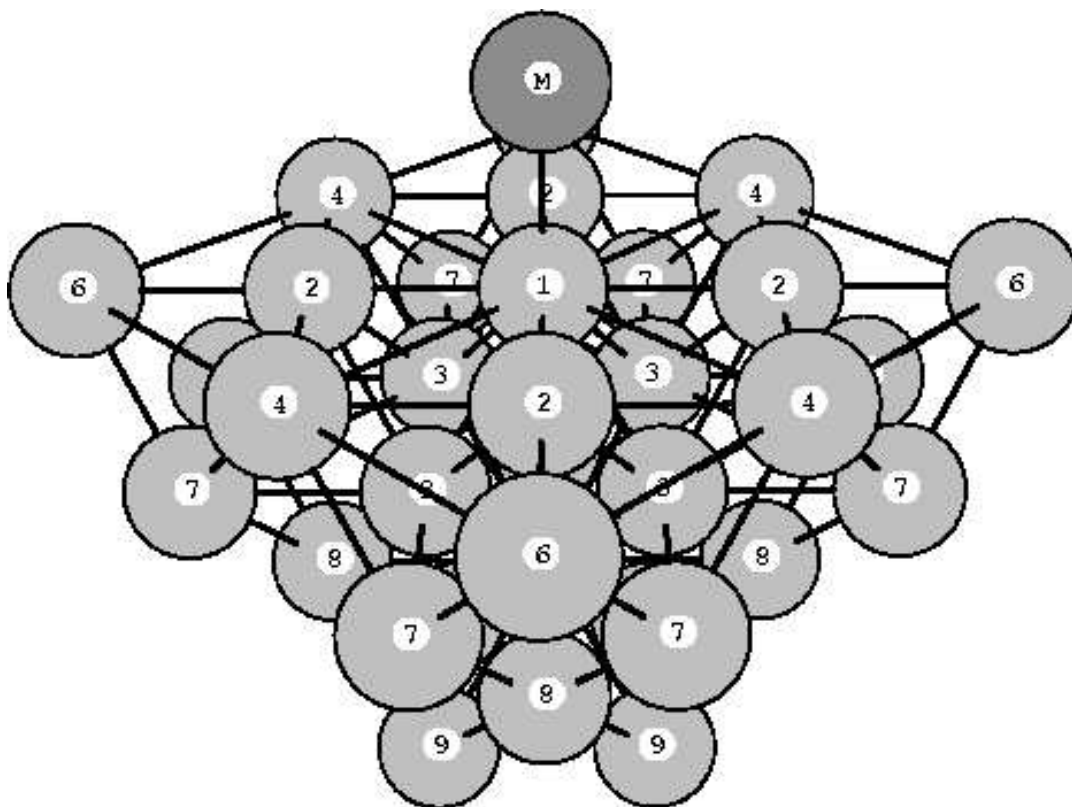
Figure 8.1: A sketch of the largest cluster investigated $(Au_{34}(13,12,4,5))$ for the on-top site.
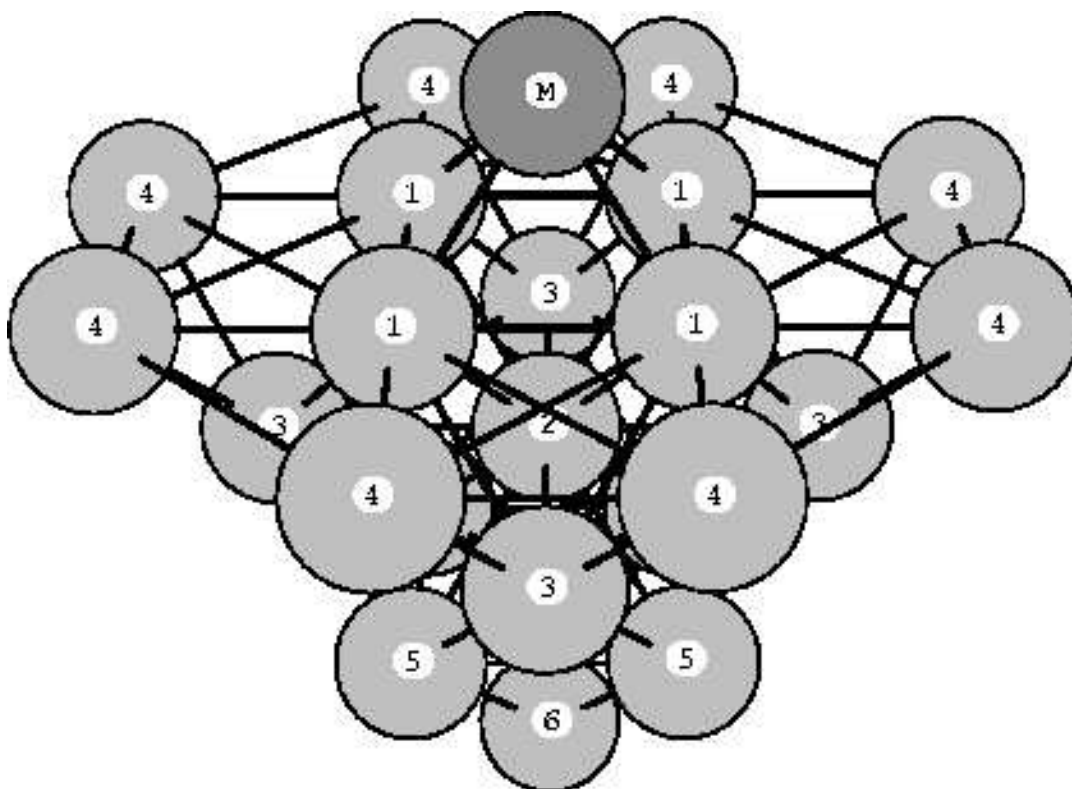
Figure 8.2: A sketch of the largest cluster investigated $(Au_{22}(12,5,4,1))$ for the fourfold site.
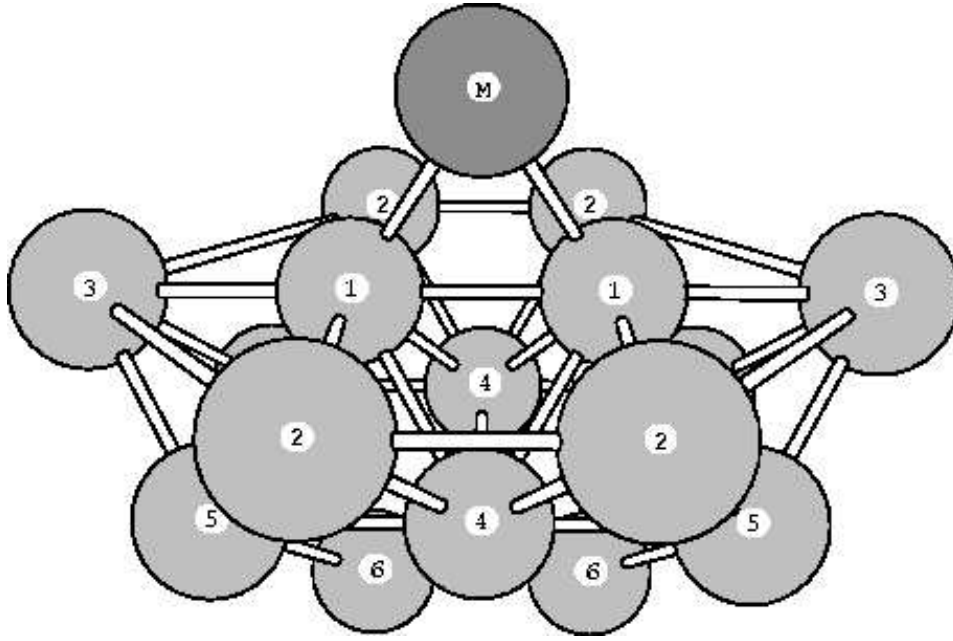
Figure 8.3: A sketch of the largest cluster investigated ($Au_{16}(8,6,2)$) for the bridge site.

The smallest clusters which were considered are the $Au_9(5,4)$ for the top position and $Au_9(4,5)$ for the hollow position, corresponding to the lowest and the highest coordination site, respectively. Further on the size of the cluster is increased. Thus for the top position $Au_{13}(9,4)$, $Au_{14}(9,4,1)$ and $Au_{34}(13,12,4,5)$ clusters are considered. As is evident from table 8.1 atomic charges are different from zero for both the atoms on the surface (constituting the first layer) and the atoms in the next layers. When one looks to the Mulliken charge of the Au atom on top where the ad–atom will coordinate, one sees that there is a deviation from the neutrality corresponding to a transfer of electronic charge from and to the neighbour atoms, which for the same type of basis is a function of the size of the clusters, and for the same cluster (see the analyses for Au_{14}) depends on the type of basis.

Table 8.2: Mulliken charge of the surface-metal atoms of different clusters used in the study of adsorption on the hollow position.

basis	system	Bl.1	Bl.2	Bl.3	Bl.4	Bl.5	Bl.6	Bl.7	Bl.8	Bl.9
opt (A)	Au_9	78.95	79.04	78.97						
opt (B)	Au_9	78.96	79.04	78.95						
opt (A)	Au_{22}	79.01	78.94	78.998	79.01	78.99	79.07			
opt (A)	Au_{26}	78.94	78.95	78.97	79.01	78.97	79.08	79.07		
opt (B)	Au_{26}	78.92	78.95	78.96	79.01	78.97	78.98	79.13		

The hollow position corresponds to the highest coordination order, the adsorbate inter-acting mainly with four atoms in the first layer of the cluster. Different cluster sizes,
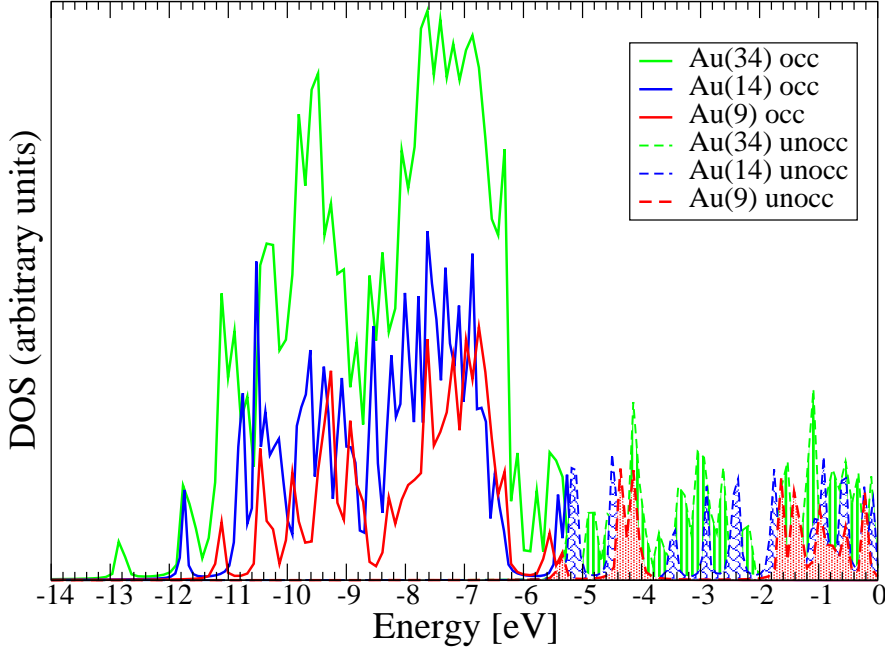
Figure 8.4: The total density of states for the $Au_9(5,4)$, $Au_{14}(9,4,1)$ and $Au_{34}(13,12,4,5)$ systems (cluster method, on–top position).

varying from the $Au_9(4,5)$ system (a small one) up to a $Au_{26}(16,5,4,1)$ system (a medium one), were considered. One should remark that the $Au_9(4,5)$ is reversed compared to the $Au_9(5,4)$ top cluster. One remark that by adding four atoms in the first layer to the $Au_{22}(12,5,4,1)$ there is a change of about 0.1 in the total charge of the atoms in the first coordination shell. From this point of view, the convergence relative to the size of the cluster is not yet achieved for none of the clusters considered. But as it was already pointed out the increase to bigger clusters is limited nowadays by the capacities of the computers.

Table 8.3: Mulliken charge of the surface-metal atoms of different clusters used in the study of adsorption on the bridge position.

basis	system	Bl.1	Bl.2	Bl.3	Bl.4	Bl.5	Bl.6
opt (A)	Au_{16}	78.99	79.02	79.02	78.93	78.99	79.02

In the bridge position the adsorbate interacts mainly with the two central atoms denoted by 1 in figure 8.3. A $Au_{16}(8,6,2)$ cluster includes the 12 atoms which constitute the second coordination shell, six in the first layer and the other six in the second one, together with 2 atoms in the third layer [68].

Information about the details of the surface electronic structure may be obtained from the analysis of density of states (DOS) diagrams. Figure 8.4 displays the total DOS for the different Au_n clusters used in the study of the adsorption on the top position. At first
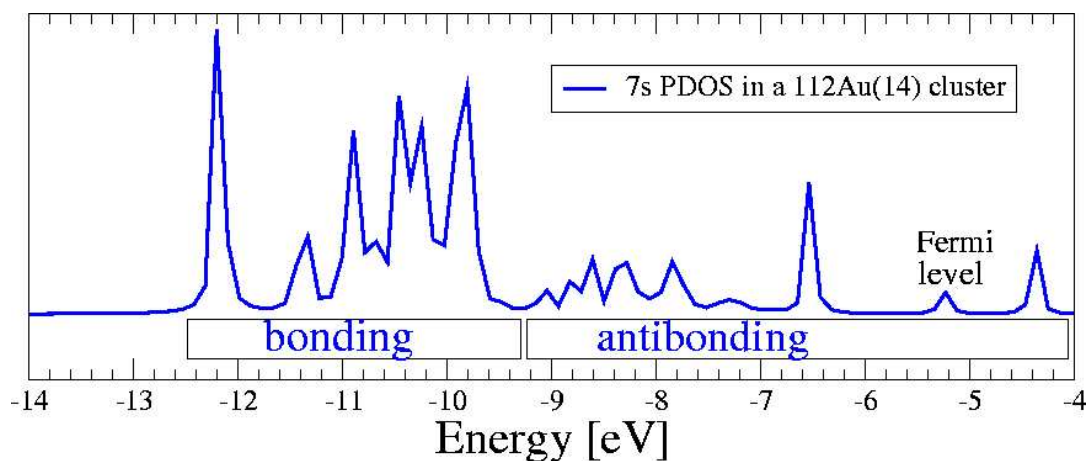
Figure 8.5: The differential density of state for the $7s$ orbital of element 112 in a $112Au_{14}$ system (cluster method, on–top position).

one notices that the $Au_9(5,4)$ cluster DOS is very different from that corresponding to the $Au_{34}(13,12,4,5)$ DOS, which indicates that 9 atoms are not sufficient for modeling the local electronic structure of a solid. The spectrum for the Au_{34} system contains one energy level at -12.81 eV which is separated by a gap of -1.07 eV from the continuum valence band. The analysis of the expansion coefficients of the corresponding MO reveals that it extends over the entire cluster and therefore the corresponding peak would lie in the valence band for a solid.

8.3 Adsorption of element 112 and Hg on the Au_n clusters

When the adsorbate and the surface start to interact, the respective states mix. This leads to new states which usually have the energy levels broadened and shifted with respect to the energy levels in the separated systems.

Lets consider the effect of the valence ($5d$ and $6s$) band of the Au substrate. The interaction of the adsorbate and the substrate leads to the hybridization of the adsorbate wave functions and the states of the substrate s–band yielding a broadening of the adsorbate levels. Moreover, the atomic levels will shift because the substrate Fermi level and the electron chemical potential of the atom become aligned. As an example, figure 8.5 displays the splitting of the $7s$–AO of element 112 over the valence energy spectra of the substrate. An analysis of the wave–function character in a such broadened peak evinces that the low energy part of the peak belongs to states which have an increased electron density between the adsorbate and the substrate. Such states are called "bonding" in contradistinction to the states belonging to the high energy part of the broadened peak which are called "anti-bonding" (and having a node between the adsorbate and the substrate).

This broadening implies a coupling of the localized electrons of the adsorbate to the substrate, and therefore a delocalization. The bonding is strongest when bonding states are occupied and anti-bonding states remain empty.

8.3.1 Adsorption on the top position

The Mulliken analysis presented in Table 8.5 shows that the change of charge between the adsorbate and surface cluster is very small. Thus there is a transfer of charge of about 0.1 from the cluster to Hg, whereas there is practically not charge transfer between element 112 and the system simulating the surface.

The smallest cluster considered for modeling the adsorption atop of a Au surface–atom is $Au_9(5,4)$, as already pointed out above. Keeping fixed the distance between the Au atoms, the binding energy of the XAu_9 system is calculated as a function of the distance R between the ad–atom and the surface. The binding energy is then calculated by subtracting the energy of the cluster Au_9 and the energy of the adsorbate at large R. The obtained potential energy curves are shown in figures 8.6, 8.7 and 8.8, together with those obtained for larger systems.

The RLDA minima of these curves are found to be -0.6 eV for Hg and -0.67 eV for element 112, corresponding to a bond length of 5.0 a.u. for $HgAu_9$ and 5.2 a.u. for $112Au_9$ system, respectively. This actually means an inversion in the relative behaviour of these elements with respect to the way in which they interact with the other Au clusters. All other results in table 8.6 and those for the dimers (table 7.4) show that Hg is stronger bound than element 112. In view to see the basis to this type of computation, the same method was applied to the XAu_9 clusters but for the basis type B, keeping the distance between the adsorbate and the cluster to the values 5.0 for Hg and 5.2 for 112, i.e. in the position of the minimum of the corresponding potential energy curves. The results are presented in table 8.4. The third set of values corresponds to the case in which an extended basis B' which contains basis B (for the Au atoms), the minimal basis set for adsorbate and in addition the next optimized spinors for Hg and element 112, as follows:

- $6p(Hg^{+1.5})+5f(Hg^{+4.0})+6d(Hg^{+3.5})+5g(Hg^{+6.0})+6f(Hg^{+5.5})$
- $7p(112^{+1.0})+6f(112^{+4.0})+7d(112^{+3.5})+5g(112^{+6.0})+7f(112^{+5.5})$.

As it results from Table 8.4, the binding energies are very depending on the basis for this size of cluster, and when the "best basis" for the ad–atom is used, the difference between the two binding energies is almost zero. The reason for this behaviour is that the size of the cluster is too small. This can be immediately observed by the analysis of the DOS of the $XAu_9(5,4)$ clusters in comparison with the DOS for the $Au_9(5,4)$ cluster which simulates the surface in figure 8.9. It is evident that the electronic distribution has not yet achieved the band structure which is characteristic to a solid, and the total DOS of the Au_9 system substantially changes by the interaction with the ad–atom.
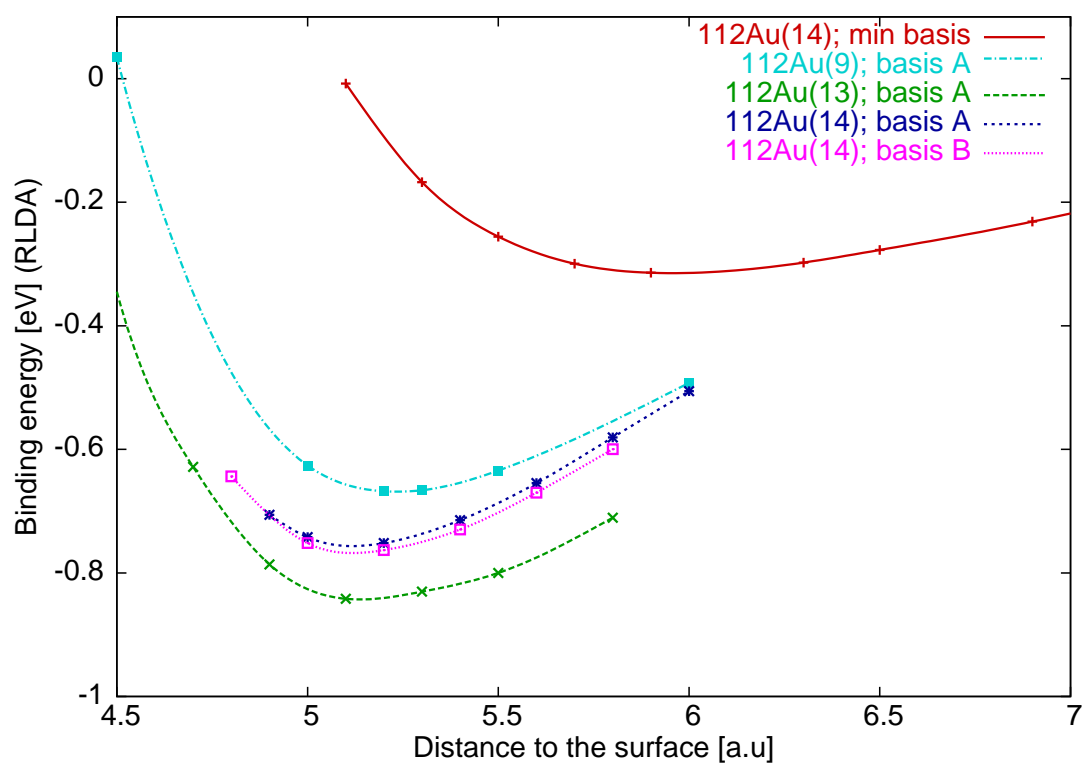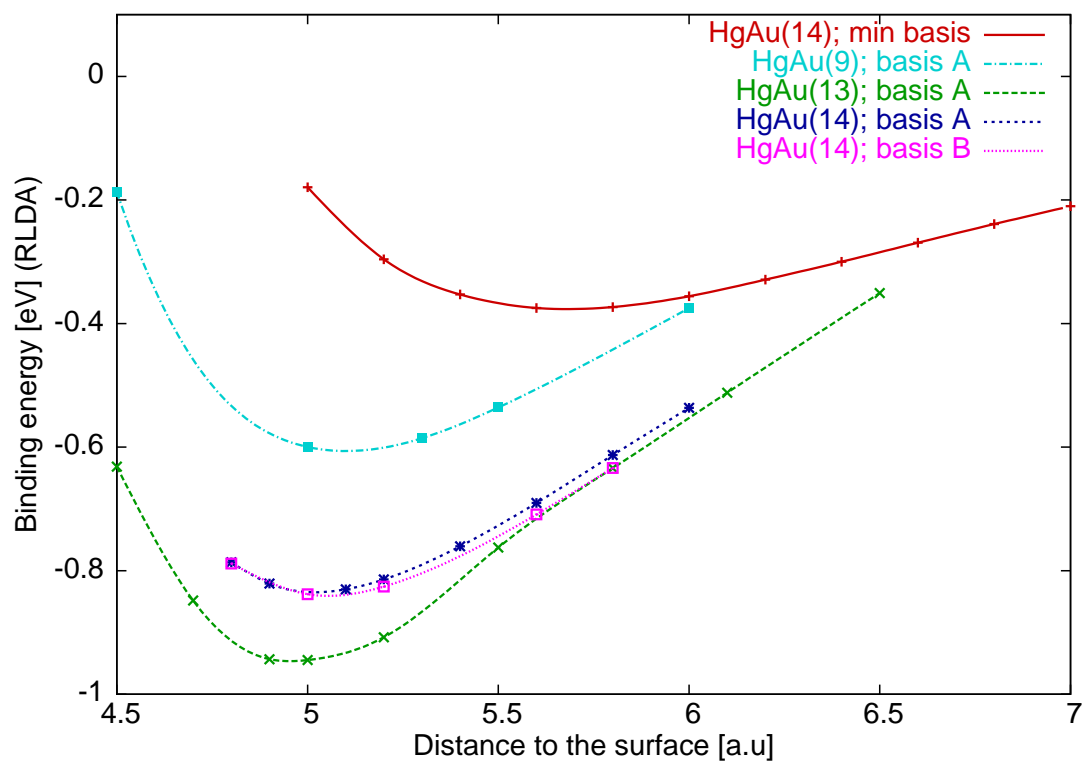
Figure 8.6: The potential energy curves (RLDA) for the adsorption of Hg and element 112 on different Au clusters on the on-top position .
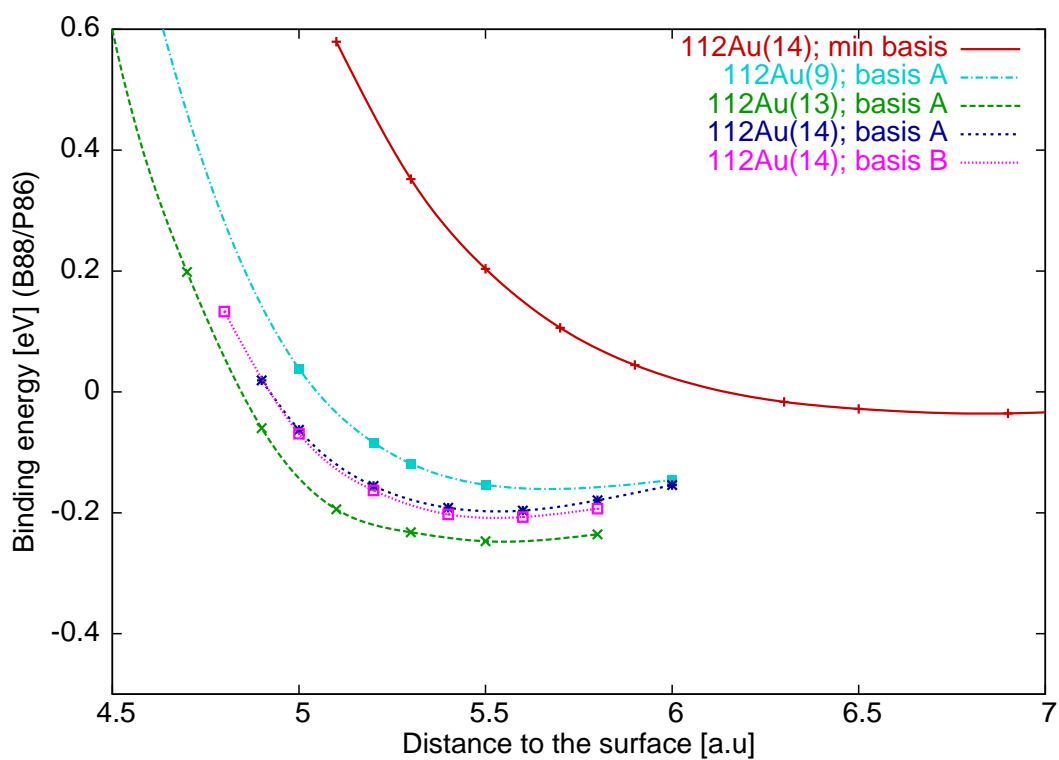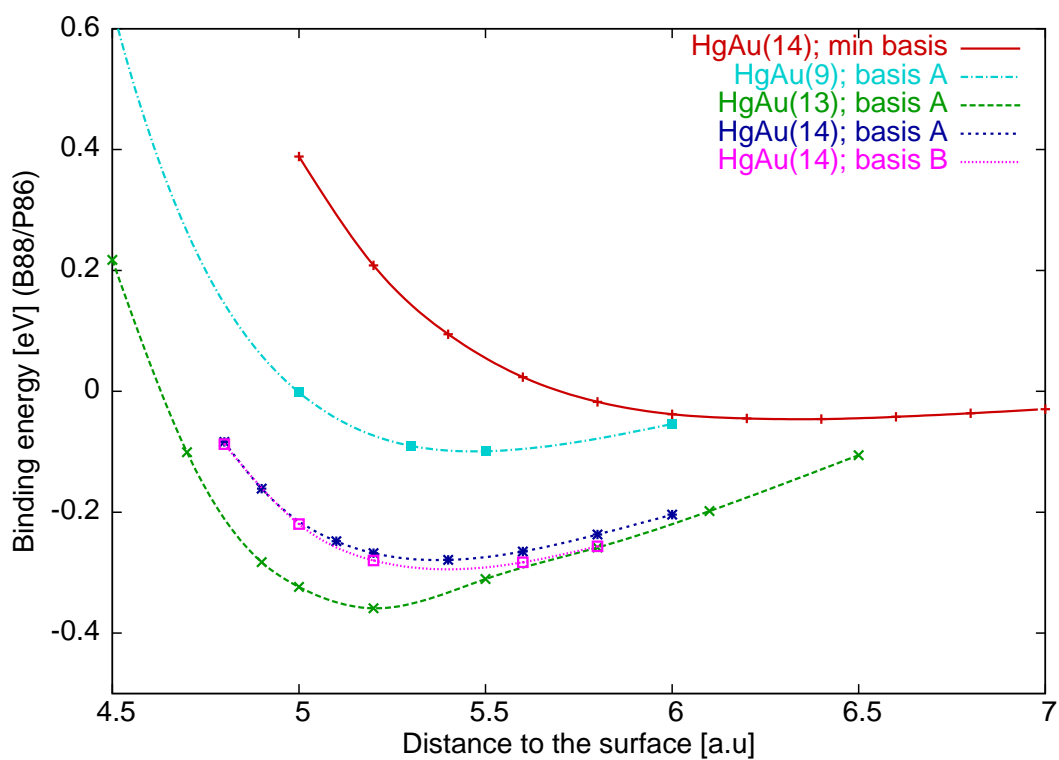
Figure 8.7: The potential energy curves (B88/P86) for the adsorption of Hg and element 112 on different Au clusters on the on-top position .
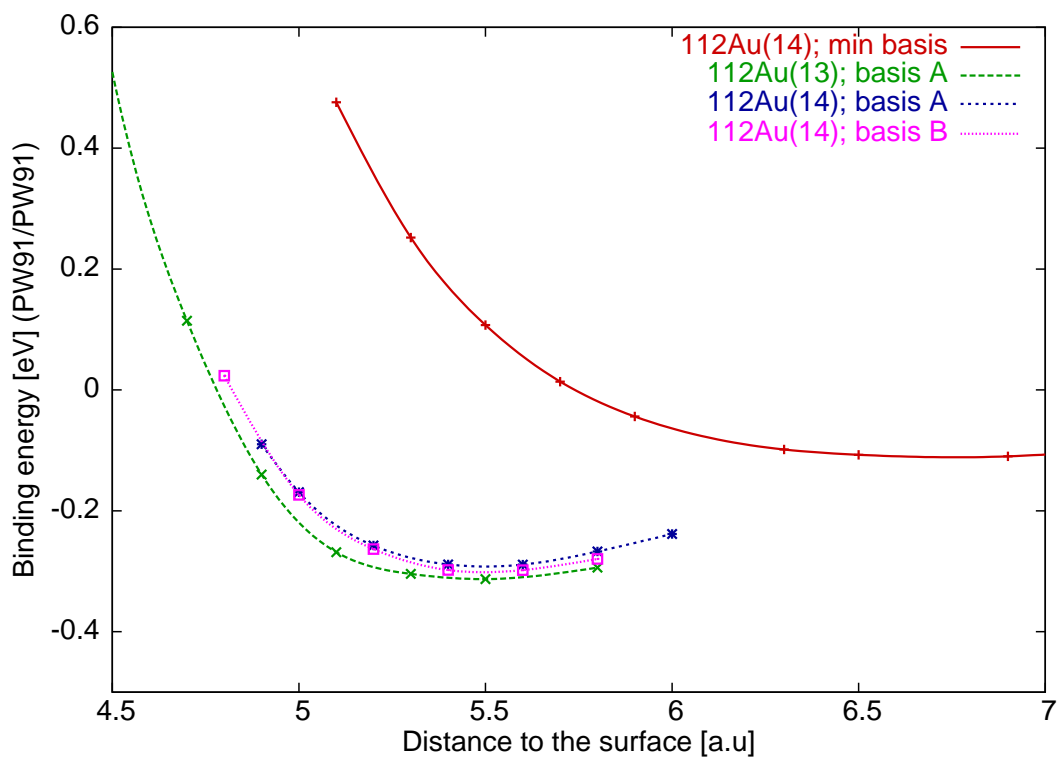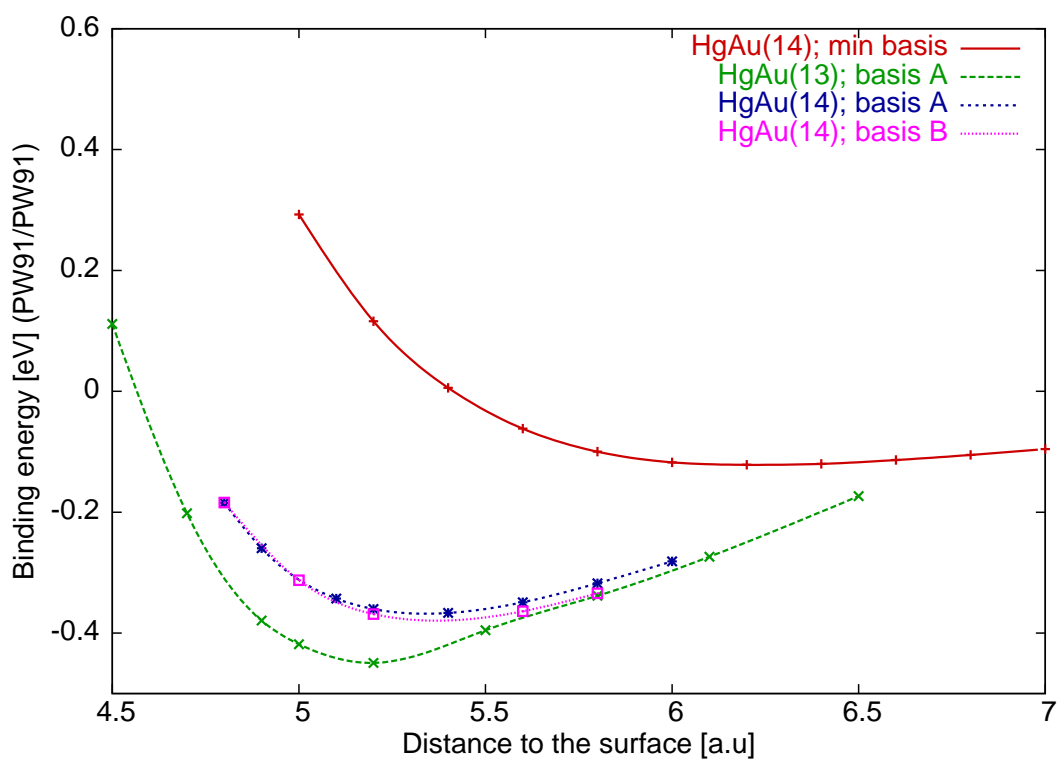
Figure 8.8: The potential energy curves (PW91/PW91) for the adsorption of Hg and element 112 on different Au clusters on the on-top position .

Table 8.4: Binding energies (RLDA) for the $XAu_9(5,4)$ clusters, when different basis sets are used keeping the distance between the adsorbate and the $Au_9(5,4)$ cluster constant.

System	Binding energy [eV]			R
	basis A	basis B	basis B'	[a.u.]
$HgAu_9(5,4)$	-0.60	-.56	-.65	5.0
$112Au_9(5,4)$	-0.67	-.60	-.67	5.2
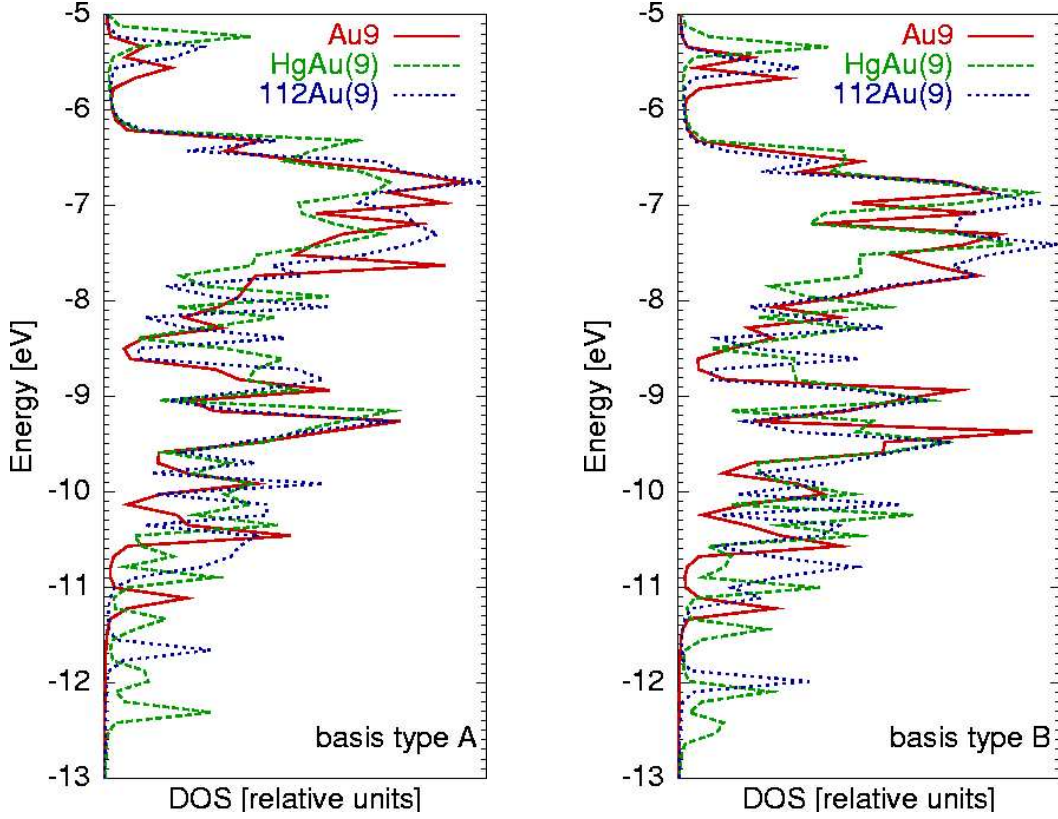
Figure 8.9: The total density of states for Au_9, $HgAu_9$ and $112Au_9$ clusters for the on-top site.

The addition of four atoms in the first layer in the Au_9 cluster, leads to $E_b = -0.95$ eV for Hg and $E_b = -0.83$ eV for element 112, which gives a difference in the binding energy of -0.12 eV (see table 8.7), comparable to that obtained for the XAu dimers (-0.1 eV (see table 7.4)). The addition of a Au atom in the third layer, i.e. a surface cluster $Au_{14}(5,4,1)$, leads to a decrease of both binding energies to the values $E_b^{Hg} = -0.86$ eV and $E_b^{112} = -0.75$ eV. This is in agreement with the previous cluster calculations ([66]) which revealed that when the cluster is enlarged in the direction perpendicular to the surface this results in a decrease in the binding energy. On the contrary, when the growing is made in the direction parallel to the surface the binding energy becomes bigger.

For the XAu_{14} the potential energy curves for the two types of basis were determined.

Table 8.5: Mulliken charge of the surface-metal atoms and of the ad–atom for different clusters used in the study of adsorption on the top position.

system	basis	Ad–atom	Bl.1	Bl.2	Bl.3	Bl.4	Bl.5	Bl.6	Bl.7	Bl.8	Bl.9
$HgAu_9$	A	79.87	79.02	79.07	78.96						
$112Au_9$	A	112.07	78.98	79.00	78.98						
$HgAu_9$	B	79.90	78.97	79.08	78.95						
$112Au_9$	B	112.05	78.94	79.04	78.95						
$HgAu_9$	B'	79.97	78.90	79.08	78.95						
$112Au_9$	B'	112.09	78.90	79.04	78.96						
$HgAu_{13}$	A	79.86	78.92	79.05	78.97	79.04					
$112Au_{13}$	A	112.02	78.92	79.04	78.96	79.02					
$HgAu_{14}$	min	79.88	78.17	79.04	78.89	79.02	79.12				
$112Au_{14}$	min	111.95	79.13	79.03	78.90	79.01	79.09				
$HgAu_{14}$	A	79.91	79.01	79.03	78.93	79.04	79.07				
$112Au_{14}$	A	112.02	78.99	79.02	78.93	79.03	79.06				
$HgAu_{14}$	B	79.90	79.01	79.03	78.90	79.06	79.11				
$112Au_{14}$	B	112.03	78.99	79.02	78.90	79.06	79.10				
$HgAu_{34}$	A	79.89	79.02	79.02	78.95	78.99	79.03	79.00	79.01	79.03	78.91
$112Au_{34}$	A	112.01	78.98	79.01	78.95	78.99	79.03	79.00	79.01	79.03	78.91

Table 8.6: The binding energies and bond length for $HgAu_n$ and $112Au_n$ on the top position, for $n = 9, 13, 14$ and 34, when the cluster method is applied.

System	basis	RLDA		GGA		
		Energy[eV]	R[a.u.]	Energy[eV] B88/P86	Energy[eV] PW91/PW91	R[a.u.]
$HgAu_9$	A	-.60	5.0	-.10	-0.18	5.3
$112Au_9$	A	-.67	5.2	-.15	-0.23	5.5
$HgAu_{13}$	A	-.95	5.0	-.36	-.45	5.2
$112Au_{13}$	A	-.83	5.1	-.28	-.34	5.5
$HgAu_{14}$	min basis	-0.38	5.6	-0.05	-0.12	6.4
$112Au_{14}$	min basis	-0.31	5.9	-0.03	-0.11	6.9
$HgAu_{14}$	A	-.86	5.0	-.27	-.36	5.2
$112Au_{14}$	A	-.75	5.2	-.20	-.29	5.6
$HgAu_{14}$	B	-.85	5.0	-.29	-.37	5.2
$112Au_{14}$	B	-.77	5.2	-.22	-.31	5.6
$HgAu_{34}$	A	-.95	5.1	-.39	-.52	5.2
$112Au_{34}$	A	-.85	5.2	-.25	-.33	5.2

Table 8.7: The differences ($\Delta E_b = E_b^{Hg} - E_b^{112}$) in the binding energies for XAu$_n$ clusters, for $n = 9$, 13, 14 and 34 for the top position and cluster method.

System	basis	Energy[eV]		
		RLDA	B88/P86	PW91/PW91
XAu$_9$	A	.07	.05	0.05
XAu$_{13}$	A	-.12	-.08	-.11
XAu$_{14}$	min basis	-.07	-.02	-.02
XAu$_{14}$	A	-.11	-.07	-.07
XAu$_{14}$	B	-.08	-.07	-.06
XAu$_{34}$	A	-.10	-.14	-.19

Figures 8.6 and 8.7 show that there is no significant difference between basis A and B. For reference and comparison with the dimer calculations, the potential energy curves for the same systems where determined in the case in which the basis sets contain only the atomic orbitals corresponding to the minimal basis. From the dimer calculations it was evident that such a basis is too poor for leading to reliable results neither for the binding energy nor for bond length. The aim is to evaluate the way in which the improvement induced by the optimization of the basis varies from dimers to bigger systems. First of all on notes a remarkable concordance in the RLDA values for the bond distance, i.e. the minimum of the binding energy is found to be as follows:

- for the minimal basis at 5.5 a.u for the HgAu dimer and at 5.6 for the HgAu$_{14}$ system, respectively at 5.9 a.u. for the 112Au dimer and at 5.9 a.u. for the 112Au$_{14}$ cluster.
- for the optimized basis sets the corresponding values are 4.9 a.u. and 5.0 a.u. for Hg, and 5.0 a.u. and 5.2 a.u. for element 112.

This outcome indicates that the interaction between the adsorbate and surface cluster is mainly with the Au atom atop of which the ad–atom is adsorbed. The binding energies are about 0.6 eV larger for the optimized basis for dimers, and about 0.46 eV larger in the case of XAu$_{14}$ systems. These differences have two principle reasons:

- firstly the interaction between the adsorbate atom with the next four substrate metal atoms in the first layer,
- and secondly, an indirect effect, the interaction between the Au–atom with its neighbours (mainly with the four nearest atoms in the first layer and the four neighbours in the second layer).

These results stress again the importance of the quality of the basis used for the expansion of the molecular orbitals. One improvement which can be done is to enlarge to basis sets. Since the use of such extension for the Au atoms would lead in a very large increase in the computation time, it remains only the possibility to keep a reduced basis for the cluster atoms and to increase the number of functions for the adsorbate only. This was done as described above for basis type B'. The results in table 8.8 indicate that the effect

of an enlarged basis consists in a deeper binding energy, but the difference in the binding energy is practically equal to that obtained for the basis B.

Table 8.8: Binding energies (RLDA) for the $XAu_{14}(9,4,1)$ clusters, when different basis sets are used keeping the distance between the adsorbate and the $Au_{14}(9,4,1)$ cluster constant.

System	Binding energy [eV]			R
	basis A	basis B	basis B'	[a.u.]
$HgAu_{14}(9,4,1)$	-0.86	-.85	-.91	5.0
$112Au_{14}(9,4,1)$	-0.75	-.77	-.85	5.2

More information regarding the details of the chemical bond can be obtained from the analysis of the differential (or partial) crystal orbital overlap population (PCOOP) diagrams for the outer electronic shells of Hg and element 112. Figures 8.11 and 8.12 show the bonding and anti-bonding components of the occupied $(n-1)d_{3/2}$, $(n-1)d_{5/2}$ and $ns_{1/2}$ valence orbitals as well as those included in the extended basis B' for Hg and element 112. The analysis refers to the $XAu_{14}(9,4,1)$ clusters, and corresponds to the binding energies shown in table 8.8. Decisive for the bonding character is the balance between the occupation of bonding and anti-bonding orbital fragments. Thus the PCOOP for the unoccupied $(n-1)d_{3/2}$, $(n-1)d_{5/2}$ and $ns_{1/2}$ atomic orbitals are drawn separately in figure 8.10

First one remembers that in element 112, due to the relativistic effects, the $7s_{1/2}$ is strongly contracted and stabilized, being situated between the two $6d$ levels (closer to $6d_{3/2}$). For this reason one expects for the $7s_{1/2}$ and $6d_{3/2}$ AO to contribute in a similar way to the bonding. The diagram 8.10 confirms this anticipation showing that both orbitals contribute to the binding in the lower energy part of the valence band and occupy anti-bonding fragments in the upper part of it. The bonding part of the PCOOP spectrum of the $6d_{5/2}$ is wider than the corresponding part of the $7s_{1/2}$ and $6d_{3/2}$, the occupation of the bonding orbital fragments being maximal in the middle of the valence band.

In comparison, the relativistic effects in Hg don't lead to an inversion between $6s_{1/2}$ and $5d_{5/2}$ levels so that the former one will lie above the later one. Therefore these two AO have a similar distribution along the energetic spectrum, the occupation of the bonding orbital fragments being maximal toward the middle of the valence band, and above the region in which the $5d_{3/2}$ contributes in a constructive way to the bonding.

As it already was pointed out, in establishing the character of a certain contribution, the occupation of anti-bonding orbital fragments is also important. From figures 8.10 one notices that $5d_{3/2}$ of Hg and $6d_{3/2}$ of element 112 both have bonding parts occupied and the anti-bonding parts almost occupied, hence they do not contribute practically to
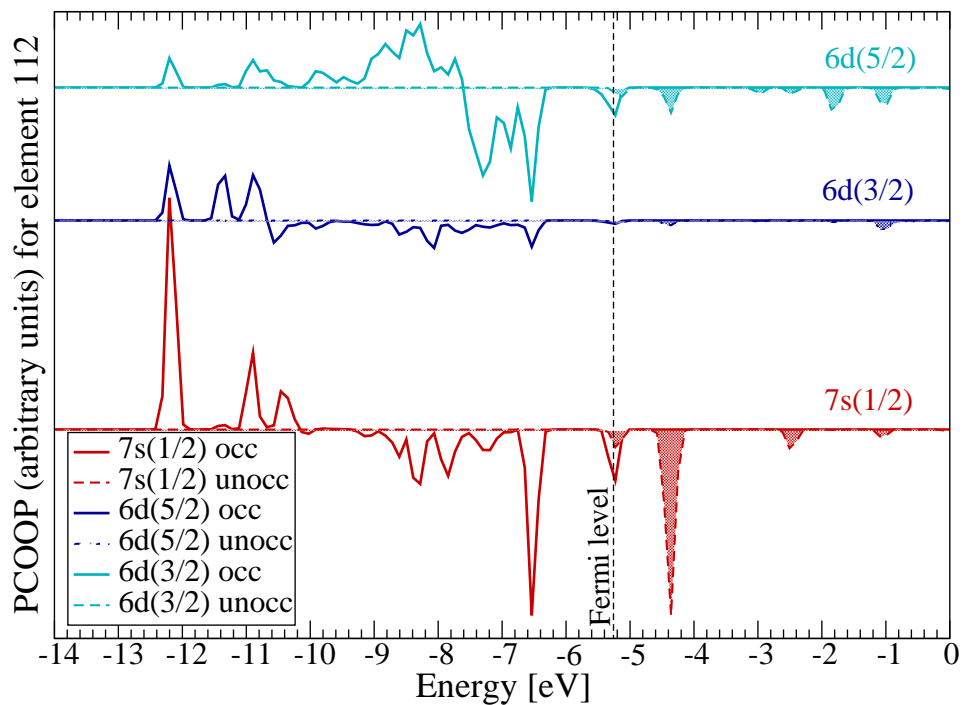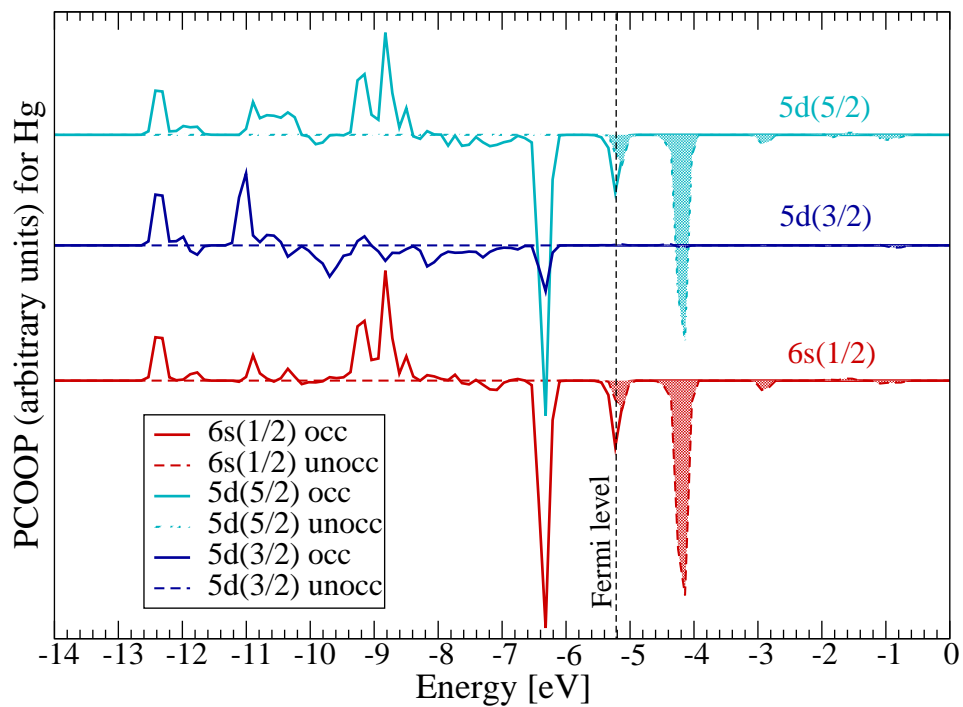
Figure 8.10: The partial crystal overlap population (PCOOP) of occupied and unoccupied states for the valence orbitals of Hg and element 112 in a $XAu_{14}(9,4,1)$ cluster (basis B', cluster method).
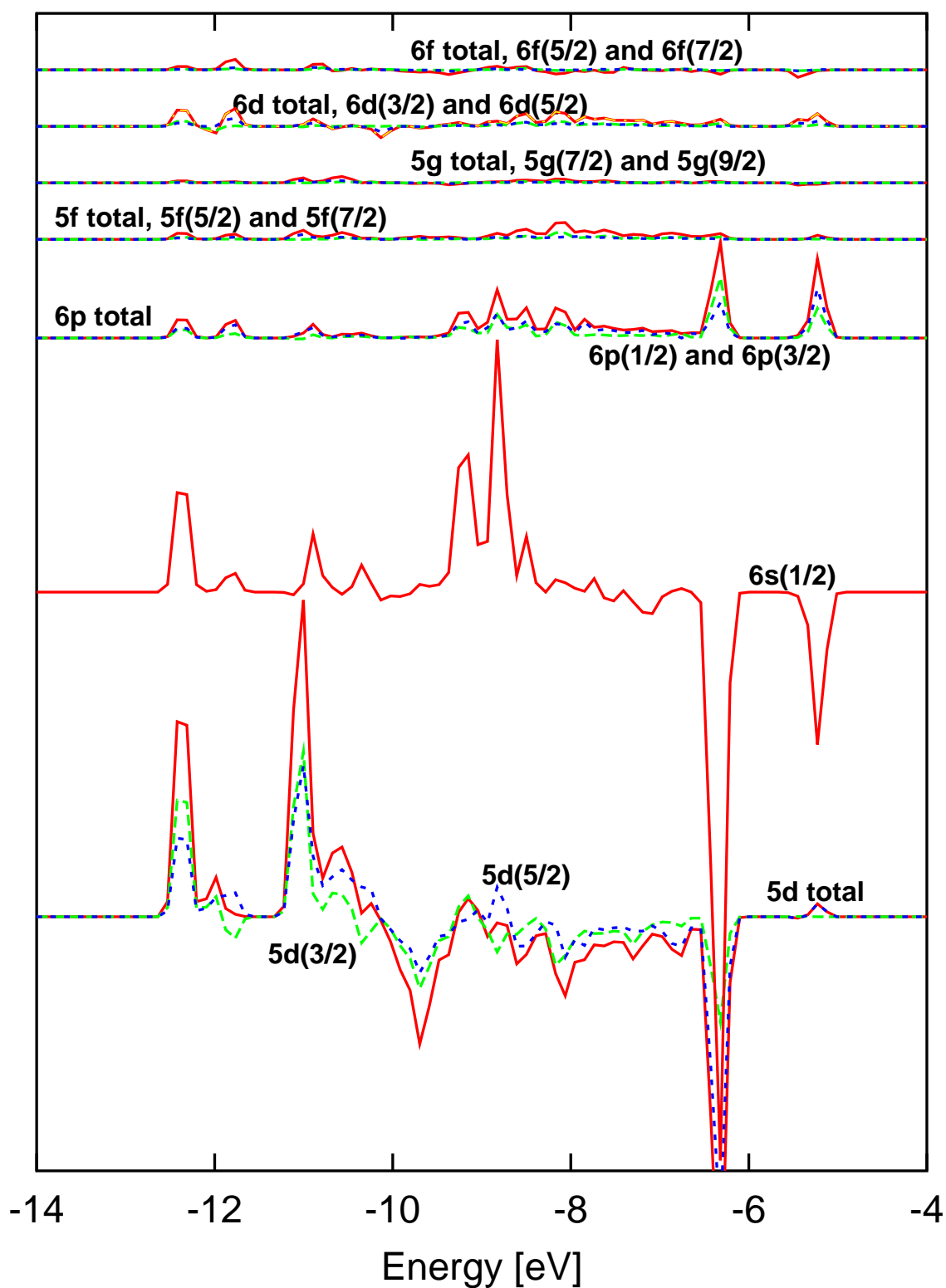
PCOOP for Hg

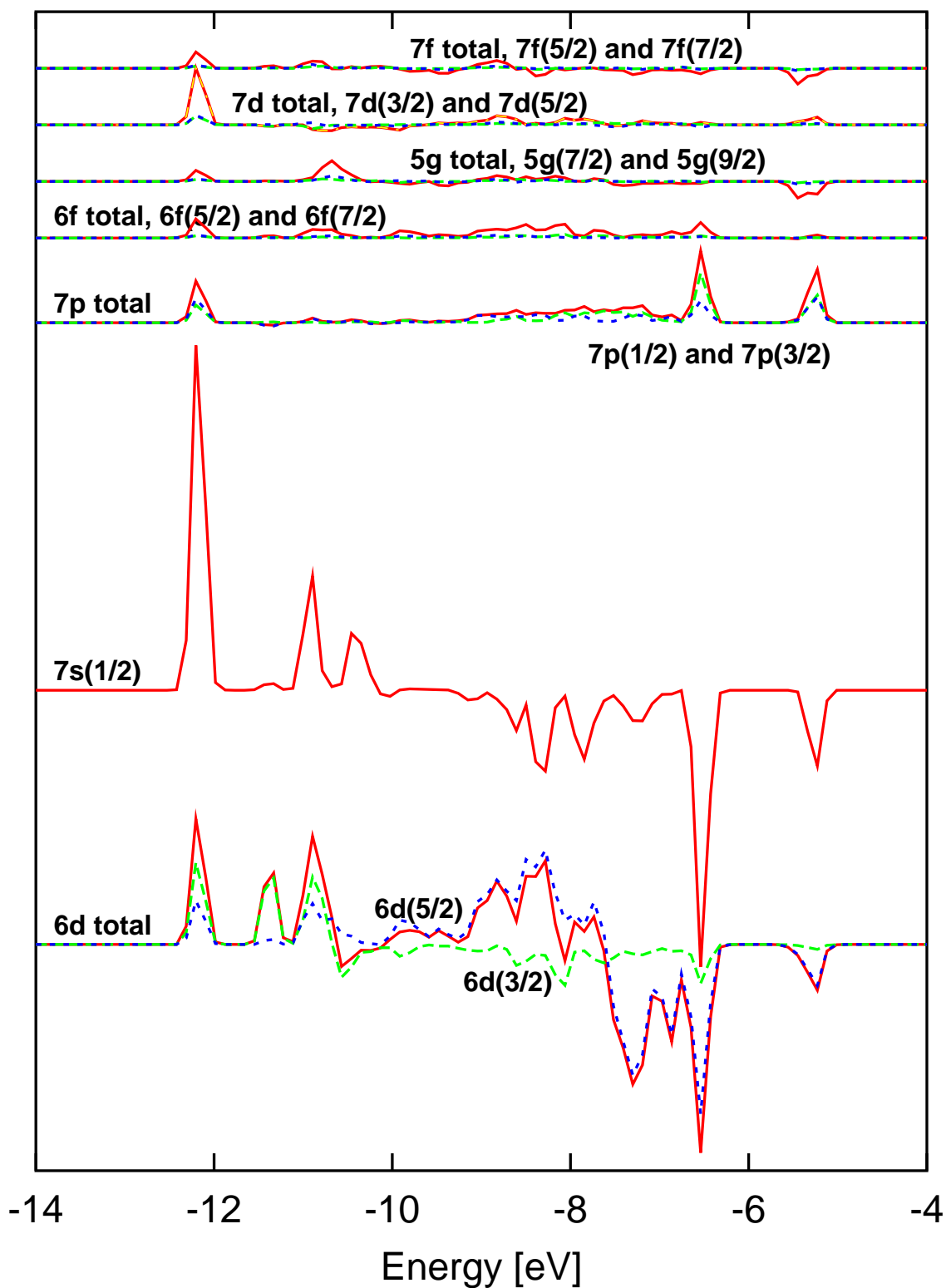Figure 8.11: The partial crystal overlap population for element Hg in a HgAu$_{14}$ cluster for the on-top site, when the basis B' is used (cluster method).

Figure 8.12: The partial crystal overlap population for element 112 in a $112Au_{14}$ cluster for the on-top site, when the basis B' is used (cluster method).

the binding. The Mulliken analysis gives an effective charge of 3.988 for $5d_{3/2}$(Hg) and 3.978 for $6d_{3/2}$(element 112), respectively. One notices that the bonding fragments for (n-1)$d_{5/2}$ and n$s_{1/2}$ are not completely occupied, corresponding to a transfer of charge from these levels to the orbitals which are not occupied in the ground state of a free atom (the additional np to nf functions). The Mulliken analysis indicates that the transfer of charge is bigger for $6s_{1/2}$ than for $5d_{5/2}$ in the case of Hg (the corresponding effective charges being 1.75 and 5.97, respectively), whereas for element 112 the two most outer shells are equal deprived of electronic charge ($q_{eff}(7s_{1/2})$=1.89 and $q_{eff}(6d_{5/2})$=5.90).
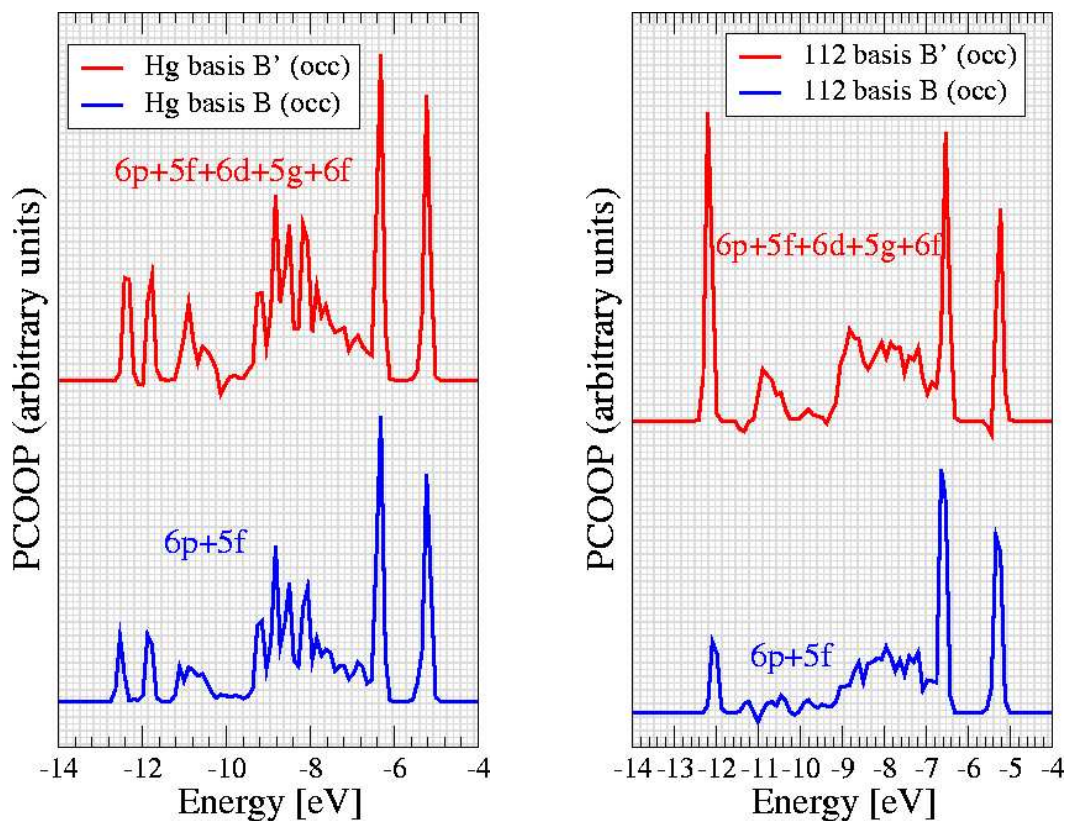
Figure 8.13: The partial crystal overlap population (PCOOP) of occupied states for the additional orbitals in the basis sets of Hg and element 112 in a XAu_{14}(9,4,1) cluster (basis B', cluster method).

Figures 8.11 and 8.12 show the proportion to which the additional optimized atomic functions influence the interaction between the adsorbate and cluster. One notice that the main contribution to the binding comes from the additional 6p–type functions for Hg and from 7p–type functions in the case of element 112. However, the way in which these participate to the binding is quite different: one have a more uniform distribution for 6p(Hg) than for 7p(element 112), the later one giving a contribution to the overlap population mainly on the extremities of the valence band. The next 5f(Hg) and 6f(element 112) behave quite similarly and spread over the entire valence energy band. One important difference is given by the 5g–type functions which contribute to the overlap population for element 112, but weaker in the case of Hg. It is interesting to make
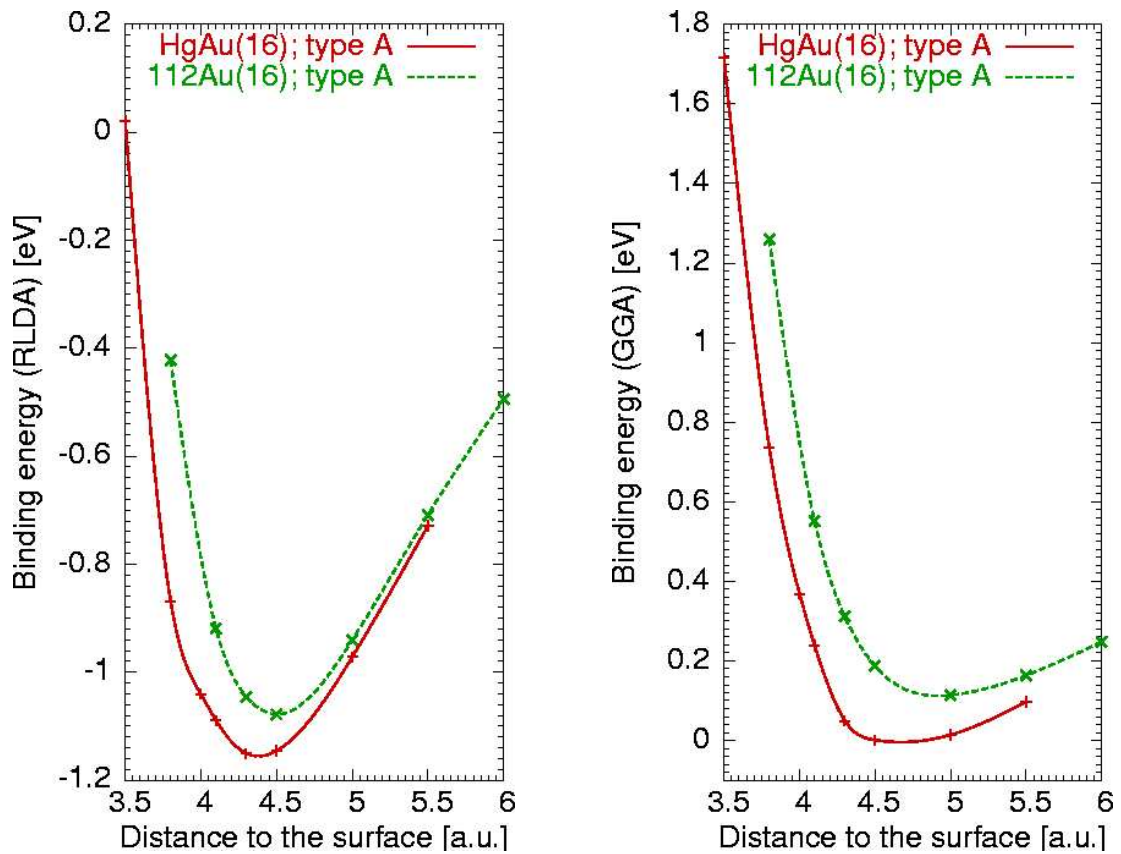
Figure 8.14: The potential energy curves (RLDA and GGA) for the adsorption of Hg and element 112 on different Au clusters for the bridge position.

a comparison between the contributions of the optimized basis functions to the COOP for two different basis sets. This is done in figure 8.10 and one immediately remark that the main difference appears in the law energy part of the spectrum for both kinds of ad–atoms.

For the larger clusters $XAu_{34}(13,12,4,5)$ one obtains a RLDA value of -0.95 eV for the binding energy of Hg and -0.85 eV for element 112, which gives a difference of 0.1 eV between the values corresponding to these elements. The difference of about 0.2 eV for the GGA values is due to the fact that it was not calculated the entire potential energy curves for both elements, and the GGA bond lengths are larger than the RLDA ones. The analysis of the RLDA energy potential curves (see figure 8.6) gives a bond length of 5.1 a.u. for Hg, and a value of 5.2 a.u. for element 112.

8.3.2 Adsorption on the bridge position

The bridge position corresponds to an adsorption of the adsorbate on a two–fold site, as shown in figure 8.3.

The Hg is found to stabilize at a distance of 4.3 a.u relative to the surface, i.e. 5.09 a.u. away from the nearest Au atoms. For element 112 the bond length relative to

Table 8.9: The total and binding energies for the bridge position, cluster method. (Basis type A was used.)

System	RLDA		GGA		
	Energy[eV]	R[a.u.]	Energy[eV] B88/P86	Energy[eV] PW91/PW91	R[a.u.]
$Au_{16}Hg$	-1.15	4.3	.01	-0.07	4.5
$Au_{16}112$	-1.08	4.5	.11	0.02	4.8

the surface is found to be 4.5 a.u., which corresponds to a distance of 5.26 a.u. to the nearest substrate atoms. These values are again close to that obtained for the dimer bond lengths and for the top position.

Table 8.9 shows that for the clusters $XAu_{16}(8,6,2)$ the binding energies have the highest value, namely -1.15 eV for Hg and -1.08 for element 112. This again show a small difference of 0.07 eV in the binding energies, as follows from the table 8.10. One should remark that the GGA value are not bound.

Table 8.10: The differences ($\Delta E_b = E_b^{Hg} - E_b^{112}$) in the binding energies for the bridge position, cluster method. (Basis type A was used.)

System	Energy[eV]		
	RLDA	B88/P86	PW91/PW91
$Au_{16}X$	-.07	-.10	-0.09

8.3.3 Adsorption on the hollow position

The adsorption on the four–fold site was considered for $XAu_9(4,5)$ and $XAu_{22}(12,5,4,1)$ clusters. The potential energy curves in figure 8.15 show that, by increasing the size of the cluster, the bond lengths changes 3.5 a.u. to 3.8 a.u. for Hg, and from 3.8 a.u. to 4.0 a.u. for element 112. This corresponds to an enlargement of the distance between the adsorbate and the nearest substrate atom (denoted by 1 in figure 8.2) from 5.2 a.u. to 5.41 a.u. for Hg, and from 5.41 a.u. to 5.55 a.u. for element 112.

Moreover, the values on table 8.11 show a different trend in the binding of the two species, element 112 being stronger bound than Hg. It follows that either the cluster is too small, and the polarization of the cluster has as consequence a different behaviour of the system relative a solid either the hollow position is not preferred for the adsorption. The results obtained for the embedded cluster method suggest that the first one is the reason for these effect.
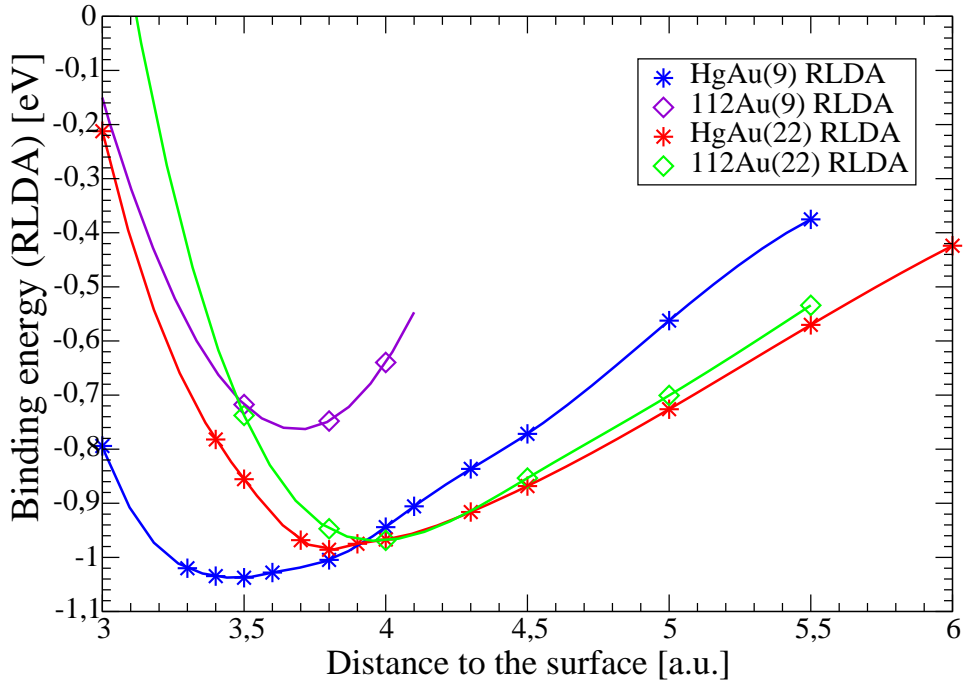
Figure 8.15: The potential energy curves (RLDA) for the adsorption of Hg and element 112 on different Au clusters on the hollow position .

Table 8.11: The total and binding energies for the hollow position, cluster method. (Basis type A was used.)

System	RLDA		GGA		
	Energy[eV]	R[a.u.]	Energy[eV] B88/P86	Energy[eV] PW91/PW91	R[a.u.]
$HgAu_9$	-1.04	3.5	-.08	-.19	4.5
$112Au_9$	-.99	3.8	-.05	-.16	5.0
$HgAu_{22}$	-.75	3.8	.32	.18	4.0
$112Au_{22}$	-.97	4.0	-.17	-.19	5.0

Table 8.12: The differences ($\Delta E_b = E_b^{Hg} - E_b^{112}$) in the binding energies for the hollow position, cluster method. (Basis type A was used.)

System	Energy[eV]		
	RLDA	B88/P86	PW91/PW91
Au_9X	-.05	-.03	-.03
$Au_{22}X$	.22	.49	.37

Chapter 9

Embedding calculations

The embedded cluster method was described in chapter 5. All three possible adsorption sites were taken in the account: top, bridge and hollow position. Calculations were performed for cluster of moderate size in the embedding environment. The biggest systems considered are shown in figure 9.1.

9.1 Unperturbed surface clusters

At first the Mulliken analysis is done, for both the unperturbed systems and the systems with adsorbate, the effective electric charge is written down in tables 9.1 and 9.2.

Table 9.1: Mulliken charge of the surface-metal atoms of different clusters used in the study of adsorption on the top position when embedded cluster method is used.

basis	system	Bl.1	Bl.2	Bl.3	Bl.4	Bl.5	Bl.6	Bl.7	Bl.8	Bl.9
min	Au_{14}	78.90	78.81	79.01	79.09	79.15				
opt	Au_{14}	78.94	78.86	79.01	79.03	79.16				
min	Au_{34}	78.83	78.83	78.95	78.92	78.84	79.06	79.11	78.97	79.12
opt	Au_{34}	78.81	78.83	78.88	78.97	78.78	79.04	79.09	79.10	79.11

Table 9.2: Mulliken charge of the surface-metal atoms of different clusters used in the study of adsorption on the bridge and hollow position when embedded cluster method is used.

basis	position	system	Bl.1	Bl.2	Bl.3	Bl.4	Bl.5	Bl.6
opt (B)	bridge	Au_{16}	78.79	78.99	79.03	78.90	79.07	79.14
min	hollow	Au_{22}	78.77	78.89	78.98	79.08	79.08	79.14
opt (B)	hollow	Au_{22}	78.83	78.76	79.04	79.04	79.06	79.20

As it is evident from these data, the polarization of the cluster is still present. The reason is the way in which the occupation of the orbitals for the atoms in the environment was obtained. One remembers that an average procedure on the orbital occupations
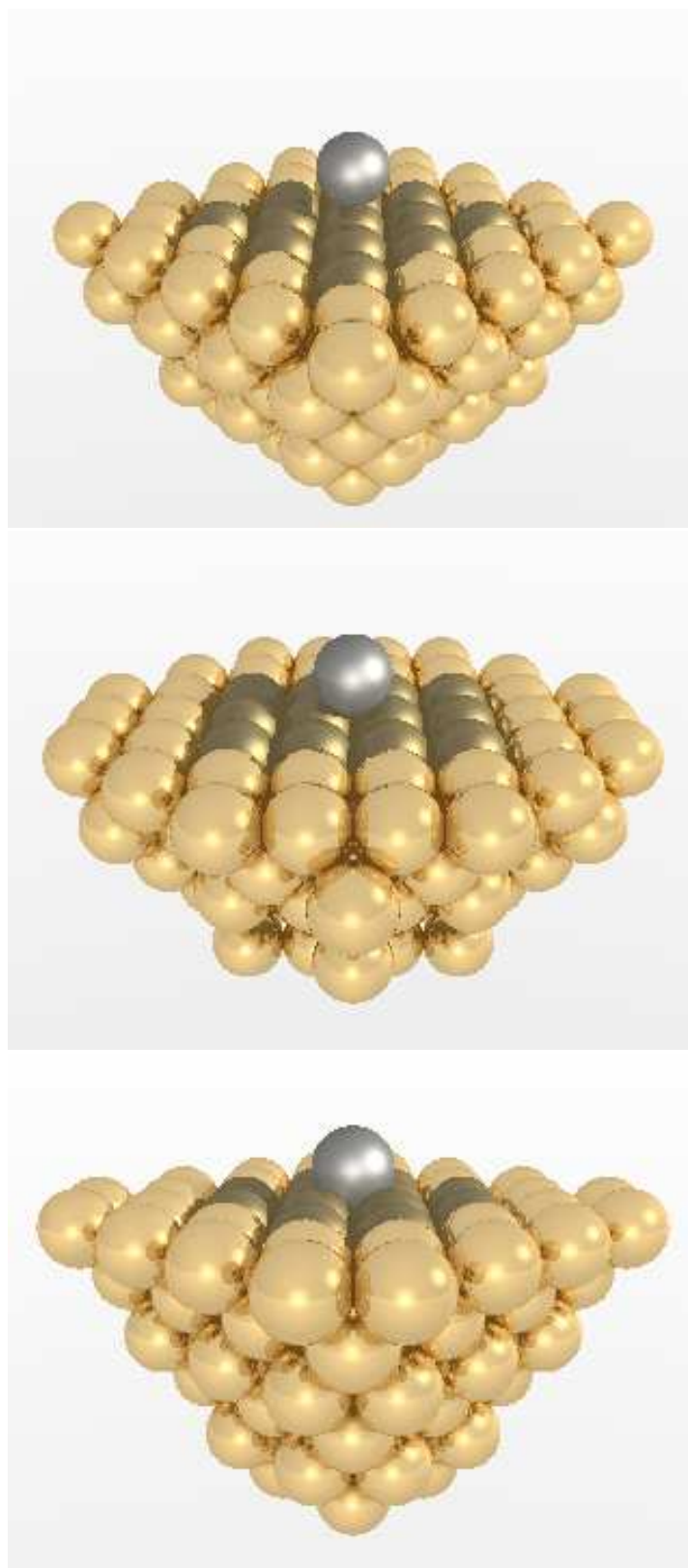
Figure 9.1: The representation of the biggest clusters used in the embedding method: top—Au_{34} cluster embedded in 109 Au atoms (top position), middle—Au_{16} embedded in 110 atoms (bridge position) and bottom—Au_{22} cluster embedded in 92 Au atoms (hollow position) .

in the Au–cluster was done in every iteration, which means that at the end all the "atoms" in the environment have the same occupation. In this situation there is no distinction in the way in which the atoms on the surface and in the bulk are treated in the environment system. This is not the case in a semi–infinite metal. However an average of the occupations of the orbitals in atoms belonging to the same layer is not possible. The reason is that during the self-consistent calculations there is a charge transfer between the atoms belonging to the same layer as well as between atoms belonging to different layers. As a result the effective charge of different layers are nonzero. If one would use the average charge of them for describing the atoms in the environment the result will be an artificial ionization of the surrounding system. Nevertheless our procedure has proven to give very good results when it was applied to other systems [57, 58, 66] .
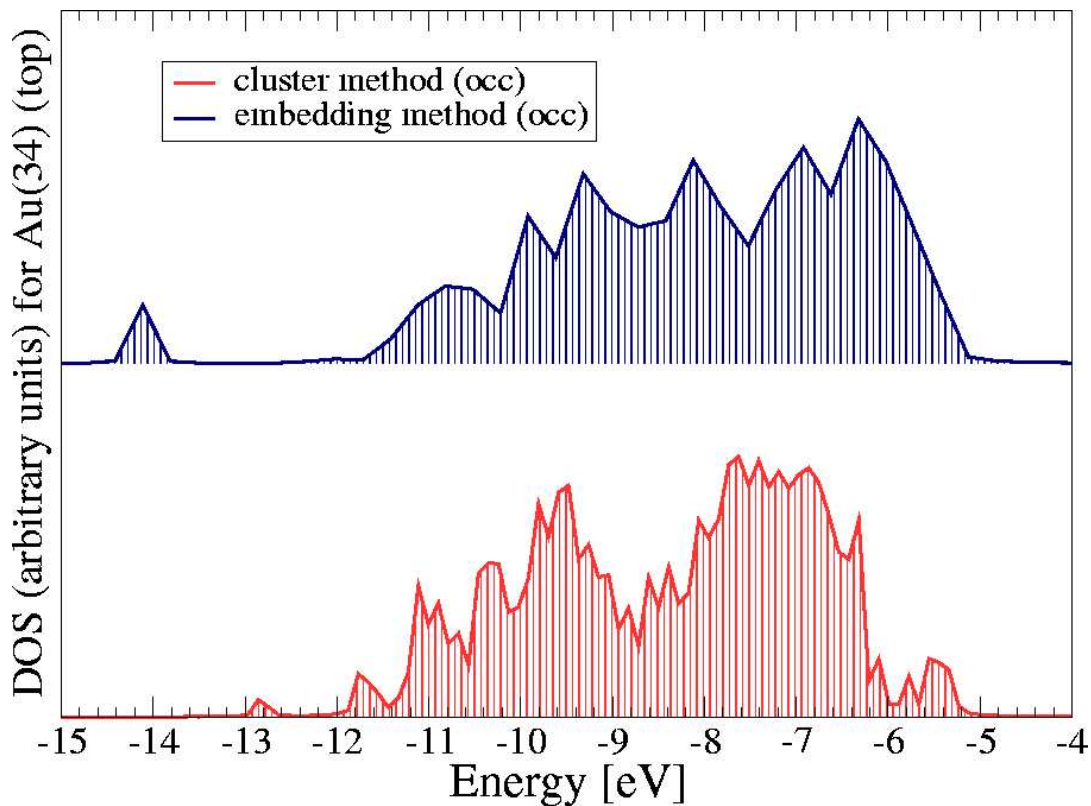
Figure 9.2: The total density of states for the occupied states in a Au_{34} system for the on-top site, when the basis B is used.

Other important information about the effect of the environment on the inner system is given by the DOS diagrams. Figure 9.2 displays the total DOS for a Au_{34} cluster for the two methods. At the first site one remarks that for the embedding method the distribution of the occupied states inside the valence band is more uniform than for the cluster method. Another aspect which may be observed is the increase of the gap between the valence band and the peak which lies below it. The analysis of the expansion coefficients of the molecular orbitals situated in that peak reveals that they are composed essentially from $6s$ atomic orbitals from all the atoms in the cluster.

9.2 Adsorption of element 112 and Hg on the embedded Au_n clusters

9.2.1 Adsorption on the top position

For the adsorption on-top of a Au surface–atom, calculations were performed for XAu_{14} and XAu_{34} systems. In both cases two types of basis sets were used: minimal basis and optimized basis B (described in chapter 7). The first type of basis was used with the aim to check how the lack of completeness of the basis is affected by the presence of the surrounding cluster.

The Mulliken analysis in table 9.3 shows that both elements stabilize as negative ions. The effective charge of Hg has a value between 79.60 and 79.65, slightly depending on the size of the system and the type of basis. For element 112 on have $111.79 \leq q_{eff} \leq 111.83$. One notice that the transfer of charge from the adsorbate to the surface-cluster is much bigger for Hg than for element 112. There is another interesting feature to be mention. There is a difference in which the enlargement of the basis influence the transfer of charge: this quantity is slightly larger for minimal basis than for the optimized basis set in the case of Hg, and slightly smaller for element 112. For both system the increase in the size of the inner cluster leads to an increasing in the charge transfer, which finally results in in increase in the binding energy.

Table 9.3: Mulliken charge of the ad-atom and the surface-metal atoms of different clusters used in the study of adsorption on the top position when embedded cluster method is used.

basis	system	Metal	Bl.1	Bl.2	Bl.3	Bl.4	Bl.5	Bl.6	Bl.7	Bl.8	Bl.9
min	$HgAu_{14}$	79.62	78.93	78.92	79.01	79.12	79.16				
opt	$HgAu_{14}$	79.60	78.97	78.88	79.03	79.08	79.15				
min	$112Au_{14}$	111.79	78.92	78.86	79.01	79.11	79.16				
opt	$112Au_{14}$	111.82	78.95	78.83	79.02	79.06	79.16				
min	$HgAu_{34}$	79.65	78.93	78.86	78.94	78.94	78.83	79.07	79.11	78.97	79.12
opt	$HgAu_{34}$	79.64	78.91	78.85	78.89	78.99	78.77	79.05	79.09	79.10	79.11
min	$112Au_{34}$	111.80	78.88	78.86	78.94	78.94	78.83	79.07	79.11	78.97	79.12
opt	$112Au_{34}$	111.83	78.84	78.84	78.89	78.98	78.77	79.05	79.09	79.10	79.11

Another aspect which we are interested in is the way in which the Mulliken charge of different substrate–atoms change in the presence of the adsorbate. The data in table 9.3 show that in the case of XAu_{14} systems the main changes occur in the effective charge of the atoms in blocks 1, 2 and 4, i.e. for the atoms in the first layer. For the XAu_{34} systems the main changes are also for the atoms in blocks 1, 2 and 4. There are also some very small changes in the atoms in blocks 3 and 5 (second layer), whereas the effective charge of the atoms in blocks 6, 7, 8 and 9 (outer atoms in the second layer and the atoms in the third and fourth layers) is practically unchanged.

Table 9.4: The total and binding energies for the top position, embedded cluster method. (Basis B type was used.)

System	RLDA		GGA		
	Energy[eV]	R[a.u.]	Energy[eV] B88/P86	Energy[eV] PW91/PW91	R[a.u.]
$Au_{14}Hg$ (min bas)	-1.09	5.2	-.57	-.66	5.5
$Au_{14}112$ (min bas)	-.67	5.5	-.25	-.34	5.9
$Au_{14}Hg$ (opt bas)	-1.80	4.8	-1.15	-1.25	5.0
$Au_{14}112$ (opt bas)	-1.28	5.1	-.66	-.75	5.3
$Au_{34}Hg$ (min bas)	-.78	5.0	-.18	-.29	5.0
$Au_{34}112$ (min bas)	-.38	5.1	.23	.13	5.1
$Au_{34}Hg$ (opt bas)	-1.66	5.0	-1.01	-1.12	5.0
$Au_{34}112$ (opt bas)	-1.22	5.1	-.52	-.62	5.1

The potential energy curves (RLDA as well as GGA) for these systems are displayed in figure 9.3. The main effect of the environment is reflected in the values of the binding energy, the adsorbate being much stronger bound in comparison with the cluster method. For the minimal basis results two aspects are remarkable:

- firstly, already mentioned above, unlike the results in table 8.6, the GGA values, although too small, become bound.
- secondly, there is a significant change in the bond length, the new values (5.2 a.u. for Hg and 5.5 a.u. for element 112) are much closer to the values obtained with extended basis sets.

When optimized basis are used, the position of the RLDA bond distance is 4.8 a.u. for Hg on Au_{14} cluster and 5.0 a.u. on Au_{34} cluster. The value of the RLDA bond length for $112Au_n$ seems to be more stable, being the same (5.1 a.u.) for n=14 and n=34.

Our main aim is to study the relative behaviour of these two elements, i.e. how strong the element 112 will be bound in comparison with his homologue in the Periodic System. To this aim the difference in the binding energies was calculated and is shown in table 9.5. The values of $\Delta E_b = E_b^{Hg} - E_b^{112}$ is four or even five times larger than the values given by the cluster method (see table 8.7). To see from where this big changes come, calculations were performed with more extended basis sets (type B'), constructed as indicated in section 8.3.

Table 9.6 gives the binding energies for Hg and element 112 on an embedded Au_{14} cluster, for two types of optimized basis, B and B', the first one being poorer than the later one. It can be seen that the quality of the basis sets is important for both the binding energy values and for the differences of these binding energies (ΔE_b). These quantities were determined only for the distances of the adsorbate to the surface corresponding to the minimum of the RLDA potential energy curves. For the most complete complete basis (B'), $\Delta E_b = -0.2$ eV, in comparison with -0.06 eV obtained with the cluster method.
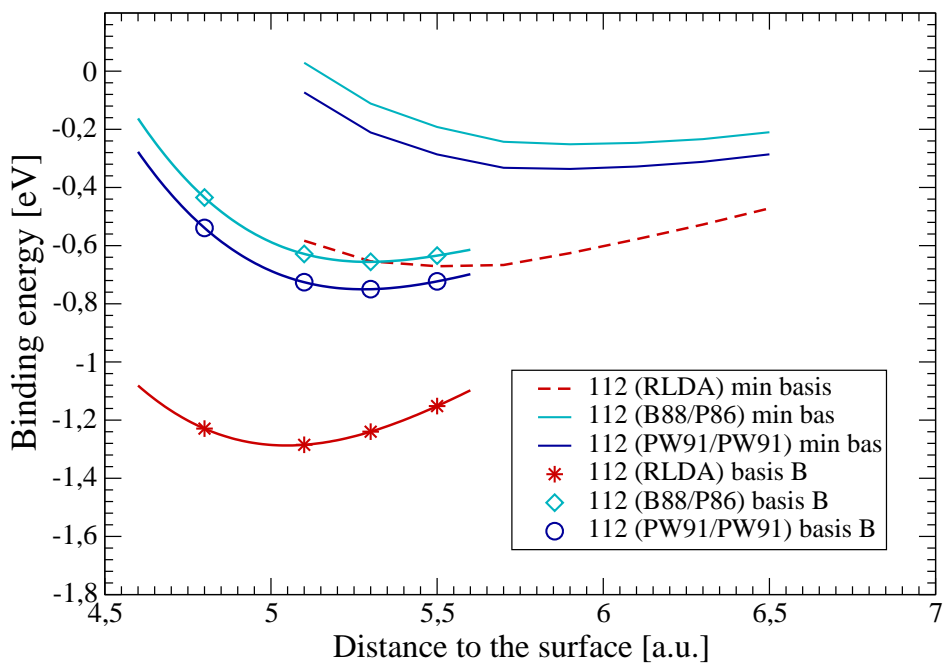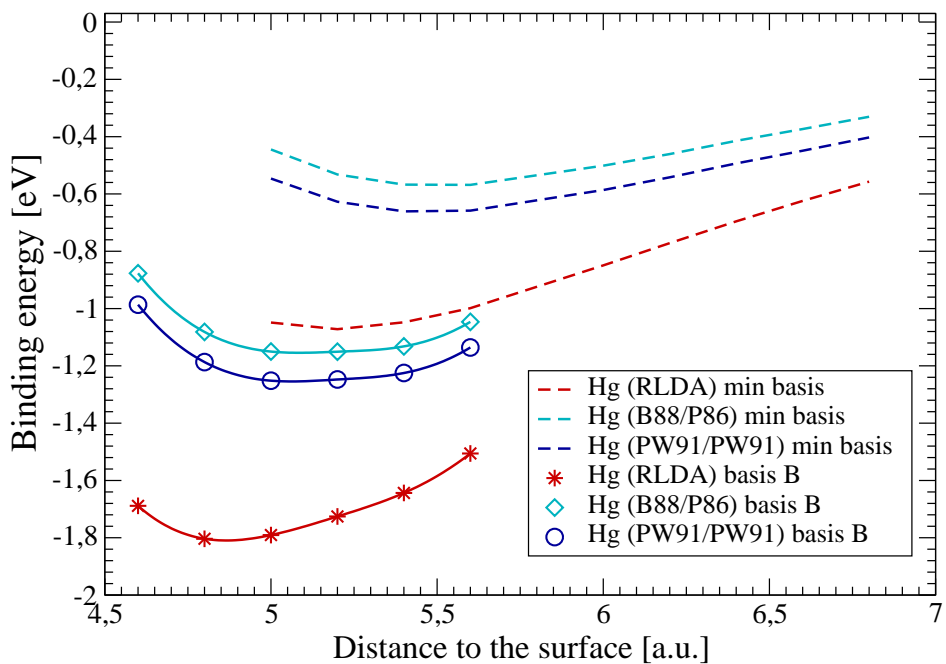
70

Figure 9.3: The potential energy curves for the HgAu$_{14}$ and 112Au$_{14}$ systems for the on-top site, embedding method, when the basis B is used.
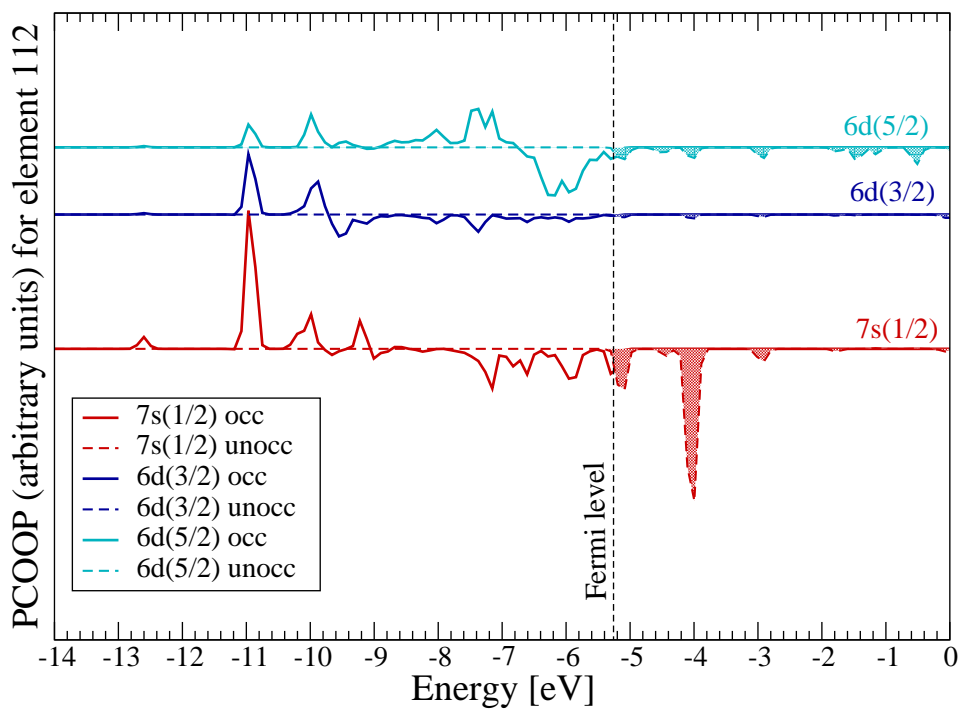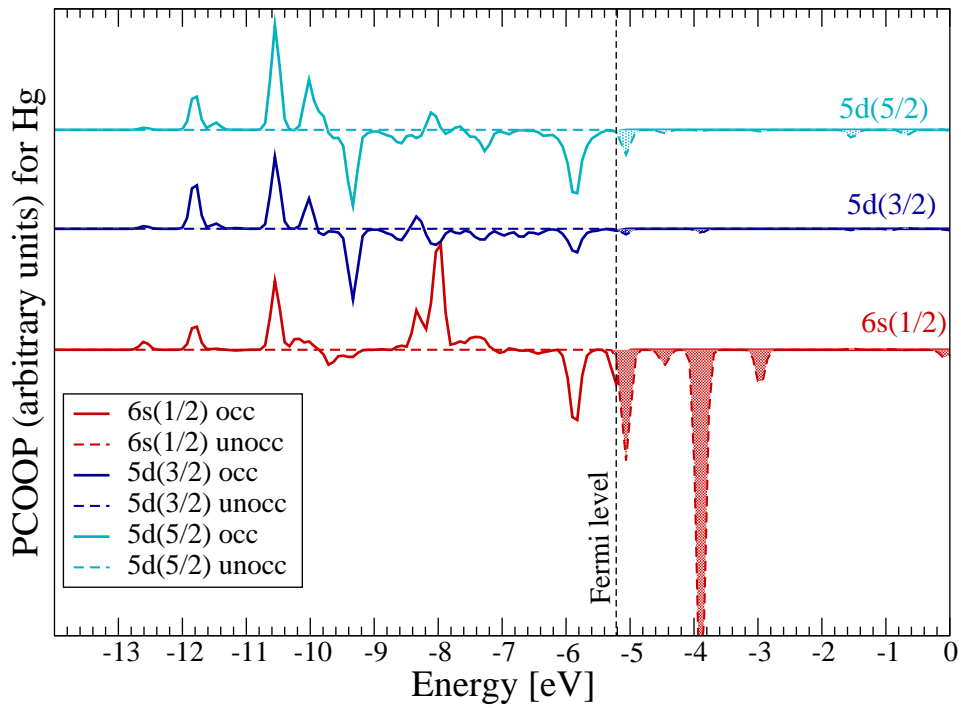
Figure 9.4: The partial crystal overlap population (PCOOP) for the occupied and unoccupied states for the valence orbitals in an embedded XAu$_{14}$ system for the on-top site, when the basis B' is used.

Table 9.5: The differences $(\Delta E_b = E_b^{Hg} - E_b^{112})$ in the binding energies for the top position, embedded cluster method. (Basis B type was used.)

System	Energy[eV]		
	RLDA	B88/P86	PW91/PW91
$Au_{14}X$ (min bas)	-.42	-.32	-.32
$Au_{14}X$ (bas B)	-.52	-.49	-.50
$Au_{34}X$ (min bas)	-.40	-.41	-.41
$Au_{34}X$ (bas B)	-.44	-.49	-.50

Table 9.6: Binding energies (RLDA) for the $XAu_{14}(9,4,1)$ clusters, when different basis sets are used keeping the distance between the adsorbate and the $Au_{14}(9,4,1)$ cluster constant.

System	Binding energy [eV]		R
	basis B	basis B'	[a.u.]
$HgAu_{14}(9,4,1)$	-1.80	-2.16	5.0
$112Au_{14}(9,4,1)$	-1.28	-1.96	5.2

Further information may be obtained from the analysis of PCOOP diagrams, 9.4. Because of the external potential produced by the environment, there is a moving of the Fermi level (ϵ_F) towards lower values. In order to make a comparison possible with the corresponding diagrams for the cluster method, the plots in figure 9.4 were drawn after the alignment of ϵ_F was done.

First we remark a decreasing of the occupation of the anti-bonding states for both ns valence orbitals. The contribution to the binding of $6s_{1/2}$ for Hg is higher than that of $7s_{1/2}$ for element 112. Moreover the occupied states for $6s_{1/2}$(Hg) are more spread along the energy spectra occupying 2/3 of the valence band, whereas the $7s_{1/2}$(element112) lies only in the left-hand side half part of the corresponding band. This is in agreement with the Mulliken analysis which give an effective charge of 1.50 for Hg and 1.83 for element 112. When one compares these values with $q_{eff}^{Hg}(6s_{1/2}) = 1.75$ and $q_{eff}^{112}(7s_{1/2}) = 1.89$ from the cluster method, it can be seen that $6s_{1/2}$(Hg) was more sensitive to the changes induced by the surrounding than $7s_{1/2}$(element112). This is not unexpected since the first is the highest occupied level in the isolated atom, whereas $7s_{1/2}$ is energetically situated between $6d_{3/2}$ and $6d_{5/2}$ in the isolated atom.

A second important difference is given by the (n-1)$d_{3/2}$ and (n-1)$d_{5/2}$ of both elements. For element 112 the $6d_{3/2}$ continues to have a similar distribution along the energetic spectrum with $7s_{1/2}$. The main difference of them relative to $6d_{5/2}$ is given by the way in which they contribute in the region around the -7.5 eV in the spectrum. Here $6d_{5/2}$ occupies binding states whereas $7s_{1/2}$ and $6d_{3/2}$ occupy anti-bonding states.

In the case of Hg the similarity in the distribution of $5d_{5/2}$ and $6s_{1/2}$ (observed in the cluster-method results) almost disappear. The Mulliken analyses gives $q_{eff}^{Hg}(5d_{3/2}) =$

Table 9.7: Mulliken charge of the adsorbate and the surface-metal atoms of different clusters used in the study of adsorption on the bridge and hollow position when embedded cluster method is used.

basis	position	system		Bl.1	Bl.2	Bl.3	Bl.4	Bl.5	Bl.6
opt (B)	bridge	HgAu$_{16}$	79.56	78.80	79.05	79.07	78.90	79.10	79.15
opt (B)	bridge	112Au$_{16}$	111.79	78.74	79.03	79.06	78.90	79.10	79.14
opt (B)	hollow	HgAu$_{22}$	79.67	78.83	78.76	79.04	79.08	79.07	79.19
opt (B)	hollow	112Au$_{22}$	111.93	78.82	78.78	79.05	79.04	79.06	79.21

3.992 and $q_{eff}^{Hg}(5d_{5/2}) = 5.977$ for embedding method, and $q_{eff}^{Hg}(5d_{3/2}) = 3.989$, $q_{eff}^{Hg}(5d_{5/2}) = 5.973$ for the cluster method.

Another aspect which should be discussed is connected with the peak lying below the continuum valence band (see figure 9.2). None of the valence orbitals of Hg or element 112 interact with MO from that region of the energy spectrum.

9.2.2   Adsorption on the bridge and hollow position

The bridge and hollow position corresponds to adsorption on sites with higher coordination numbers. The Mulliken analysis was done and the effective charges of the atoms in different symmetry blocks (labeled as in figures 8.3 and 8.2) are shown in table 9.7. Both species stabilize as negative ions as follows:

- for the XAu$_{16}$(8,6,2) embedded systems (bridge position) $q_{eff}(Hg) = 79.56$ and $q_{eff}(112) = 111.79$

- for the XAu$_{22}$(12,5,4,1) embedded clusters (four-fold site) $q_{eff}(Hg) = 79.67$ and $q_{eff}(112) = 111.93$

In the case of the two-fold adsorption site, one can see that the distribution of charge in the embedded Au$_{16}$ system slightly differs for the two elements. Thus in the case of Hg, despite of a transfer of charge of 0.44 from the adsorbate to the inner cluster, the effective charge of the two atoms in symmetry block 1 is almost unchanged. The main change in the electronic charge occurs for the atoms in symmetry blocks 2, 3 and 5 which are in contact with th surrounding environment. In the case of element 112 there is a change also in the effective charge of the atoms (labeled by 1 in figure 8.3) with which the adsorbate mainly interact. In the case of the four–fold site, the main change in the effective charge of Au atoms corresponds to the 4-th and 6-th symmetry blocks. For element 112 the induced changes are very small.

For the bridge position calculations were performed only for a distance between adsorbate and surface which corresponded to the bond length obtained for the same system when the cluster method was applied. The corresponding binding energies are shown in table 9.8 together with the minima of the potential energy curves of XAu$_{22}$ systems. The

Table 9.8: The total and binding energies for the bridge and hollow position, embedding method. (Basis B type was used.)

System	RLDA		GGA		
	Energy[eV]	R[a.u.]	Energy[eV] B88/P86	Energy[eV] PW91/PW91	R[a.u.]
$HgAu_{16}$ (opt B)	-1.99	4.3	-1.09	-1.21	4.3
$112Au_{16}$ (opt B)	-1.50	4.5	-.61	-.72	4.5
$HgAu_{22}$ (opt B)	-2.30	3.3	-1.26	-1.44	3.5
$112Au_{22}$ (opt B)	-1.90	4.0	-.88	-1.02	4.4

Table 9.9: The differences ($\Delta E_b = E_b^{Hg} - E_b^{112}$) in the binding energies for the bridge and hollow positions, embedding method. (Basis B type was used.)

System	Energy[eV]		
	RLDA	B88/P86	PW91/PW91
$Au_{16}X$ (opt B)	-.49	-.48	-.49
$Au_{22}X$ (opt B)	-.40	-.38	-.42

difference in the GGA binding energy (see table 9.9) are 0.49 eV for the XAu_{16} and 0.42 eV for the XAu_{22} system, at the same order with those obtained for the top position.

Figures 9.7 display the PCOOP diagrams for the occupied valence orbitals of Hg and element 112, corresponding to the RLDA minimum of the potential energy curves (i.e. $R^{Hg} = 3.3$ a.u., $R^{112} = 4.0$ a.u.). One can see that the strong bond for $HgAu_{22}$ is due mainly to the fact that the occupation of anti-bonding states for $6s_{1/2}$ is important (the two filled dashed peaks on the right of the Fermi level). For element 112 one remarks that the overlap population of both bonding and anti-bonding orbital fragments is quite small. These corresponds to the fact that for a 4.0 a.u. distance relative to the surface, the distance to the nearest neighbours (the atoms in the symmetry block 1 in figure 8.2) is 5.56 a.u. In this case the overlap between the valence orbitals in the basis set of element 112 overlap only weakly with the MO of the embedded Au_{22} cluster considered as a separate system.

Figures 9.6 evince that the region of the total DOS of states probed by Hg lies in low energy part of the valence band, whereas for element 112 it stand most on the middle part of these band.
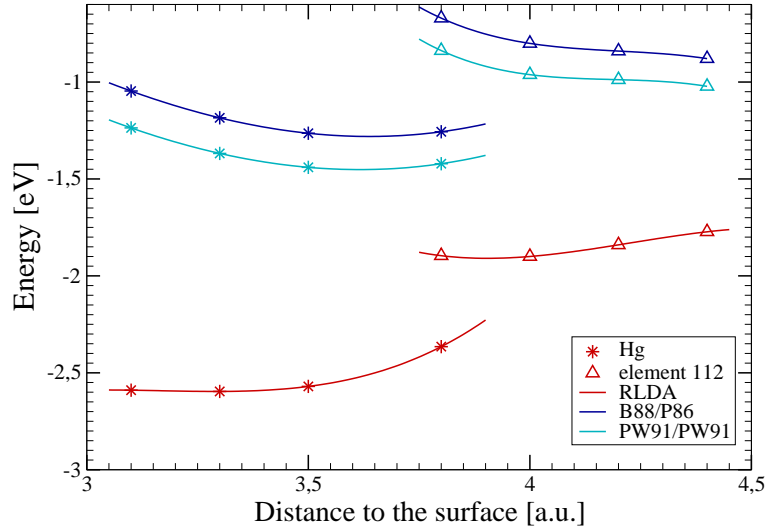
Figure 9.5: The RLDA and GGA binding energies for the XAu_{22} embedded systems.

9.3 Comparison of the cluster and embedding method results

Figures 9.8, 9.9 and 9.10 display the binding energies of different XAu_n systems as a function of the number of atoms considered in the cluster. As can also be seen in Tables 8.7, 8.10 and 8.12 the difference in the binding energy of Hg and element 112 is about 0.1 eV. As discussed in details in chapter 8 this result is not consistent because small systems are not able to describe the surface which we would like to model in order to describe the adsorption energy. This can be seen e.g. for XAu_9 in top position or XAu_{22} for hollow position where an inversion of the order of the binding occurs. This definitely is not astonishing because these systems are too small to describe this physical situation. The embedding method on the other hand, which allows a much better modeling of the surface of a solid leads to a systematic behaviour of the binding energies which are presented in Figures 9.8, 9.9 and 9.10 or Tables 9.5 and 9.9. The remaining problem is the use of the various basis sets. The results obtained with basis set B give a difference of the binding energy of about 0.4 eV, which is quite large in comparison with the value of 0.1 eV mentioned above for the cluster calculations. The reason became evident when we included the best basis set which we obtained from diatomic optimization. At the beginning we assumed that the basis set B was good enough. This is was not true. The argument which we had was that the error in the calculation with the cluster and the embedding calculation would be eliminated by the difference with respect to the calculation without the adsorption atom. To our astonishment we observed that the basis B and B' lead to the same results in the cluster calculation whereas the embedding calculation showed a different behaviour.
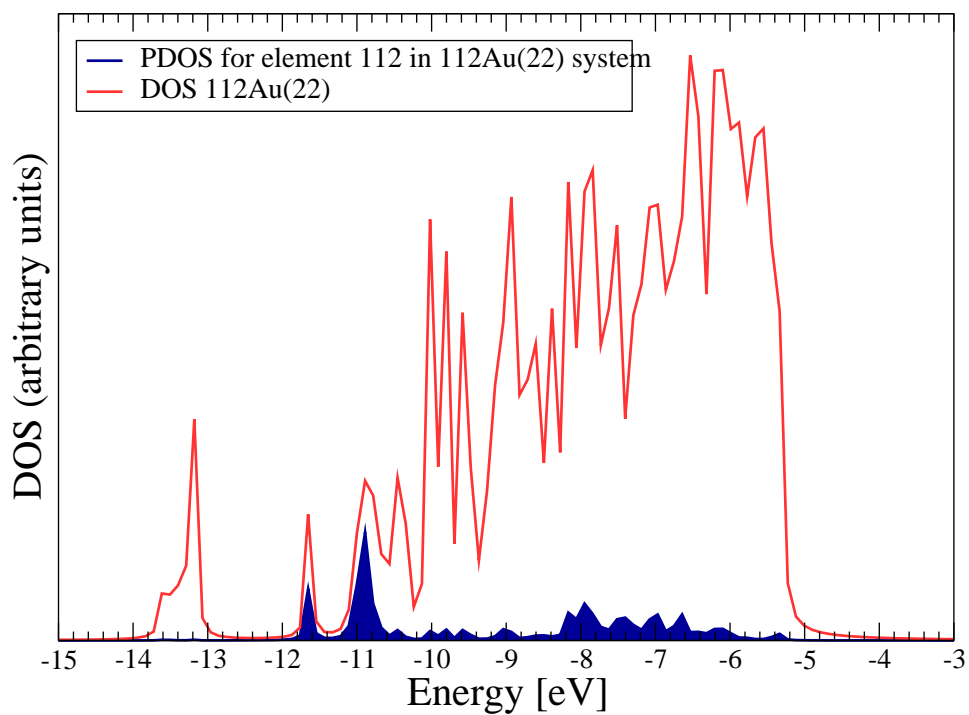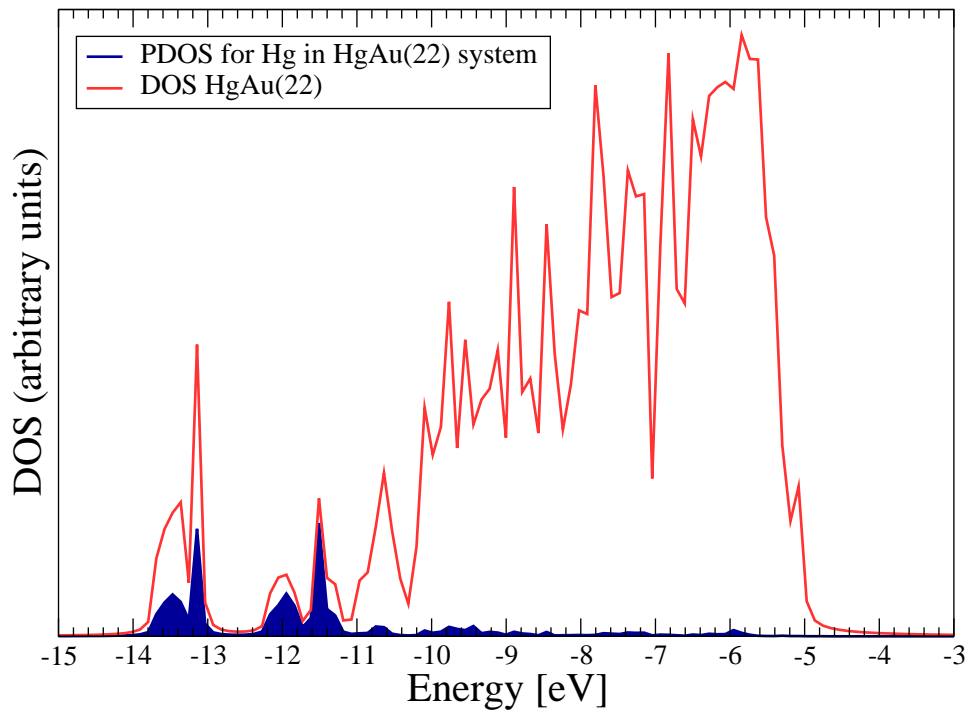
76

Figure 9.6: The total DOS of an embedded XAu_{22} system and the PDOS for the ad–atom of the occupied states for the hollow position, when the basis B is used.
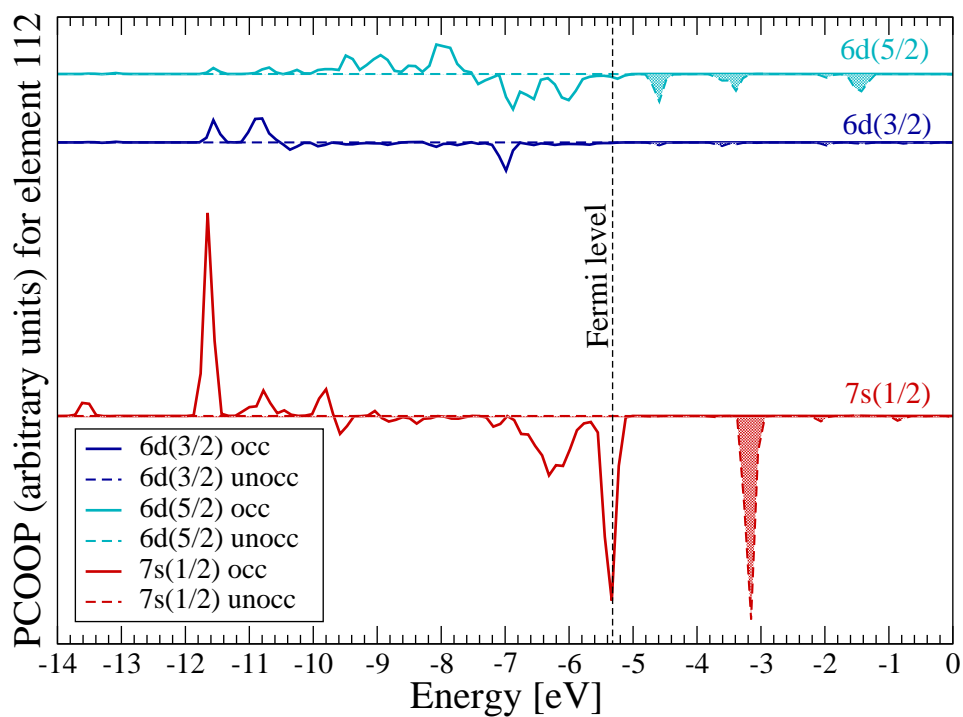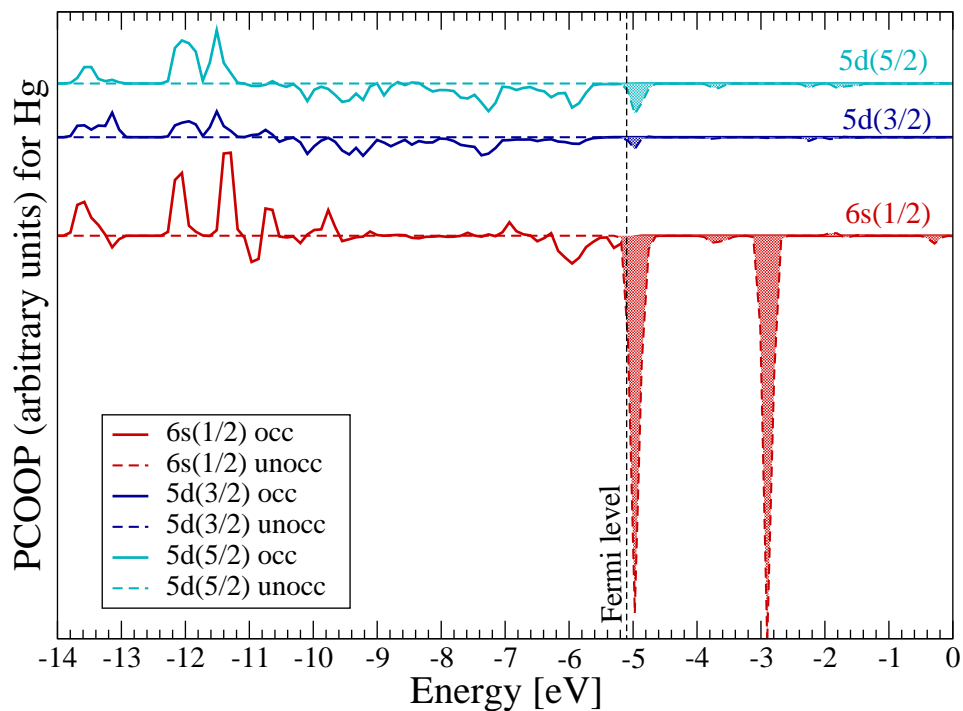
Figure 9.7: The partial crystal overlap population (PCOOP) for the occupied and unoccupied states for the valence orbitals in an embedded XAu_{22} system for the hollow position, when the basis B is used.
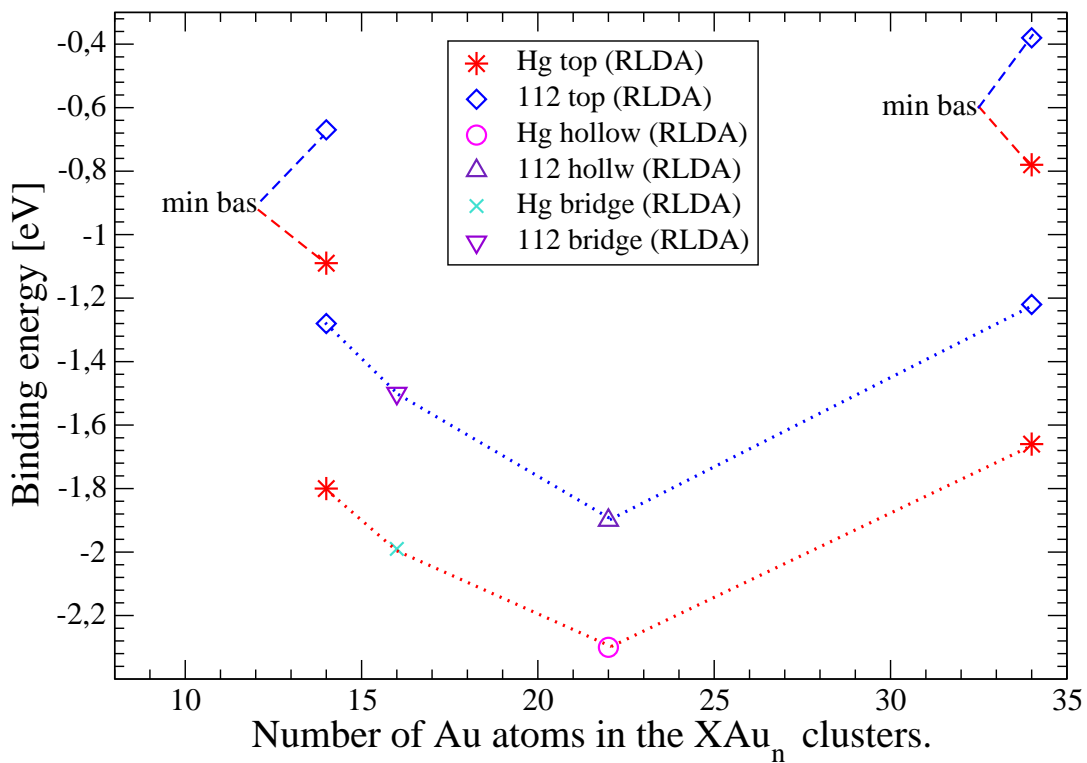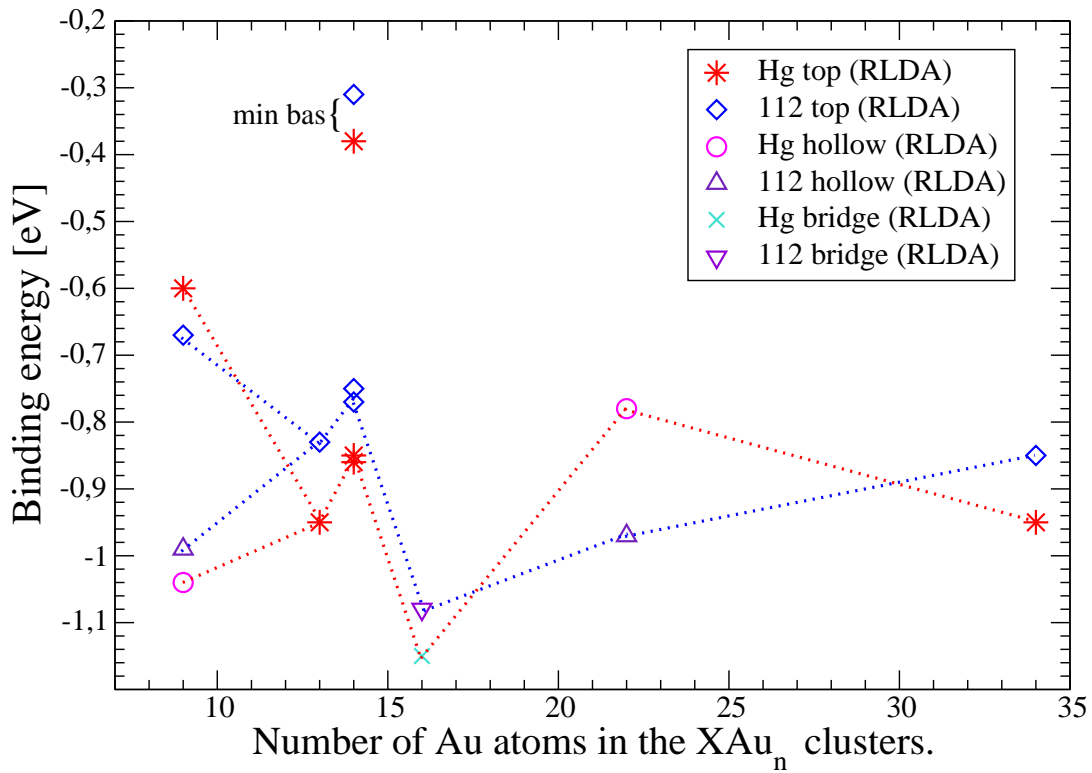
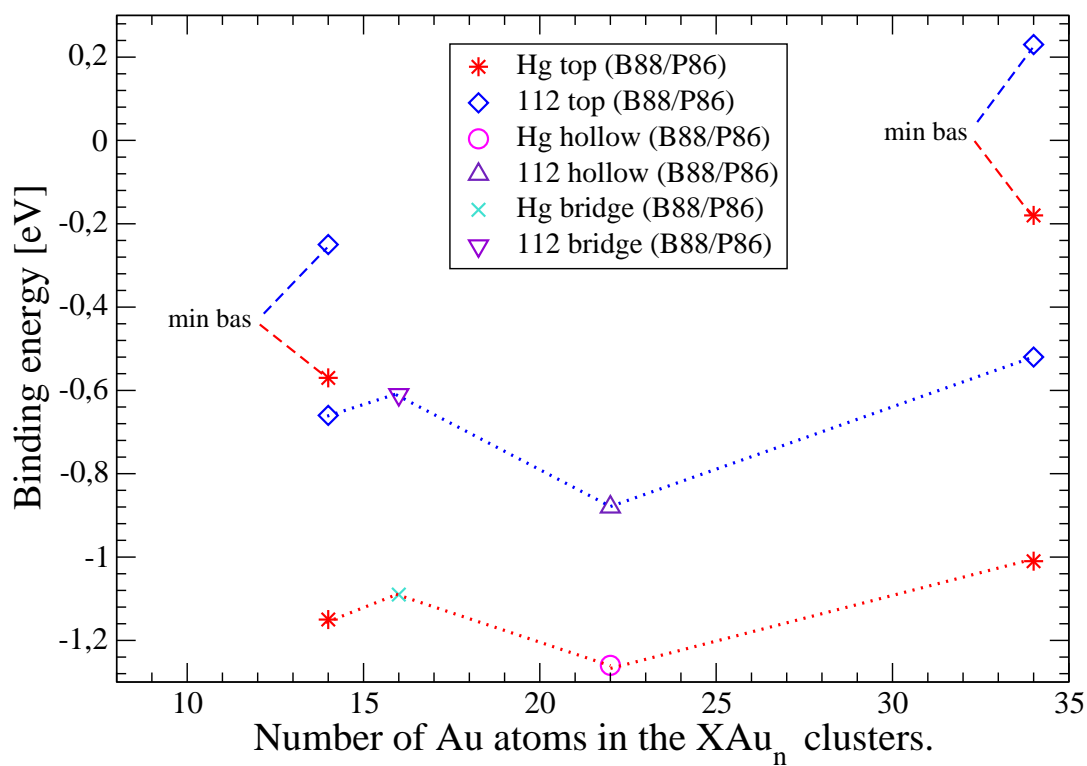Figure 9.8: The RLDA binding energies as a function of the number of atoms used to model the surface.(top—cluster method; bottom—embedding method)
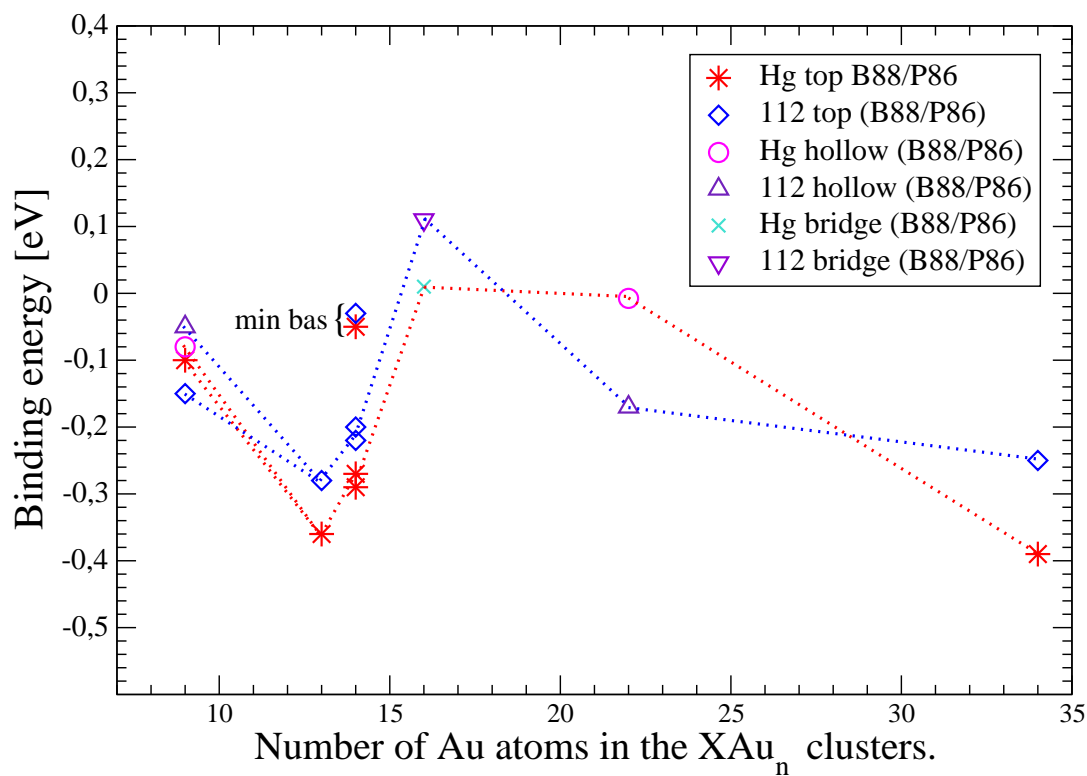
Figure 9.9: The GGA (B88/P86) binding energies as a function of the number of atoms used to model the surface.(top—cluster method; bottom—embedding method)
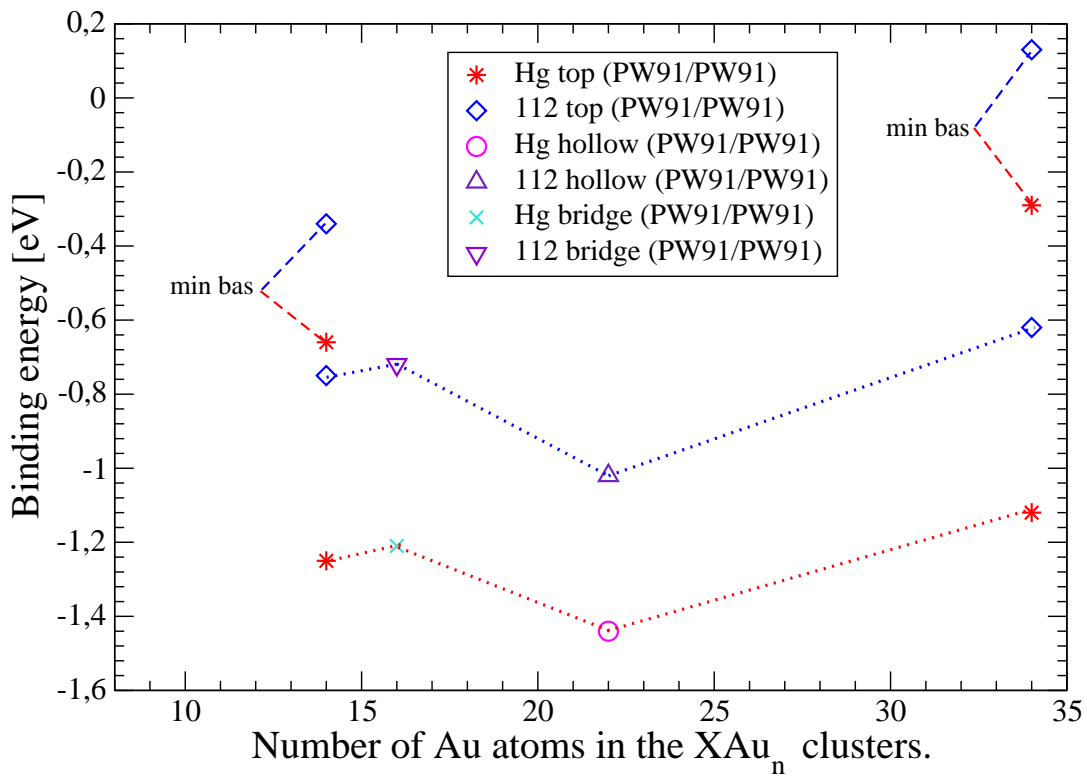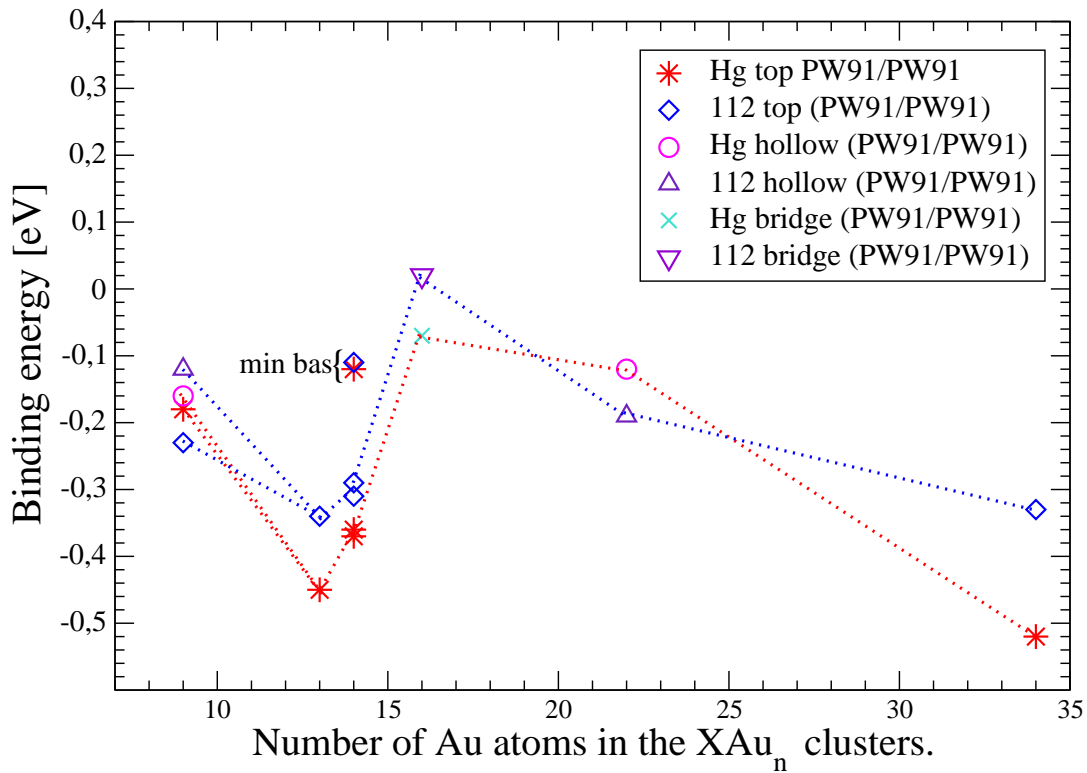
Figure 9.10: The GGA (PW91/PW91) binding energies as a function of the number of atoms used to model the surface.(top—cluster method; bottom—embedding method)

Chapter 10

Summary and outlook

One has to be aware that such ab–initio calculations of the adsorption energy of an ad–atom on a surface is on the verge of the possibility of a relativistic molecular program which we are using here. Of course a number of similar calculations has been performed by other authors. In these cases the method was much simpler (like the Diophantine method), or the clusters were quite small. The use of various exchange correlation potentials was another challenge of the present work.

In our case we have chosen the most complicated system. Hg and element 112 are elements with a closed electronic shell, thus behaving like van der Waals systems. One knows that usually van der Waals bonding can not be described with the usual form of density functionals. Since we deal here with these elements interacting with the surface of gold the method can be applied.

We have learned during the course of this work that one has to take great care in the choice of the basis. As was discussed in the text we were not able to use the best optimized basis for the cluster, as well as for the embedded cluster, otherwise calculations would have not been finished within any realistic time interval. A calculation with such an optimized basis for Au with 50 atoms, of C_{4v} symmetry, would need about 1/2 a year and double for a system with C_{2v} symmetry.

We have seen that the cluster calculations have not converged to the true value of adsorption energy for the two systems: Hg and 112 on the gold surface. Even 34 atoms do not seem to be sufficient to reach the convergence in size for the cluster calculations. From analogous calculations for Cu on a Cu surface we know that we need at least 60 atoms in the cluster to arrive at a converged value. As was mentioned above this is not possible for a gold cluster. On the other hand, we definitely have reached the cluster size convergence with the embedded cluster method. Using the external potential (both Coulomb and exchange-correlation) in this method resulted in a better convergence to the desired energy state. As was shown in the last chapter, the energy difference between Hg and element 112 interacting with a gold cluster became very reasonable. The further work here could be the usage of better basis sets.

As a final result we can state that the binding energy difference between the adsorption of these two elements is about 0.2 eV. Since we know the adsorption energy for Hg on

gold to be 1.05 eV we can predict that the binding energy of element 112 on gold is about 0.85 eV. The largest binding energy will not be on the top site but at the hollow site.

One of the unsolved questions in this work is the use of other optimized basis sets. In our calculations we optimized basis set for the dimer, which could be the case for the adsorbtion in the top position. If we arrive at the bridge or the hollow site then this basis may not be the optimal. In our future research we will optimize the basis with 3 atoms, which we can use for the bridge site, or with 5 atoms which we can use for the four–fold site.

Nevertheless, we hope that the obtained value of the binding energy of element 112 on the gold cluster can now be used for the identification of this superheavy element in a chemical thermo-chromatographic experiment.

Bibliography

[1] S. Hofmann, V. Ninov, F.P. Heßberger, P. Armbruster, H. Folger, G. Münzenberg, H. H. Schött, A.G. Popeko, A.V. Yeremin, S. Saro, R. Janik, M. Leino, *Z. Phys.*, A **354**, 229 (1996).

[2] S. Hofmann, "Superheavy elements", *J. Radioanal. Nucl. Chem*, **243**, 13–20 (2002)

[3] S. Hofmann, F.P. Heßberger, D. Ackermann, G. Münzenberg, S. Antalic, P. Cagarda, B. Kindler, J. Kojouharova, M. Leino, B. Lommel, R. Mann, A.G. Popeko, S. Reshitko, S. Saro, J. Uusitalo, A.V. Yeremin, *Eur. Phys. J.*, A **14**, 147 (2002).

[4] Yu.Ts. Organessian, A.V. Yeremin,G.G. Gulpbekian, S.L. Bogomolov, V.I. Chepigin, B.N. Gikal, V.A. Gorshkov, M.G. Itkis, A.P. Kabachenko, V.B. Kutner, A.Yu. Lavrentev, O.N. Malyshev, A.G. Popeko, J. Rohac, R.N. Sagaidak, S. Hofmann, G. Münzenberg, M. Veselsky, S. Saro, N. Iwasa, K. Morita, *Eur. Phys. J.* A **5**, 63 (1999).

[5] Yu.Ts. Organessian, A.V. Yeremin, A.G. Popeko, S.L. Bogomolov, G.V. Buklanov, M.L. Chelnokov, V.I. Chepigin, B.N. Gikal, V.A. Gorshkov, G.C. Gulpekian, M.G. Itkis, A.P. Kabachenko, A.Yu. Lavrentev, O.N. Malyshev, J. Rohac, R.N. Sagaidak, S. Hofmann, S. Saro, G. Giardina, K. Morita, *Nature*, **400**, 242 (1999).

[6] Yu.Ts. Organessian, V.K. Utyonkov, Yu.V. Lobanov, F.Sh. Abdulin, A.N. Polyakov, I.V. Shirokovski, Yu.Sl. Tsyganov, G.G. Gulbekian, S.L. Bogomolov, B.N. Gikal, A.N. Mezentsev, S. Iliev, V.G. Subbotin, A.M. Sukov, G.V. Buklanov, K. Subotic, M.G. Itkis, K.J. Moody, J.F. Wild, N.J. Stoyer, M.A. Stoyer, R.W. Lougheed, *Phys. Rev. Lett.*,**83**,3154 (1999).

[7] Yu.Ts. Organessian, V.K. Utyonkov, Yu.V. Lobanov, F.Sh. Abdulin, A.N. Polyakov, I.V. Shirokovski, Yu.Sl. Tsyganov, G.G. Gulbekian, S.L. Bogomolov, B.N. Gikal, A.N. Mezentsev, S. Iliev, V.G. Subbotin, A.M. Sukov, G.V. Buklanov, K. Subotic, M.G. Itkis, K.J. Moody, J.F. Wild, N.J. Stoyer, M.A. Stoyer, R.W. Lougheed, *Phys. Rev. C*,**63**,011301 (2000).

[8] B. Fricke, *Structure and Bonding* **21**, 89 (1975)

[9] G. G. Hall. The Hall equations. Proc. Roy. Soc., 208 A:328, 1951.

[10] P. A. M. Dirac, *Proc. Cambridge Phil. Soc.* **26**, 376 (1930).

[11] F. Bloch, *Zeitschrift für Physik* **57**, 545 (1929)

[12] D. R. Hartree, Proc. Cambridge Phil. Soc. **24**, 89 (1928)

[13] V. Fock, Z. Phys. **61**, 126 (1930)

[14] C. C. J. Roothaan, Rev. Mod. Phys. **23**, 69 (1951)

[15] C. Møller and M. S. Plesset, Phys. Rev. **46**, 618 (1934)

[16] J. Čìžek, Adv. Chem. Phys. **14**, 35 (1969)

[17] G. D. Purvis and R. J. Bartlett, J. Chem. Phys. **76**, 1910 (1982)

[18] J. A. Pople, M. Head-Gordon, and K. Raghavachari, Chem. Phys. **98**, 8718 (1993)

[19] J. D. Watts, J. Gauss and R. J. Bartlett, J. Chem. Phys. **98**, 8718 (1993)

[20] M. Häuser and R. Ahlrichs, J. Comp. Chem. **10**, 104 (1988)

[21] I. Panas, J. Almlöf, and M. W. Feyereisen, Inst. J. Quantum Chem. **40**, 797 (1991)

[22] M. C. Strain, G. E. Scuseria, and M. J. Frisch, Science **271**, 51 (1996)

[23] C. Ochsenfeld, C. A. White, and M. Head-Gordon, J. Chem. Phys. **109**, 1663 (1998)

[24] P. Y. Ayala and G. E. Scuseria, J. Chem. Phys. **110**, 3660 (1999)

[25] M. Schütz, G. Hetzer, and H.-J. Werner, J. Chem. Phys. **111**, 5691 (1999)

[26] M. Schütz and H.-J. Werner, Chem. Phys. Lett. **318**, 370 (2000)

[27] P. Hohenberg and W. Kohn. *Phys. Rev.*,**136**, B864-B871, 1964

[28] W. Kohn and L. J. Sham. *Phys. Rev*, **140**, A1133-1138, 1965.

[29] A. K. Rajagopal, *Adv. Chem. Phys.*, **41**, 59 (1980)

[30] S. Varga, E. Engel, W.–D. Sepp, and B. Fricke, *Phys. Rev. A*,**59**, 4288 (1999)

[31] S. Varga, B. Fricke, H. Nakamatsu, T. Mukoyama, J. Anton, D. Geschke, A. Heitmann, E. Engel, and T. Baştuğ, *J. Chem. Phys.*, **112**, 3499 (2000)

[32] E. Engel, R. M. Dreizler, S. Varga, and B. Fricke, *Relativistic Effects in Heavy-Element Chemistry and Physics.*, edited by B. A. Hess, John Wiley & Sons, 2001

[33] E. Engel, *Relativistic Electronic Structure Theory, Part 1: Fundamentals*, edited by P. Schwerdtfeger, Elsevier, Amsterdam, 2002

[34] L. D. Landau, E. M. Lifschitz, *Quantenelektrodynamik*, Akademie-Verlag, Berlin 1986

[35] J. P. Perdew. *Phys. Rev. Lett.*, **55**,1665, 1985.

[36] A. D. Becke. Density functional calculations of molecular bond energies. J. Chem. Phys., 84(8):4524-4529, 1986.

[37] A. D. Becke. Density-functional thermochemistry I. The effect of the exchange-only gradient correction. J. Chem. Phys., 96(3):2155-2160, 1992.

[38] A. D. Becke. Density-functional thermochemistry II. The effect of the Perdew-Wang generalized-gradient correlation correction. J. Chem. Phys., 97(12):9173-9177, 1992.

[39] A. D. Becke. Density-functional thermochemistry III. The role of exact exchange. J. Chem. Phys., 98(7):5648-5652, 1993.

[40] A. D. Becke. Density-functional thermochemistry IV. A new dynamical correlation functional and implications for exact-exchange mixing. J. Chem. Phys., 104(3):1040-1046, 1996.

[41] A. D. Becke. Density-functional thermochemistry V. Systematic optimization of exchange-correlation functionals. J. Chem. Phys., 107(20):8554-8560, 1997.

[42] A. D. Becke. A new mixing of Hartree-Fock and local density-functional theories. J. Chem. Phys., 98(2):1372-1377, 1993.

[43] D. C. Langreth and J. P. Perdew. Theory of nonuniform electronic systems. I. Analysis of the gradient approximation and a generalization that works. Phys. Rev. B, 21(12):5469-5493, 1980.

[44] J. P. Perdew and Wang Y. Accurate and simple density functional for the electronic exchange energy: Generalized gradient approximation. Phys. Rev. B, 33(12):8800-8802, 1986.

[45] J. P. Perdew. Density-functional approximation for the correlation energy of the inhomogeneous electron electron gas. Phys. Rev. B, 33(12):8822-8824, 1986.

[46] J. P. Perdew. Unified Theory of Exchange and Correlation Beyond the Local Density Approximation. Electronic Structure of Solids '91, edited by P. Ziesche and H. Eschrig, pages 11-20, 1991.

[47] Y. Wang and J. P. Perdew. Spin scaling of the electron-gas correlation energy in the high-density limit. Phys. Rev. B, 43(11):8911-8916, 1991.

[48] J. P. Perdew and Y. Wang. Accurate and simple analytic representation of the electron-gas correlation energy. Phys. Rev. B, 45(23):13244-13249, 1992.

[49] K. Burke, J. P. Perdew, and Y. Wang. Derivation of a Generalized Gradient Approximation: The PW91 Density Functional. Electronic Density Functional Theory: Recent Progress and New Directions, edited by J. F. Dobson, G. Vignale and M. P. Das, pages 81-121, 1997.

[50] J. P. Perdew, K. Burke, and M. Ernzerhof. Generalized Gradient Approximation Made Simple. Phys. Rev. Lett., 77:3865-3868, 1996.

[51] W. Ludwig, C. Falter, Symmetries in Physics, Springer-Verlag, Berlin, Heidelberg, New York, London, Paris, Tokyo 1988

[52] B. I. Dunlap, J. W. D. Connolly, J. R. Sabin, *J. Chem. Phys.*, **71**(8), 3396– 3402 (1979)

[53] S. Varga, B. Fricke, H. Nakamats, T. Mukoyama, *Journal of Chem. Phys.* ,**112** ,8 (200)

[54] M. Schädel, *The Chemistry of Superheavy Elements*, Kluwer Academic Publishers, 2003

[55] V. Pershina, T. Bastug, C. Sarpe–Tudoran, J. Anton, B. Fricke, *Nucl. Phys. A*, **734**, 200 (2004)

[56] R. A. van Santen, *Progr. Surf. Sci.*, **25**, 253 (1987)

[57] T. Jacob., S. Fritzsche, W.-D. Sepp *Physics Letters A*, **300**, 71–75 (2002)

[58] T. Jacob, J. Anton, C. Sarpe–Tudoran, W.-D. Sepp *Surf. Sci.*, **536**, 45–54 (2003)

[59] *Advances in Quantum Chemistry* **6**, Academic, New York (1972)

[60] S.J. Rose, I.P. Grant and N.C. Piper, *J. Phys. B: At. Mol. Phys.*,**11**, 1171, 1978

[61] J.P. Desclaux, *At. Data Nucl. Data Tables*,**12**, 311, 1973

[62] E. Eliav, S. Shhmulyian, U. Kaldor, Y. Ishikawa, *J. Phys. B*, **35**, 1693 (2002)

[63] J. Kordis, K. A. Gingerich, Ber. Bunsenges, *J. Chem. Phys.* ,**83** ,5114 (1974)

[64] J. Anton, B. Fricke, E. Engel, *Phys. Rev A*, **69**, 0125505 (2004)

[65] C. Kittel, *Introduction to Solid State Physics*, John Wiley &Sons, 7-^{t}h edition (1996)

[66] T. Jacob *Inaugural–Disertation zur Erlagung des akademischen Grades eines Doktors der Naturwissenschaften,*, Kassel, Dezember 2001

[67] T. Jacob, W.A. Goddard, J. Anton, C. Sarpe–Tudoran, B. Fricke, *Eur. Phys. J. D***24**, 61–64 (2003)

[68] C. Sarpe–Tudoran, V. Pershina, B. Fricke, J. Anton, W.D. Sepp, T. Jacob *Eur. Phys. J. D***24**, 65–67 (2003)

Lebenslauf

07 November 1968   born in Craiova, Romania

1975–1983   Elementary School, Scoala Generals Nr. 23, Craiova

1983–1987   Highschool, "Nicolae Balcescu" in Craiova

1987   Begin the study of physics at University of Craiova

1992 Jan.–July   Research mobility stage for diploma work in a Tempus program at Université Jean–Monnet du Saint–Etienne, Laboratoir du Signal et Instrumentation

1992   Diploma in Physics

1992–1997   physics theacher, "Elena Cuza" High School, Craiova

1997–1999   Associate at University of Craiova, Faculty of Physics

1999–Feb 2001   Assistent professor at University of Craiova, Faculty of Physics

since March 2001 PhD Student at University of Kassel